THE UNIVERSITY OF
WARWICK

University of Warwick institutional repository: http://go.warwick.ac.uk/wrap

A Thesis Submitted for the Degree of PhD at the University of Warwick

http://go.warwick.ac.uk/wrap/45871

This thesis is made available online and is protected by original copyright.

Please scroll down to view the document itself.

Please refer to the repository record for this item for information to help you to cite it. Our policy information is available from the repository home page.

Multi-layered nanocomposite polymer latexes and films

By

Roberto F. A. Teixeira

A thesis submitted in partial fulfilment of the requirements for the degree of Doctor of Philosophy in Chemistry

University of Warwick, Department of Chemistry

December 2011

Table of Contents

Figures

Tables

Acknowledgments

First of all I would like to thank my supervisor Assoc. Prof. Stefan Bon for giving me the opportunity to work in his team, for his continuous encouragement throughout my PhD and also for giving me the opportunity to present my work in leading conferences/journals.

I would like to thank all the past and present members of the Bon Polymer Colloid group. Special thanks to Dr. Catheline Colard for her contribution in our collaborative work. Thank you all for your support, advices and friendship – Andy, Nick, Nicole, Rong, Gabit, Yunhua, Tom, Holly, Adam, Attyah, Ashton, Sang and other students, under graduates and masters.

I also would like to thank my industrial sponsor BASF (Ludwigshafen) for their financial support. Also a special thanks to Dr. Harm Wiese, Dr. Bas Lohmeijer and Dr. Alexander Martin for their advices and interesting discussions.

I would like to thank Prof. Joseph Keddie and Gareth Davies (Department of Physics, Surrey University) for our successful collaborative work.

A special acknowledge to Ian Portman for his help and training with TEM. I also acknowledge Steve York for the help with SEM, Birmingham Science city Innovative for some of equipment used in this research (Uses for Advanced Materials in the Modern World (West Midlands Centre for Advanced Materials

Project 2) with support from Advantage West Midlands (AWM) and partly funded by the European Regional Development Fund (ERDF)).

Most importantly would like to thank all my family and friends. Special thanks to my mother and father for their support. Finally, I am especially grateful to Andreia for keeping me sane, motivated and for constant help and support during the last three years.

Declaration

I hereby declare that I am the major contributor of all work presented in this PhD thesis except for the work in chapter II which was done in collaboration with Dr. Catheline Colard. Also the mechanical analysis presented in chapter IV was done in collaboration with Prof. Joseph Keddie and Gareth Davies from Surrey University, UK. Any other sources of work previously published, are acknowledged and referenced on the first page of each chapter.

Signature: Roberto Fernando Almeda Teixeira Date: 1, December, 2011

Abstract

Clay platelets and silica nanoparticles are used as Pickering stabilizers in the fabrication of hybrid armored polymer particles through a Pickering emulsion polymerization process. A variety of hydrophobic comonomers (i.e., styrene-*co*-(*n*-butyl acrylate) (Sty:BA), methyl methacrylate-*co*-(*n*-butyl acrylate) (MMA:BA)), styrene-*co*-(2-ethyl hexyl acrylate) (Sty:2-EHA), vinyl acetate (VAc) and vinyl pivalate (VPiv) are used as organic film forming components. Polymerization kinetics and particle size distributions were examined as a function of monomer conversion. Additionally, key mechanistic features of the polymerization process by quantitatively analyzing the concentration of silica nanoparticles in the water phase during monomer conversion by disc centrifugation are unraveled. It is also showed the crucial role of Laponite clay discs in the particle formation (nucleation) of the Pickering emulsion polymerization process. Increasing amounts of clay nanodiscs leads to smaller average particles sizes, but broader particle size distributions.

Polymer films of poly(styrene-*co*-*n*-butyl acrylate) armored with Laponite clay were studied as a function of clay amount. Improvements in mechanical, thermal and surface topography provided by clay platelets are reported. In addition, advantages are shown in use of hybrid polymer particles in comparison with simple blend mixtures of polymer particles plus inorganic particles.

Humidity properties of poly(styrene-*co*-*n*-butyl acrylate) films as a function of clay content are investigated. It is demonstrated that the presence of Laponite clay improves the water storage capacity of polymer films. Also water barrier properties are improved when clay platelets are applied.

Finally, a versatile two step Pickering emulsion polymerization for the fabrication of core-shell particles armored with Laponite clay XLS is developed. The obtained particles contain a “hard” core and a “soft” shell armored with clay. The different in the refractive indexes between the core and shell makes these core-shell particles interesting for possible use as colloidal crystals.

Abbreviations

(FEG)-SEM	(Field Emission Gun-) Scanning Electron Microscopy
2-EHA	2-ethylhexyl acrylate
ABIN	2,2'-azobis(2-methyl)propionitrile
APS	Amonium persulfate
BA	*n-b*utyl acrylate
BMA	Butyl methacrylate
CPS	Disc Centrifuge Particle Sizing
D_I	Dispersity index (polydispersity index)/ -
DLS	Dynamic Light Scattering
DMA	Dynamic mechanical analysis
DMTA	Dynamic mechanical thermal analysis
DSC	Differential Scanning Calorimetry
DVS	Dynamic vapour sorption
d_z	Hydrodynamic diameter/ m
EELS	Electron energy loss spectroscopy
fcc	Face-centred cubic
hcp	Hexagonally closed packed
HDMS	Hexamethyldisiloxane
KPS	Potassium persulfate
MAA	Methacrylic acid
MMA	Methyl methacrylate
NASS	Sodium styrene sulfonate
PBA	Poly(butyl acrylate)

PMMA	Poly(methylmethacrylate)
PMAA	Poly(methacrylic acid)
PEHA	Poly(2-ethylhexylacrylate)
PS	Poly(styrene)
PVAc	Poly(vinyl acetate)
PVPiv	Poly(vinyl pivalate)
RH	Relative humidity
SDS	Sodium dodecyl sulfonate
TEM	Transmission Electron Microscopy
VAc	Vinyl acetate
VPiv	Vinyl pivalate
T_g	Glass transition temperature/ K
X_m	Monomer conversion/ -
XPS	X-ray photoelectron spectroscopy/ J

Chapter I.

General Introduction

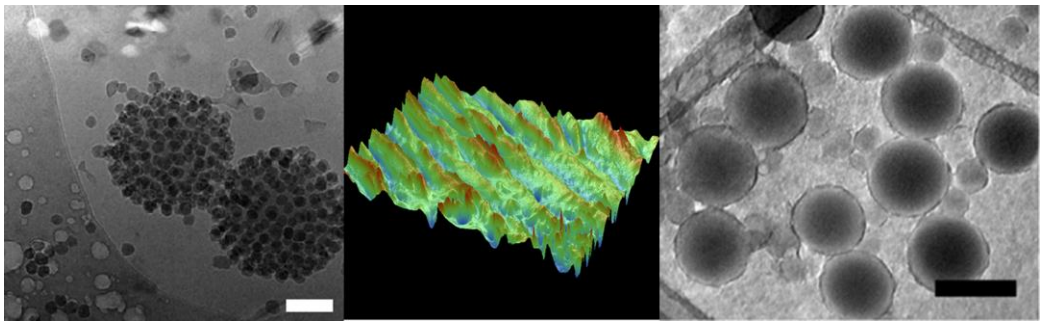

In this chapter the conceptual physical approaches towards the fabrication of nanocomposite polymer latexes are introduced, in which each individual latex particle contains one, or more "hard" nanoparticles, such as clays, silicates, titanates, or other metal(oxides). With "physical approaches" it is mean that the "hard" nanoparticles are added as pre-existing entities, and are not synthesized in situ as part of the nanocomposite polymer latex fabrication process. The discussion is narrow and focus on physical methods that rely on the assembly of nanoparticles onto the latex particles after the latex particles have been formed, or its reciprocal analogue, that is the adhesion of polymer onto an inorganic nanoparticle. In this section, the phenomenon of heterocoagulation, and various driving forces such as electrostatic interactions, the hydrophobic effect and secondary molecular interactions are discussed. It is also addressed methods that will involve assembly of nanoparticles onto, or around, the more liquid precursors (*i.e.* swollen/growing latex particles or monomer droplets). It will focus hereby on the phenomenon of Pickering stabilization. Features of particle

interactions with soft interfaces, and see how the adhesion of particles onto emulsion droplets can be applied in suspension, miniemulsion and emulsion polymerization will be discussed. Then, some interesting methods to make well defined assembled clusters and supracolloidal structures of particles which make use of interface-driven templating will be briefly mentioned. Finally, a brief outline of each thesis chapter is presented.

Part of this work was published

[1]Roberto F. A. Teixeira, and Stefan A. F. Bon, *Adv.Polym.Sci.*, **2011**, 233, 19-52.

I.1. Assembly of nanoparticles onto prefabricated "larger" particles via heterocoagulation

Heterocoagulation is the mutual adhesion of particles of a dissimilar nature upon collision, as a result of their individual Brownian motion. Brownian motion is a stochastic, or random, movement of colloidal particles suspended in a fluid (or gas) as a result of the internal thermal energy of the system, and thus collisions with the solvent (or gas) molecules, as pointed out independently by Einstein and Smoluchowski. Derjaguin pointed out that the term heteroadagulation should be used for adhesion of small particles that move through Brownian motion onto much larger objects, whose Brownian motion can be neglected, such as fibres.[2] For example, Jachowicz and Berthiaume[3] reported the deposition of cationic, anionic and neutral silicon oil droplets in the form of oil-in-water emulsions on native or cationically modified human hair fibers, driven by electrostatic forces.

Since heterocoagulation is a stochastic process great care needs to be taken not to end up with large fractal clusters or flocks of the two colloidal components. Driving forces to promote adhesion of inorganic nanoparticles onto the surface of polymer latex particles, or *visa versa*, can be based on a variety of forces, such as on electrostatic attraction, hydrophobic interactions, and secondary molecular interactions such as (multiple) hydrogen bond interactions, specific molecular recognition *e.g.* complementary proteins, for example, avidin-biotin.

I.1.1. Electrostatic interactions

When an inorganic nanoparticle has the opposite charge to a larger polymer latex particle they will attract each other. On the other hand, particles with the same charge sign will repel each other. This is the base of Coumlomb's law, where the force (F) between two charged points can be described as:

$$F = Ke\frac{q_1 q_2}{r^2}$$

Equation I-1

In which, r is the distance between two charged particles, q_1 is the charge of one particle and q_2 is the charge of the other particle and Ke is the Coulomb constant (9.0 x10^9 N. m^2. C^{-2}). The range in which an attractive force is felt depends on the charge densities and more importantly on the extent of the diffuse double layers of the two interacting colloids. When one wants to adhere more than one nanoparticle onto a polymer latex sphere the small particles already present on the surface of the latex particle will influence the adsorption behavior of the next to-be-adsorbed nanoparticle. The spatial distribution for sorption of the nanoparticles on the surface is logically influenced, and a close encounter can even locally be of a repulsive nature. This charge inversion is also the reason why typically only a single layer of nanoparticles can be adhered onto the surface of the central particle.

The attraction between oppositely charged colloids can be understood and modeled using the DLVO theory. [4-7] The DLVO theory links the van der Waals attraction between particles with the electrostatic effects resulting from the presence of a double layer of counterions. A detailed theoretical discussion lies

outside the scope of this Chapter. One of the difficulties of the DLVO theory is that an exact analytical description of interaction of overlapping double layers is only know for flat, infinite parallel surfaces. For spherical double layers approximations need to be made or numerical theoretical simulations need to be performed.

Hogg, Healy and Fuerstenau[8] developed their HHF theory to describe the interactions of two particles of different size. In 1985, Matijevi and Barouch,[9] evaluated the validity of the HHF theory for the electrostatic interaction between two surfaces of different sizes for both unlike particles with potentials opposite in sign, and particles with same sign potentials. The computational calculations performed overcame the problem of the accuracy in the evaluation of incomplete elliptic integrals of the first kind that is a direct consequence of a non-linearity of the Poisson-Boltzman equation. They concluded that for systems with dissimilar particles with either opposite or same sign, the approximation of the HHF theory achieved good results. However, when potential differences increased, marked deviations from the HHF theory were found.

In 1976, Bleier and Matijevic[10] reported the interaction of two different monodisperse hydrous chromium(III) oxide sols of approximate radii of 110 and 186 nm with poly(vinyl chloride) latexes of *ca.* 169 nm and 255 nm in radius and of relatively narrow particle size distribution, in aqueous solution. Zeta-potential measurements of the Chromium(III) oxide sols as a function of pH in a 8.9 mM background electrolyte solution of $NaNO_3$ showed an isoeletric point (IEP) between pH 7.2-7.6. Below the IEP the sols were positively charged,

above the IEP negatively. Dispersions of the inorganic sols were stable below pH 4.6 and above pH 9.0. Both PVC latexes were stable and negatively charged throughout the pH range 3.0-11.0 investigated. They found that rapid coagulation of mixtures of the inorganic sol with the polymer latex occurred between pH 3.0 and pH 4.6. Whereas both individual dispersions were stable, this therefore was directly ascribed to mutual coagulation of oppositely charged particles. These experimental observations were in agreement with the earlier predictions by the HHF theory[8]. Obviously bulk coagulation needs to be avoided. A logical parameter therefore is the geometric ratio of the sizes of the two different colloids involved, the larger the easier it would be to avoid mass coagulation. Note that Vincent *et al.*[11-13], showed that small particles in the presence of a low electrolyte concentration, can act as bridging flocculants of large particles of opposite charge.

Vincent and coworkers described the adsorption-desorption behavior of small positively charged poly(styrene) latex particles onto much larger negatively charged poly(styrene) spheres.[14,15] In addition to surface charges both sets of particles had a layer of adsorbed poly(vinyl alcohol) to investigate the influence of the extent of the diffuse double layer upon variation of the electrolyte concentration. At low electrolyte concentration the diffuse double layers are extended and the small particles adhere in a way that shows a relatively large spatial distance between them on the surface of the large sphere. The extended double layers effectively cause a strong and irreversible adsorption. The lateral repulsion force and the electrostatic adsorption force both decrease when the electrolyte concentration is increased. The spatial arrangement of the small

particles may now experience a lateral net attractive rather than repulsive force, which lead to clustering of the nanoparticles on the surface. The adsorption behavior also can become reversible, being a direct function of the thickness of the sterically stabilizing poly(vinyl alcohol) layers around both the small particles and the larger latex spheres, and the volume fractions of the particles in the system.

Hansen and Matijević[16] studied the adsorption of negatively charged (carboxylic acid functionality) poly(methyl methacrylate) latex of average particle radius of 40 nm onto much larger positive inorganic sols made from either hydrated aluminium oxide (particle radius 250 nm) or heamatite (radius of 272-276 nm). The polymer latex showed an IEP of pH 3.8 the hydrated aluminium hydroxide particles an IEP of pH 8.7, and the heamatite had a value of pH 7.2, all measured in 0.01 M KNO_3 background electrolyte. Above the IEPs of these dispersions the latex and the sols were negatively charged. The absorption process of the smaller latex particles proceeded in a reversible manner, implying equilibrium conditions. The maximum number of small particles adsorbed onto a large particle was shown to increase with increasing KNO_3 concentration, reaching practically a "fully covered" monolayer. This is in agreement with the findings by Vincent.[14] It was possible to compare the interactions energies obtained from the adsorption isotherm of the latex poly(methyl methacrylate *co*-methacrylic acid) onto positive oxide(alumina or haematite) to the calculated values according to the derived expression based on the two-dimensional Poisson-Boltzman equation.[17]

Furusawa and Anzai investigated the heterocoagulation of a highly monodisperse amphoteric polymer latex (particle diameter 250 nm, IEP *ca.* pH 6.8 in 5.0 mM KCl background electrolyte, positively charged at low pH) onto various silica spheres (diameter 240, 460, 960 and 1590 nm, IEP *ca.* pH 3.0) dispersed in pure water or upon addition of various hydroxypropyl celluloses (HPCs). [18, 19] Stable dispersions for both individual particles under the condition that they had opposite surface charge only occurred in the narrow pH window between pH 5-6. Stable raspberry like heterocoagulates were obtained when the ratio of the diameter of the silica to latex particle was greater than 3. For ratios of a lower value larger irregular aggregates were obtained (see **Figure I.1**).

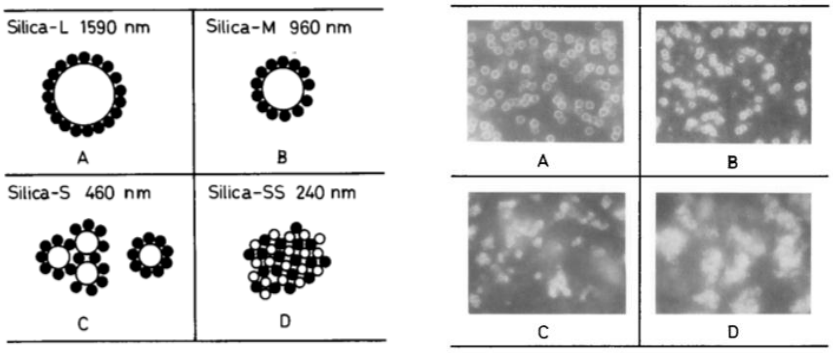

Figure I.1. The left is a schematic representation of the different morphologies of heterocoagulate particles that can be obtained when the relative sizes of the two colloids are varied. The right is a collection of micrographs obtained from the experiments in the heterocoagulation of an amphoteric latex at pH 5.6 where it has a cationic surface charge (diameter 250 nm) with negatively charged silica particles of various sizes (diameters of 1590 (A), 960 (B), 460 (C) and 240 (D) nm). Reproduced Figs 2 and 3 from Ref [18].

Harley, Thomson and Vincent used thin-film freeze-drying scanning electron microscopy (TFFDSEM)[20] as a visualization method to study the heterocoagulation of monodisperse anionic polymer latexes of various diameters made using potassium persulfate as initiator, that is poly(styrene) spheres of 696, 320, and 180 nm and a poly(vinylidene chloride) latex of 116 nm, onto a large cationic poly(styrene) latex of 2170 nm in diameter using azobis(isobutylamidine)dihydrochloride as initiator.[21] Adsorption isotherms of the four sets of negatively charged particles onto the large cationic microspheres were of the "high-affinity" type, in 0.5 mM KCl background electrolyte. This was logical and ascribed directly to extended interacting double layers. The particles pack beautifully symmetrically onto the surface (**Figure I.2**) implying that lateral electrostatic repulsion between neighboring adhered particles plays a key role.

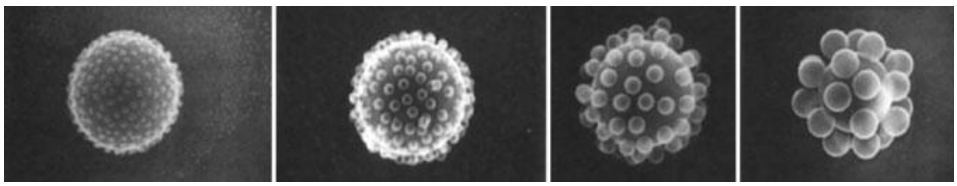

Figure I.2. TFFDSEM images of various anionic polymer latexes of different sizes, that is a poly(vinylidene chloride) latex of 116 nm, and poly(styrene) particles of 180, 320, and 696 nm in diameter, assembled onto a large cationic poly(styrene) latex of 2170 nm via heterocoagulation in 0.5 mM KCl background electrolyte. Images reproduced from Fig 7 from reference [21].

The influence of the concentration of the background electrolyte was beautifully captured in a series of images using the anionic poly(vinylidene chloride) latex of 116 nm, at KCl concentrations of 0.01, 0.1, 0.5 and 5.0 mM

(See **Figure I.3**) Increasing the background eletrolyte concentration and thus effectively reducing the thickness of the double layer led to closer spatial arrangements of the particles onto the surface of the central microsphere. At the highest electrolyte concentration one could even argue the onset of an attractive force rather than repulsive between neighboring particles.

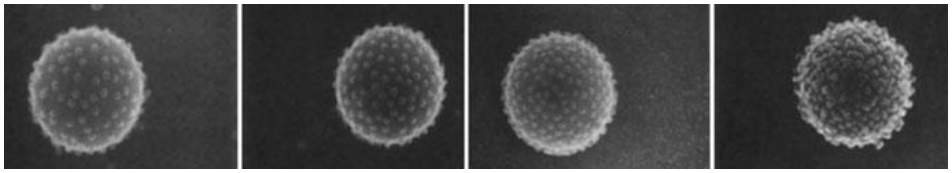

Figure I.3. TFFDSEM images of an anionic poly(vinylidene chloride) latex of 116 nm latexes, assembled onto a large cationic poly(styrene) latex of 2170 nm via heterocoagulation at various background electrolyte concentrations of KCl, i.e. 0.01, 0.1, 0.5 and 5.0 mM. Images reproduced from Fig 9 from reference [21].

Ottewill and coworkers used hetercoagulation as a route to hard core/soft shell polymer composites. Small cationic latex particles of poly(butyl methacrylate) were adhered onto the surface of larger anionic poly(styrene) latex particles.[22] Upon raising the temperature of the assembled colloidal dispersion the poly(butyl methacrylate) latex particles underwent film formation leading to a smooth shell. Okubo played with the reciprocal concept of using heterocoagulation as a method to prepare soft core/hard shell polymer composites. The source for hard particles, however, were not inorganic nanoparticles but cationic poly(styrene) spheres of 103 nm in diameter, assembled onto a soft poly(ethyl acrylate-*co*-ethyleneglycol dimethacrylate-*co*-methacrylic acid) latex spheres of 714 nm.[23]

Xu *et al*. heterocoagulated cationic poly(methyl methacrylate) latex particles of an estimated 150-200 nm in diamater with various clays Montmorillonite (GelWhite GP® and Cloisite® Na+) and (fluoro)hectorites (Laponite® RD, RDS, B, S, JS), having various plate dimensions in between 25-600 nm. No details on the stable colloidal armored structures were reported. Mass coagulation was induced in order to obtain a nanocomposite bulk material that was further analysed.[24] Chen et al[25] added TiO_2 and SiO_2/TiO_2 nanoparticles with a positive surface charge at very low pH 0-2 to both anionic and cationic latexes based on poly(methyl methacrylate). A bulk nanocomposite blend was analyzed.

Voorn *et al*. heterocoagulated both anionic "hard" poly(styrene) and "soft" poly (*iso*-butyl methacrylate) latex particles onto large positively charged gibbsite clay platelets. The soft latex was allowed to spread and wet the surface of the clay platelets to form a more uniform layered film by curing at 80 °C[26] (See **Figure I.4**). At low number ratios of latex particles to clay platelets, that is <180, multilayered aggregates were formed. Increasing the amount of latex particles resulted in coverage of isolated clay particles. The use of small latex particles at low ionic strength proved beneficial to warrant overall colloidal stability.[27]

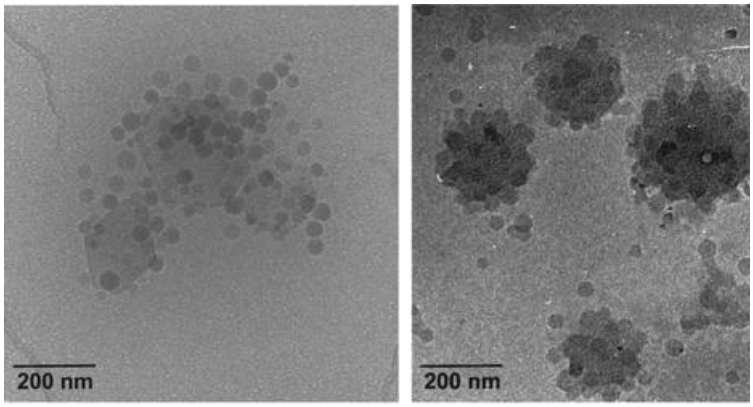

Figure I.4. Cryo-TEM micrographs of cationic gibbsite with anionic poly(*iso*butyl methacrylate) latex particles at different NaCl concentrations: (a) 3.1 × 10-4 M and (b) 9.1 × 10-4 M. The image is a reproduction of Figure 8 from reference [26].

I.1.2. Hydrophobic/ van der Waals interactions

Amphiphilic molecules, such as sodium dodecyl sulfate, above a certain critical concentration form assembled structures in which the hydrophobic units are clustered together. This hydrophobic or van der Waals interaction was brought to light by Walter Kauzmann, whilst studying forces which influenced protein denaturation.[28] An excellent critical review on interfaces and the driving forces of hydrophobic assembly has been written by Chandler in 2005.[29]

The hydrophobic effect is the tendency of nonpolar species to cluster in water in order to decrease the overall interfacial area between the hydrophobic species and water. It can be seen as predominantly driven by the large cohesive energy of water. Clustering of a set of individual hydrophobic particles into an agglomerate structure initially looks entropy driven. However, one should look

at the overall change in free energy, and thus also at enthalpy. The latter is a measure for the average potential energy of interaction between molecules. Assembly processes that involve considerable changes in the number of molecular interactions, therefore could (also) be enthalpy driven.

There are numerous attempts to define hydrophobic interactions, but there is not one that can explain all experimental results.[30] In 1989 Eriksson[31] postulated that the long range hydrophobic forces (LRHF) occurred due to structural changes on the boundary layers of water when in contact with hydrophobic surfaces. Other theory that assume the LRHF was related by Attard[30] that said that these forces are due to electrostatic correlations induced by the surface. Stillinger has suggested that the interface of liquid water near a large hydrophobic particle can be modeled analogous to a water-vapor interface [32].

Yaminsky et al[33] evaluated theoretically a hydrophobic surface in water with a contact angle more than 90º concluding that the water-vapour cavity is thermodynamically favored at small separations. The existence of such a hydrophobic "gap" between liquid water and the hydrophobic surface has been experimentally confirmed by for example Mezger and coworkers in high-resolution X-ray studies at the water-octadecyltrichlorosilane interface.[34] The reason is that the persistence of a hydrogen-bonded network of water molecules is geometrically impossible on a "large", in approximate excess of 1nm, interface, and therefore leads to drying. This dewetting effect can lead to very strong interactions between hydrophobic objects, as seen for example in surface force measurements. When two hydrophobic objects approach each other water depletes in between.[35]

These hydrophobic interactions are reported to be "long-range" commonly covering distances of 1-100 nm,[36] greatly exceeding the interaction range of van der Waals forces. Singh and coworkers[37] investigated the hydrophobic effect between naturally occurring superhydrophobic rough surfaces (water contact angle of 170 °) beneath a water surface using force measurements in which a superhydrophobic tip was placed in contact with a flat superhydrophobic substrate, both immerged in water, the tip being subsequently rectracted. They found a very-long-range hydrophobic interaction that was due to out-of-contact 'cavitation' of the intervening water at tip-to-substrate separations ranging from 0.8 μm to and impressive 3.5 μm. Cavitation is a first-order phase transition which was the reason for the observed sudden, strong attractive force identified as a vapor bridge spanning the tip-to-substrate gap.

Nagai and coworkers reported a heterocoagulation study driven by the hydrophobic effect of cationically charged "hard" poly(styrene-*co*-(methacryloyloxyphenyl-dimethylsulfonium methylsulfate)), or "soft" poly(styrene-*co*-(n-butylacrylate)-*co*-(methacryloyloxyphenyl-dimethylsulfonium methylsulfate)) latex particles of *ca.* 220-240 nm in diameter onto neutral microspheres of crosslinked poly(styrene) (8.5 μm in diameter). [38] A separate study on the small cationic latex particles showed that their interface was hydrophobic as the cationic surfactant cetyltrimethylammonium bromide (CTAB) adsorbed onto the surface, clearly driven by a hydrophobic effect. [39] The assembly of the cationic latex particles onto the larger microspheres was studied against increasing NaCl concentrations, which influenced the packing patterns from individually spaced to clusters (see **Figure I.5**).

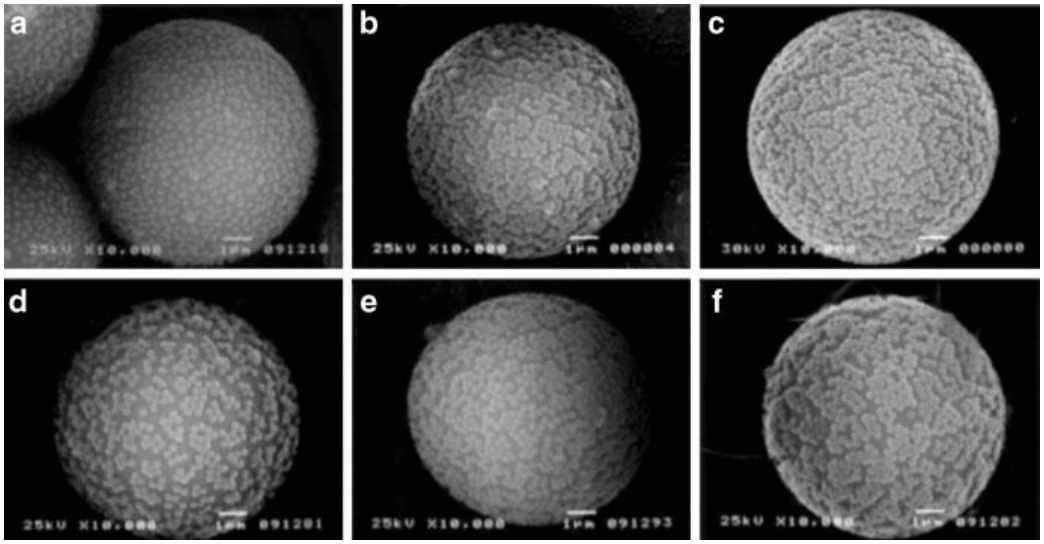

Figure I.5. SEM photographs of cationic polymer latex particles heterocoagulated onto the surface of crosslinked poly(styrene) microspheres driven by the hydrophobic effect, against increasing NaCl concentrations. (a), (b) and (c) are the "hard" "hard" poly(styrene-*co*-(methacryloyloxyphenyl-dimethylsulfonium methylsulfate)) particles at 0.5 mM, 50 mM, and 200 mM of NaCl.; (d), (e) and (f) are the "soft" poly(styrene-*co*-(*n*-butyl acrylate)-*co*-(methacryloyloxyphenyldimethylsulf-onium methylsulfate)) latex particles at 0.5 mM, 50 mM, and 200 mM of NaCl.

I.1.2.1. Self-assembly of amphiphilic particles driven by the hydrophobic effect

An interesting "molecular" approach using the hydrophobic effect to assemble gold nanoparticles was taken by Zubarev and coworkers who attached V-shaped (twin-tailed) amphiphilic poly(styrene)-*block*-(ethylene oxide) with a central carboxylic acid moiety which binds to the gold nanoparticle, effectively giving it its biphasic, Janus-type, characteristics.[40] Self-assembly led to worm-like aggregates (See **Figure I.6**)

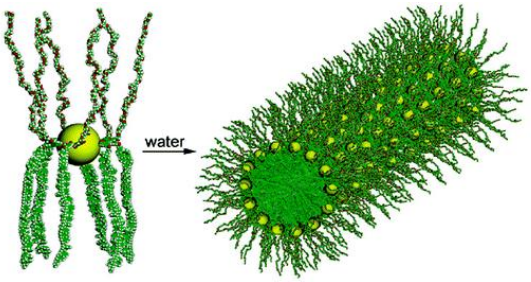

Figure I.6. Schematic representation of the amphiphilicity-driven self-assembly of Au-(PS-PEO)n nanoparticles (for simplicity reasons only six PS-PEO molecules are shown). This figure is a reproduction of Fig 1A from ref[40]

Along this line of using amphiphilic features of particles to drive assembly using a hydrophobic effect the recent surge in interest in fabrication and behavior of anisotropic "patchy" or Janus-type colloidal particles will be a promising route to innovative nanocomposite materials [41,42]. Whereas a thorough review lies outside the scope, we would like to highlight a few examples. Müller and coworkers prepared disc-like polymer Janus particles from assembled films of poly(styrene)-*block*-poly(butadiene)-*block*-poly(methyl methacrylate) triblock copolymer (SBM),[43] selective crosslinking of the poly(butadiene) block and dissolution via sonication, and assembled them into supracolloidal Janus micelles. They revisited this in another paper by hydrolyzing the poly(methyl methacrylate) into poly(methacrylic acid) [44]. Again assembly into supracolloidal micelles was driven by the hydrophobic effect. Daoyong Chen and coworkers prepared polymeric Janus particles from divinylbenzene and *N*-isopropylacrylamide via an yttrium hydroxide nanotube (YNT) supported route. Upon removal from their support these asymmetric particles assembled into flower-like supracolloidal structures (See **Figure I.7**). [45]

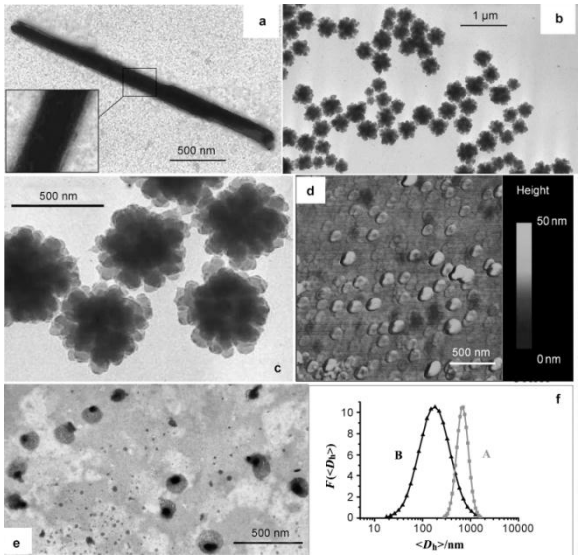

Figure I.7. a) TEM image of a hybrid nanotube, and the same HN at a larger magnification to show the polymer layer surrounding the YNT; b) TEM image of the supermicelles; c) TEM image of the supermicelles at a larger magnification; d) AFM image of petal-like (Janus) particles that result from the dissociation of the supermicelles on mica; e) TEM image of the Janus particles stained with RuO_4; f) distribution of the hydrodynamic diameter <Dh> of the supermicelles (A) and the Janus particles (B). This Figure is reproduced from Figure 2 in ref.[45]

Granick and coworkers studied both experimentally and by Monte Carlo simulations the assembly of amphiphilic colloidal microspheres into clusters. [46] Not only supracolloidal spherical micellar structures were observed, but also wormlike strings. Fluorescent carboxylated poly(styrene) microspheres were partially coated (hemisphere) with a thin gold layer, the latter subsequently modified with octadecanethiol to promote a hydrophobic nature. The hemisphere with the free carboxylate groups was occasionally made more hydrophilic by grafting of DNA oligomers onto the surface of the microsphere.

Upon increasing salt concentration (KNO_3) a transition from unimers, spherical clusters, and wormlike strings was observed in both simulations and experiments.

Recently, Miller and Cacciuto explored the self-assembly of spherical amphiphilic particles using molecular dynamics simulations.[47] The found that, next to spherical micellar-type structures and wormlike strings, also bilayers and faceted polyhedra were possible as supracolloidal structures. Whitelam and Bon [48] used computer simulations to investigate the self-assembly of Janus-like peanut-shaped nanoparticles, finding phases of clusters, bilayers, non-spherical and spherical micelles and faceted polyhedral structures (see **Figure I.8**). In both studies faceted polyhedra and bilayers are coexisting, a phenomenon still unexplained.

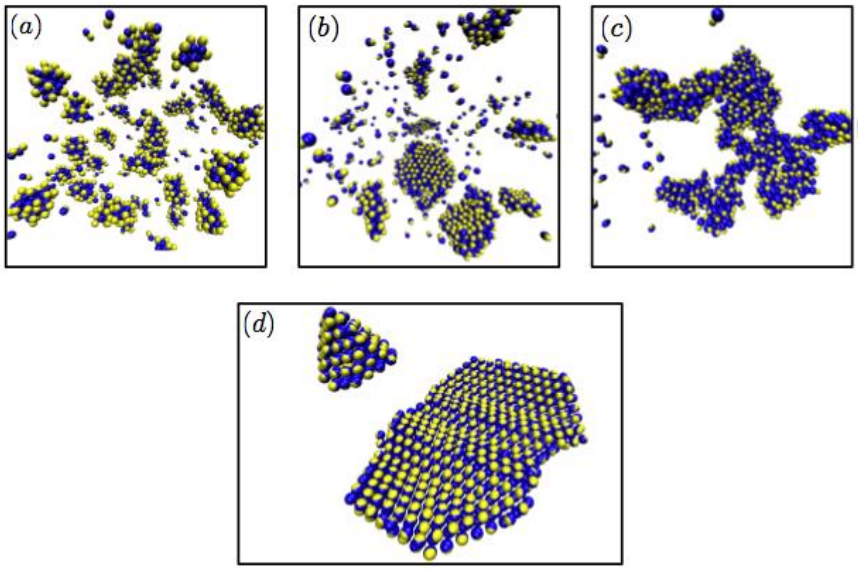

Figure I.8. Various configurations for assembled peanut-shaped amphiphilic nanoparticles of variable particle geometry. (a) Micelles of various morphologies; (b) coexisting bilayers and micelles, (c) disordered wormlike

micelle, and (d) coexisting polygon and bilayer. This Figure is reproduced from Figure 6 in reference.[48]

I.1.3. Secondary molecular interactions

Beyond electrostatic and hydrophobic forces, the heterocoagulation process could be controlled by secondary molecular interactions. We will briefly highlight with some examples hydrogen bonding, π-π interactions, and specific molecular interactions obtained from complementary DNA strands, and biotin-avidin complexation.

I.1.3.1. Hydrogen bonding

Hydrogen bonding is one of the most common interactions, which can aid the assembly process of colloidal particles. Hydrogen bonding is an attractive interaction of a hydrogen atom with an electronegative atom (typically oxygen, nitrogen, or fluor) and strength-wise typically lies in between van der Waals, and ionic attraction. We restrict ourselves by mentioning some typical examples.

Armes and coworkers studied the preparation of polypyrrole particles in the presence of silica sols.[49,50] Hydrogen bonding between the silica surface and the polypyrrole particles, next to electrostatic and hydrophobic interactions, led to raspberry shaped nanocomposite colloids.

Yang and coworkers[51] assembled particles of poly(ethylene glycol dimethacrylate-co-acrylic acid) (poly(EGDMA-co-AA)) onto larger poly(ethylene glycol dimethacrylate-co-4-vinylpyridine) (poly(EGDMA-co-

VPy)) microspheres to form a core−corona structure with a raspberry-like polymer composite by a hydrogen interaction mechanism through an affinity complex between the carboxylic acid group and pyridine group.

Li et al[52] prepared monodisperse microspheres by distillation precipitation polymerization of divinylbenzene (DVB) and N-isopropylacrylamide (NIPAM) with 2.2 – azobisisobutynotrile (AIBN) as initiator in acetonitrile in the absence of any surfactant. Subsquently latex particles of poly(ethyleneglycoldimethacrylate-*co*-acrylic acid) were assembled onto the microspheres affording a core-corona composite polymer particle with a raspberry-like morphology, strengthened by hydrogen-bonding interaction.

I.1.3.2. π-π Interactions

Li and coworkers[53] described the formation of supracolloidal balls with a mean diameter of 148±5 nm by self-assembly of Fe_3O_4 nanoparticles (6.0±1.3 nm) which were functionalized with 2-carboxyterthiophene (TTP-COOH). The driving force behind self-assembly in DMF was shown to be π-π stacking of the thiophene units (See **Figure I.9**)

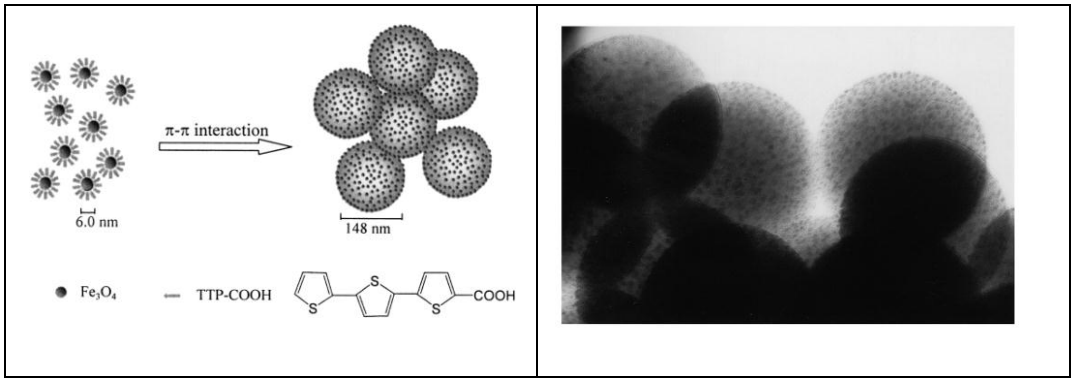

Figure I.9. Structure model proposed for the self-assembly process of individual nanoparticles to form microspheres through π-π interactions. The

sizes of individual nanoparticles and microspheres can be determined directly by TEM. Figure reproduced from Figs 2 and 3 from reference [53]

I.1.3.3. Specific recognition of complementary DNA-strands

An interesting approach using specific multiple hydrogen-bond recognition is to functionalize nanoparticles with DNA-based oligonucleotides. Mirkin and coworkers[54] functionalized two batches of Au colloids of 13-nm diameter dispersed in water with separate non-complimentary oligonucleotides, that is 3'-thiol-TTTGCTGA and 3'-thiol-TACCGTTG. Combination of the two separate functionalized gold nanoparticles led to a stable colloidal sol, the grafted oligonucleotides providing steric stabilization thereby improving the stability of the sol upon increasing temperature and or electrolyte concentration. Upon addition of a duplex consisting of 5'-ATGGCAACTATACGCGCTAG and 3'-ATATGCGCGATCTCAGCAAA, containing 8-base-pair sticky ends, complementary to the gold sols, aggregation of the gold nanoparticles was achieved.

Valignat [55] demonstrated that this powerful assembly method could be used to lock reversibly directed assembled (with optical tweezers) microspheres grafted with complementary polymer brushes into a prearranged suprastructure.

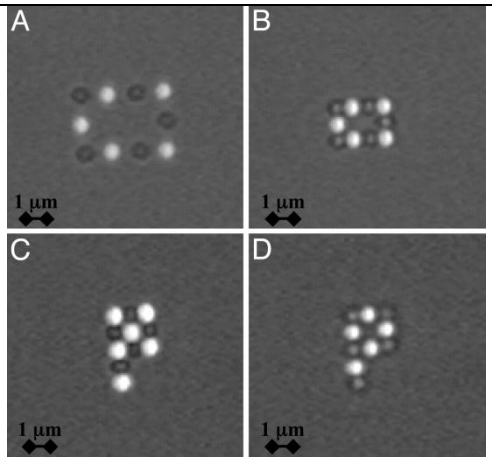

Figure I.10. Directed assembly of particles. Fluorescent and nonfluorescent particles bear complementary strands of DNA. (A) Particles are first captured in discrete time-shared traps induced by laser tweezers. (B–D) Particles are moved in contact to promote hybridization between the DNA strands and form the following rigid structures: a rectangle (B), a "full" P (C), and an "empty" P (D). This figure is reproduced from Figure 4 in reference [55].

I.1.3.4. Avidin-biotin recognition

There are alternatives to complementary DNA-strand recognition, for example the strong interaction between avidin (or its related streptavidin) and biotin. Avidin is a tetrametric glycoprotein which has the ability to interact strongly with up to four biotin units. Biotin, also known as vitamin H or B7 is a soluble B complex of ureido(tetrahydroimidizalone) ring fused with a tetrahydrothiophene ring. The interaction between avidin-biotin is widely explored. An interesting example related to heterocoagulation of small poly(styrene) particles on larger silica microspheres was reported by Fleming

and coworkers.[56] Amine-functionalized silica microspheres of 5 μm-diameter were either treated with biotin sulfosuccinimdyl ester, or reacted with avidin after activation of the silica spheres with gluteraldehyde. Biotin labeled poly(styrene) particles of *ca.* 200 nm in diameter were made in a similar manner. However, avidin labeled poly(styrene) particles were obtained by treatment of the biotin-labeled ones with excess amounts of avidin. Upon mixing the complementary colloids strong adhesion of the poly(styrene) particles onto the surface of the silica spheres was observed. From earlier work by Chern[57] it should be noted that the interaction between avidin is not able to induce flocculation of biotin labeled particles, as its size, approximately 4 nm, is not large enough to bridge the overlapping double layers of the particles. The armored structure obtained by Fleming [56] therefore is strengthened by the biotin-avidin interaction, though the heterocoagulation process itself is not induced by this.

I.2. Assembly of nanoparticles onto prefabricated larger particles via repetitive heterocoagulation: the Layer-by-Layer technique

The layer-by-layer (LbL) technique for the assembly of nanoparticles onto a substrate can be seen as a repetitive extension of heterocoagulation. Driving forces for adhesion can be based on the same interactions, that is electrostatics, hydrophobic, and secondary molecular interactions. For example in the case of LbL assembly driven by eletrostatic interactions alternating layers of positive

and negatively charged particles and/or (macro)molecules are deposited sequentially onto the underlying substrate, the latter obviously also undergoing surface charge-inversion in alternating fashion.[58] Hydrogen-bonding as a driving force to LbL self-assembly was investigated by Rubner *et al*.[59] and Zhang *et al.*,[60,61] The LbL technique based on biotin-avidin recognition was described by Osa[62] and Hoshi.[63]

The excess amount of material used is removed in between steps. The LbL technique is easy to carry out and very versatile. Due to a great range of polyelectrolytes, biopolymers (proteins and nucleic acids), lipids and inorganic particles have been used as building blocks in the preparation of multilayer composite films[64,65], and in the fabrication of micro- and nanometer-sized capsules, the latter introduced in 1998 by Donath and Caruso.[66-68]

Caruso *et al.*,[69] reported the preparation of negatively charged poly(styrene) latex particles (640 nm-diameter) armored with a nanocomposite multilayer of SiO_2 nanoparticles (Ludox TM-40; 26±4 nm-diameter) and poly(diallyldimethyl-ammonium chloride (PDADMAC). These two components were sequentially adsorbed onto the surface of the poly(styrene) latex spheres (see **Figure I.11**), after adsorption of a precursor polyelectrolyte multilayer film of (PDADMAC/poly(4-sodium styrenesulfonate)/PDADMAC) which provided a uniformly charged surface and facilitated subsequent SiO_2 nanoparticle adsorption. The process was driven by electrostatic interactions. With electrophoteric mobility (EPM) measurements, reversal of the ζ-potential after each deposition step was shown. Single-particle light scattering (SPLS) measurments showed the linear increase of the particle dimensions upon

increasing SiO_2/PDADMAC multilayer number. Electron microscopy showed the evidence of a stepwise multilayer growth, with TEM data yielding an average diameter increment of *ca.* 65 nm corresponding to a layer thickness of approximately 32 ± 5 nm for each SiO_2/PDADMAC layer pair. A similar approach was undertaken using nanoparticles of Fe_3O_4 (diameter 10-15 nm). [69]

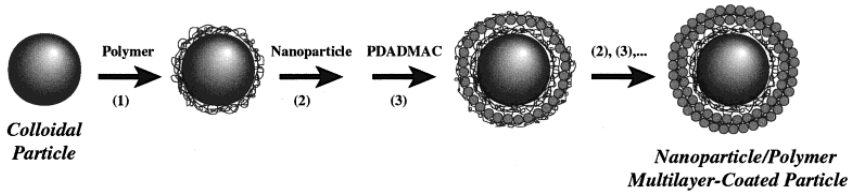

Figure I.11. The first stage involves the formation of a three-layer polyelectrolyte multilayer film (PDADMAC/PSS/PDADMAC), formed by the sequential adsorption of PDADMAC and PSS under conditions where they are oppositely charged (step 1). The outermost layer, PDADMAC, positively charged, aids the subsequent adsorption of negatively charged SiO2 nanoparticles. SiO_2/PDADMAC multilayer shells on the PS latices are then formed by the sequential adsorption of SiO_2 (step 2) and PDADMAC (step 3). Additional SiO_2 and PDADMAC cycles result in further growth of the multilayer shell thickness on the PS latices. The excess/unadsorbed polyelectrolyte and nanoparticles are removed by a series of centrifugation/water wash/redispersion cycles before additional layers are deposited. Figure and legend taken from reference.[69]

I.3. Assembly of nanoparticles onto emulsion monomer droplets and their subsequent polymerization

In the previous section we have seen that "hard" inorganic nanoparticles can adhere onto the surface of polymer latex particles via a stochastic process of collisions, which was referred to as heterocoagulation. Once deposited onto the surface of the latex particles the strength of adhesion governed by attractive forces such as eletrostatic attraction, the hydrophobic effect, and hydrogen bond interactions, needs to exceed repulsive forces, and the entropy gain achieved when nanoparticles detach. This potential detachment of nanoparticles from the surface of the polymer latex particle is typically induced by the thermal energy of the system, k_BT.

What now happens if we replace the polymer latex particle with a monomer droplet onto which we first assemble the "hard" nanoparticles and in a subsequent step polymerize the now armored droplet?

I.3.1. Pickering stabilization: Adhesion of particles to "soft" interfaces

The phenomenon that solid particles adhere onto an emulsion droplet, that is a liquid-liquid interface, was first observed and reported by Ramsden[70] and Pickering[71] in the 1900s. They found that these emulsion droplets were stable against coalescence, as the adhered solid particles effectively provided a barrier. Emulsions stabilized by adhered solid particles were coined Pickering emulsions.[72,73] Hildebrand *et al.* [74]suggested that the reason the particles place themselves in the liquid-liquid interface is that they partially wet the two liquid

phases. In line with the Bancroft rule for emulsification, which links whether a water-in-oil emulsion or *visa versa* is preferred for a certain type of emulsifying agent, they suggest that the type of emulsion produced by a solid powder is determined by the contact angle between the solid and the liquid-liquid interface. "In order for the powder to remain in the interface the angle must be finite, and unless the angle is 90°, the interface will be on one side or the other of the points of contact of the particles, and its tension will cause the film to be concave on that side."

The observations by Ramsden and Pickering that emulsion droplets armored with solid particles were "stable" against coalescence led to believe that the particles are in essence trapped, and cannot leave the interface to re-enter one of the two liquid phases.

I.3.1.1. The interaction of a single spherical particle with a "soft" interface

Pieranski[75] developed a simple macroscopic model to calculate the free energy as a function of the position of a spherical particle with respect to the "soft" liquid-liquid (or as was the case in his manuscript, a liquid-air interface).

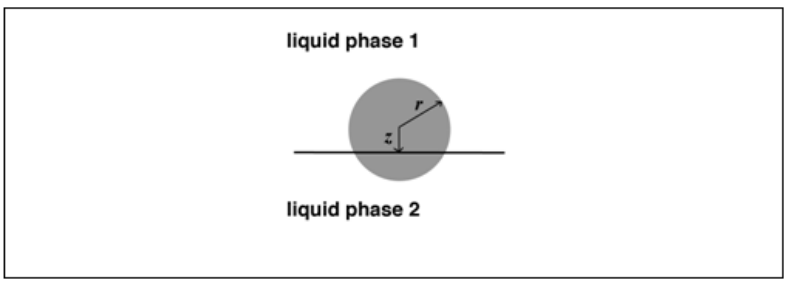

In this macroscopic continuous model three interfacial energy contributions can be derived as the product of the interfacial tension and the respective contact areas:

$$\begin{aligned} E_{p1} &= \gamma_{p1} 2\pi r^2 \left(1 + \frac{z}{r}\right) \\ E_{p2} &= \gamma_{p2} 2\pi r^2 \left(1 - \frac{z}{r}\right) \\ E_{12} &= -\gamma_{12} \pi r^2 \left(1 - \left(\frac{z}{r}\right)^2\right) \end{aligned}$$

Equation I-2

In which γ_{p1}, γ_{p2}, and γ_{12} are the interfacial tensions between the particle and liquid phase 1, the particle and liquid phase 2, the two liquid interfaces. When we define the following dimensionless numbers:

$$z_0 = \frac{z}{r}; \quad \sigma_1 = \frac{\gamma_{p1}}{\gamma_{12}}; \quad \sigma_2 = \frac{\gamma_{p2}}{\gamma_{12}}; \quad E_0 = \frac{E_{p1} + E_{p2} + E_{12}}{k_B T}$$

we find for the relative free energy E_0:

$$E_0 = \left[\frac{\gamma_{12}\pi r^2}{k_B T}\right]\left(z_0^2 + 2(\sigma_1 - \sigma_2)z_0 + 2\sigma_1 + 2\sigma_2 - 1\right)$$

Equation I-3

The equilibrium position for the particle can easily be found from:

$$\begin{aligned} \frac{dE_0}{dz_0} &= 2z_0 + 2(\sigma_1 - \sigma_2) = 0 \\ z_0^{\min} &= \sigma_2 - \sigma_1 \end{aligned}$$

Equation I-4

For values of $z_0^{\min}$ between -1 and 1 the particle adheres to the liquid-liquid interface. The energy it will take to remove the particle from the interface into either the bulk of phase 1 or phase 2 can easily be obtained from:

$$\begin{aligned} \Delta E_1 &= \mathrm{E}_0(z_0 = 1) - \mathrm{E}_0(z_0^{\min}) \\ \Delta E_2 &= \mathrm{E}_0(z_0 = -1) - \mathrm{E}_0(z_0^{\min}) \end{aligned}$$

Equation I-5

Whereas this model gives a good feel for the order of magnitude of the energy well in which the particles are trapped, it is rather crude and thus a simplification of reality. It does ignore surface charges (chemical heterogeneity of the surface, or "patchyness") and potential morphological surface roughness of the spherical particle, and as previously mentioned it assumes absence of external fields (such as gravity), or flow. A problem also ignored is the three-phase interaction at the contact line between the two liquids and the particle. Gibbs suggested qualitatively that this three-phase contact line should be treated as a one-dimensional "line tension", in analogy with the two-dimensional surface tension between the interphase of two bulk phases. An expression for the free energy as a function of particle-interface separation for a spherical particle

or radius *R*, extended to account for line tension (τ), was given by Aveyard and Clint[76] in which they basically added one extra term to the Pieranski equation:

$$E_0 = \left[\frac{\gamma_{12}\pi r^2}{k_B T}\right]\left(z_0^2 + 2(\sigma_1 - \sigma_2)z_0 + 2\sigma_1 + 2\sigma_2 - 1\right) + \frac{2\pi r\tau}{k_B T}\sqrt{\left(1 - z_0^2\right)}$$

Equation I-6

As can be seen from this expression the effect of line tension becomes increasingly important for smaller spherical particles as it scales linear with the radius of the particle, whereas contributions arising from interfacial tensions scale quadratically. A debate on experimental realistic values of line-tension is ongoing, especially when the spherical particles become of nanoscale dimensions and line tension may become important.

One key question that remains is what is the validity of these macroscopic models when we scale the size of our spherical particle down to nanoscale dimensions? The liquid-liquid interface can no longer be modeled as flat (capillary waves need to be considered), and additional small-scale effects, such as discrete rather than continuous wetting of the spherical nanoparticle by the liquid molecules, need to be taken into account. Can this be reflected in line tension?

Cheung and Bon[77] investigated the behavior of a non-charged nanoparticle in proximity and adhered to an ideal liquid-liquid interface, using molecular simulations. In the model a two-component Widom-Rowlinson (WR) fluid[78] was used to generate the two phase-separated bulk liquids and the corresponding

soft interface, hereby neglecting eletrostatic and attractive van der Waals forces. Calculated free energy profiles as function of the distance of the nanoparticle from the soft liquid-liquid interface confirmed that macroscopic models, such as the Pieranski model,[75] gave a poor description or the energy well. The energy well was considerably wider, and thus the distance of interaction greater between the particle and the interface. The reason for this is most likely due to the existence of capillary waves (the liquid-liquid interface can no longer be considered flat). Moreover, the smaller the nanoparticle was, the larger the underestimation of the depth of the energy well by the Pieranski model was, with deviations of up to 50%. The binding energy was found to increase quadratically with the radius of the nanoparticle, with an additional linear dependency (which could plausibly be seen as line tension). The overall good news from these simulations is that nanoparticles adhere considerably stronger to, and are trapped over a longer range by, the liquid-liquid interface than predicted by macroscopic models.

A question often asked is; do the parabolic energy wells as predicted by Pieranski do not have an activation barrier that prevents the particle from "falling" in spontaneously? One can argue that, especially for a large spherical particle, upon its approach to the soft interface, the interface needs to deform and liquid has to drain. This event adds an activation barrier that needs to be overcome for the particle not to bounce off the interface, and clearly the interfacial tension between the two soft bulk phases (liquid-liquid, or liquid-air), and the viscosity of both phases play a key role. Note that a potential hydrophobic effect[29] can counter-balance such a barrier, as the dewetting of the

liquid in between a hydrophobic particle and the hydrophobic liquid phase or air, stimulates long range attraction and eases the adhesion process.

Obviously one also should take into account the shape of the particle, as often the particles used will differ from spheres. This clearly can have dramatic effects on where and how the particle adheres to the interface when it tries to minimize energy from interfacial as well as line tensions. The three point contact angle needs to be constant, which means that the contact line has to undergo curvature in order to accommodate this. This has pronounced influences on interaction (of a long range nature) between adhered particles on the surface. An in depth discussion lies outside the scope of this review, but the interested reader is referred to (as a starting point) work by Vermant and coworkers.[79,80]

I.3.1.2. Droplets armored with a layer of adhered particles

The above discussion only considers the existence of a single isolated particle onto a liquid-liquid interface. Experimentally, however, the number of nanoparticles adhered to a single monomer droplet or growing polymer particle will be greater than unity. This means that particle-particle interactions, both attractive and/or repulsive in nature need to be taken into account. An elegant example confirming the existence of attractive particle-particle interactions can be found in work reported by Russell and coworkers.[81] They prepared a dispersion of 2.8 nm (diameter) tri-*n*-octylphosphine (TOPO)-covered cadmium selenide (CdSe) nanoparticles in toluene. Upon introduction of a water droplet

the nanoparticles organized themselves onto the toluene-water interface. Introduction of 4.6 nm (diameter) CdSe nanoparticles let to displacement of the smaller ones from the liquid-liquid interface. A clear phase-separation was seen on the surface of the waterdroplet, showing distinct regions of the 2.8 nm and 4.6 nm CdSe nanoparticles respectively.

When particles of a narrow particle size distribution (monodisperse) adhere to the interface of a spherical droplet, 2D crystallization can occur. As a direct result of the curved surface of the droplet, packing into infinite hexagonal 2D arrays is no longer possible. The determination of the packing geometry is often referred to as the Thomson problem,[82] generalized by Tammes. In short, 12 defects either in the form of point dislocations, or grain boundary scars (the latter for large droplets which have a great number of particles on the surface). Bausch *et al.*[83,84]showed that for large droplets onto which thousands of microspheres were assembled, this rule of 12 defects prevailed in the form of five- and seven-neighbor line defects, or grain boundary scars. Bon and coworkers[85] studied a system of intermediate size (tens to hundreds of particles on a sphere), that is the packing patterns of silica nanoparticles on poly(styrene) latex particles made via Pickering miniemulsion polymerization[86,87] were investigated. The found an excellent correlation between the experimental morphology and the nearest-neighbour distribution using metropolis Monte Carlo simulations, using a 12-24 LJ potential. Moreover, they addressed the effect of polydispersity of the nanoparticles used in preparing the armored droplets. They found that upon broadening of the particle size distribution, the

packing geometry no longer can be described in terms of 12-point dislocations, or grain boundary scars.[85]

I.3.2. Polymerization of emulsion droplets armored with inorganic nanoparticles: Pickering suspension and miniemulsion polymerization

We have seen from the above discussion that solid particles can adhere to a "soft" interface, and thus to monomer droplets. The effect of Pickering stabilization protects the droplets from coalescence. The use of solid particles as stabilizers in emulsion-based polymerization techniques was first described in open literature by Hohenstein[88,89] for suspension polymerizations in the 1940s. Winslow and Martreyek[90] investigated the influence of both solid inorganic particles such as bentonite and $Ca_3(PO)_4$ and organic stabilizers on the suspension polymerization of mixtures of divinylbenzene with ethylvinylbenzene. Wiley,[91] in 1954, showed that monomer droplets of styrene dispersed in water in presence of Dowex 50 ion exchange resin beads or bentonite clay led to adhesion of the solid particles onto the surface of the droplets. The Pickering stabilized droplets underwent so-called limited coalescence, a process which after a certain time period effectively yielded a stable set of solids-armored liquid droplets. Pickering stabilization could be promoted upon addition of, for example, gelatin, and/or inorganic salts. Assuming monolayer adsorption of the colloid onto the surface of the monomer liquid droplets he was able to predict the average droplet size, by assuming cubic (square) packing of spherical solid particles onto a spherical monomer

droplet. This yielded the following equation, after a slight addition from Bon *et al.* to account for coverage:

$$R_{mon} = C\,\pi\left(\frac{m_{mon}}{m_{part}}\right)\left(\frac{\rho_{part}}{\rho_{mon}}\right) R_{part}$$

Equation I-7

in which R_{mon} is the radius of the monomer droplet, R_{part} the radius of the spherical Pickering stabilizer, C accounts for coverage (for full monolayer coverage following 2D square, or cubic, packing C = 1), and m and ρ stand for the masses and densities.

In suspension polymerization inorganic solids, such as hydroxyapetite [3 $Ca_3(PO_4)_2 \bullet Ca(OH)_2$], are often used in conjuction with (polymeric) surfactants. Deslandes[92] reported in 1987 a study in which he investigated the morphology of the beads obtained in the suspension copolymerization of styrene and butadiene. A thin layer composed of very uniformly distributed hydroxyapetite particles was adhered to the surface of the polymer bead, and surrounded with a thicker and flakier layer of loosely packed agglomerates of hydroxyapetite and small polymer beads which were also covered by a monolayer of inorganic matter. Despite this paper, the focus on the use of solid particles in suspension polymerization remained their effective use as stabilizers.

A shift of interest in the area of Pickering suspension polymerization towards the morphologies of the polymerized emulsion droplets was reported by Bon and coworkers.[93-96] They demonstrated that microgels of poly(methyl methacrylate-*co*-divinylbenzene) could be used to stabilize emulsion droplets composed of various monomers, that is styrene, divinylbenzene, and *n*-

butylacrylate.[93] A substantial amount of hexadecane was added as a porogen. Upon Pickering suspension polymerization the *in situ* generated polymer phase separated towards the interface and formed an interpenetrating network with the microgel particles. A variety of microcapsules with a raspberry-type morphology were synthesized. They showed the fabrication of TiO_2 nanoparticle (ca. 150 nm in diameter) armored microspheres and capsules made via Pickering suspension polymerization of styrene and divinylbenzene, for the capsules hexadecane was used as a non-solvent for the polymer.[95] Upon polymerization the polymer phase-separated at the interface of the droplet. The average size of the capsules could be varied by altering the amount of TiO_2 nanoparticles. The polymer wall thickness could be controlled by variation of the monomer to hexadecane ratio. They also reported on the fabrication of complex silica-based microcapsules via a two-stage templating route,[97] in which nanocomposite poly(styrene) latex particles armored with Laponite clay discs (made via Pickering miniemulsion polymerization) were used as Pickering stabilizers of emulsion droplets which contained poly(diethoxysilane) and oil. Upon hydrolysis and sol-gel reaction of the poly(diethoxysilane) hollow capsules were obtained. The organic components could be removed via an additional calcination step. The capsule walls could be decorated on either the outside or inside with nanocapsules composed of Laponite clay.

A variety of other nanoparticles have been used in Pickering suspension polymerizations, including magnetic Fe_3O_4,[98] [99] [100] and CdS nanoparticles stabilized by poly(ethylene glycol-*block*-styrene-*block*-2-(dimethylamino) ethyl methacrylate).[101]

Wu and coworkers[102] reported on the inverse Pickering suspension polymerization of poly(*N*-isopropylacrylamide). They used various sizes of silica particles, ranging from 53nm to 962 nm in diameter as solids stabilizer. Suspension polymerizations were successful for the silica particles of diameter <500 nm. Similar work was reported by Wang and coworkers.[103]

Bon, Kumacheva and coworkers[104] demonstrated that monodisperse solids stabilized droplets could be generated in microfluidic flow focusing device, whereby the solid particles were initially present in the dispersed phase. Polymerization of the monomer droplets led to hybrid polymer microspheres. They also showed that non-spherical particles could be obtained by geometric confinement of the droplets in the channel.[104 105]

A logical extension from Pickering suspension polymerization would be to miniaturize the size of the droplets into the regime of miniemulsion polymerization. Landfester and coworkers[106] described miniemulsion copolymerizations of styrene with 4-vinylpyridine in the presence of Ludox TMA silica nanoparticles. The use of 4-vinylpyridine was required to warrant the fabrication of armored latex particles. Bon and coworkers[87] described the Pickering miniemulsion polymerization of styrene using Laponite RD clay discs as a solids stabilizer in the absence of any auxiliary comonomer or surfactant. In a detailed mechanistic study[86] they described that this Pickering miniemulsion polymerization using Laponite clay discs (*ca.* 25 nm in diameter and 1 nm in height) was successful and yielded armored polymer latexes for a variety of hydrophobic monomers, including styrene, laurylmethacrylate, butylmethacrylate, octylacrylate, and 2 ethylhexylacrylate. Studying the

polymerization rates they found a pronounced retardation effect up to intermediate conversion, more prominent for smaller particles. A model was presented that allowed for prediction of the average particle sizes of the latexes produced as function of the amounts of monomer and clay discs used. A linear relationship between the number of clay discs used and the total surface area of the latex particles was shown. Key herein was that the sonication process to prepare the armored miniemulsion droplets warranted reversible adhesion of the Laponite clay discs throughout the emulsification step. Bon and coworkers[85] also performed Pickering miniemulsion polymerizations of styrene using spherical silica nanoparticles of approximately 25 nm in diameter (Ludox TM-40), in which the packing arrangements of the silica nanoparticles on the surface were investigated and modeled with the aid of Monte Carlo simulations. Zhang and coworkers used organically modified silica nanoparticles to carry out a Pickering miniemulsion polymerization of styrene. [107] The co-use of sodium dodecyl sulfate (SDS) and 2-(methacryloyl) ethyltrimethylammonium chloride (MTC) as auxiliary monomer was also reported in the Pickering miniemulsion polymerization of styrene stabilized by silica nanoparticles. [108]

Bon, Keddie and coworkers[109] demonstrated that "soft" armored polymer latex made via Pickering miniemulsion polymerization, that is poly(lauryl acrylate) armored with Laponite clay discs, could be used as a nanocomposite additive in standard poly(*n*-butyl acrylate-co-acrylic acid) waterborne pressure-sensitive adhesives (PSAs) leading to marked mechanical property enhancements (see **Figure I.12**). A maximum tack energy enhancement of 45 J m^{-2} was found in nanocomposite PSAs containing 2.7 wt% hybrid particles, which was about 70% greater than found for the PBA adhesive alone. In

comparison, the tack energy for nanocomposites containing an equivalent amount of non-armored PLA, Laponite clay discs, or both did not lead to increases of the same magnitude, therefore showing a synergistic effect as a direct result of the supracolloidal armored structure of the clay poly(lauryl acrylate) additive.

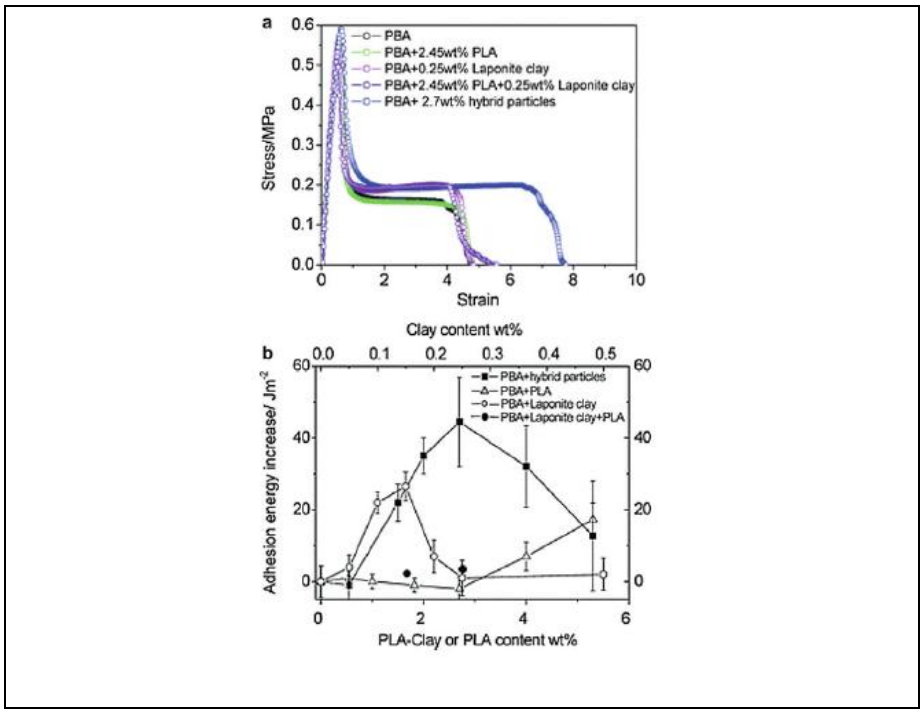

Figure I.12. (A) A comparison of the probe-tack stress–strain curves for the model PBA adhesive with the presence of 2.7 wt% clay-armored soft–hardhybrid particles with the equivalent amount of non-armored PLA (2.45 wt%), Laponite clay discs (0.25 wt%), and a blend of non-armored PLA (2.45 wt%) and Laponite clay (0.25 wt%). (B) An illustration of the synergistic effect of PLA–nanoclay hybrid particles on the tack energy of the model PSA. The increase in the tack energy above PBA is compared as a function of the nanofiller content. Figure and Legend are taken from reference.[109]

Voorn and coworkers demonstrated the inverse Pickering miniemulsion polymerization of aqueous acrylamide and 2-hydroxyethyl methacrylate in cyclohexane using hydrophobically modified montmorillonite platelets (cloisite 20A) as solids stabilizer.[110]

I.4. Assembly of nanoparticles onto the surface of polymer colloids throughout emulsion polymerization: Solids-stabilized, or Pickering, emulsion polymerization

The use of a high-energy homogenization step required to prepare the sub-micronsized monomer droplets for the Pickering miniemulsion process could be a drawback for industrial scale-up. The equivalent emulsion polymerization process in which solid nanoparticles would be used as solids stabilizer would bring great outcome.

Müller and coworkers prepared disc-like polymer Janus particles from assembled films of poly(styrene)-*block*-poly(butadiene)-*block*-poly(methyl methacrylate) triblock copolymer (SBM), and after hydrolysis of the ester groupgs into methacrylic acid units, used these as Pickering stabilizer in the soap-free emulsion polymerization of styrene and *n*-butyl acrylate. [111] Armes and coworkers described the synthesis of poly(methyl methacrylate)-silica nanocomposite particles in aqueous alcoholic media using silica nanoparticles as stabilizer,[112] extending this method to operate in water with a glycerol-modified silica sol.[113] [114] Sacanna showed that methacryloxypropyltrimethoxysilane,[115] in the presence of nanosized silica led to spontaneous emulsification in water,

which upon a two-step polymerization procedure afforded armored particles with an outer shell of poly(methyl methacrylate).[116] Bon and coworkers demonstrated the preparation of armored hybrid polymer latex particles via emulsion polymerization of methyl methacrylate and ethyl methacrylate stabilized by unmodified silica nanoparticles (Ludox TM-40).[117] Performance of an additional conventional seeded emulsion polymerization step provided a straightforward route to more complex multilayered nanocomposite polymer colloids. (See **Figure I.13**)

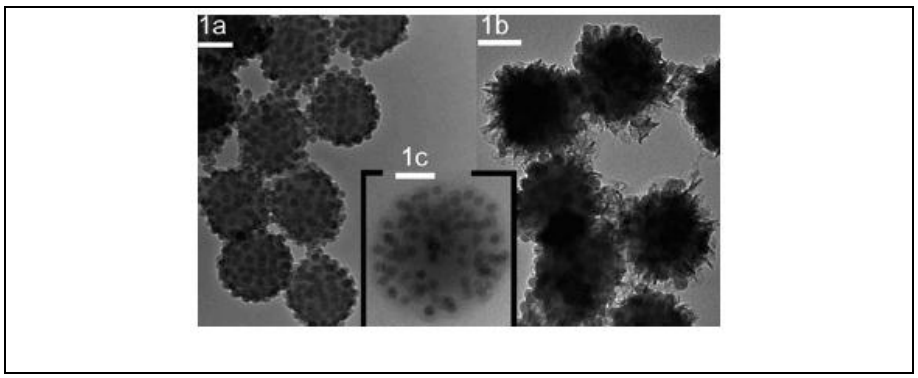

Figure I.13. TEM images (scale bar = 100 nm) of (a) poly(methyl methacrylate) latex armored with silica nanoparticles obtained by Pickering emulsion polymerization. Multilayered nanocomposite polymer colloids with (b) a "hairy" outer-layer of poly(acrylonitrile) and (c) a soft shell of poly(*n*-butyl acrylate). Figure and reference were reproduced from ref. [117]

The use of either styrene or butyl methacrylate as monomer led to stable latexes that were not covered by silica particles. They proposed a mechanism for the solids-stabilized, or Pickering, miniemulsion polymerization effectively combining coagulative nucleation with heterocoagulation throughout the polymerization process, in which effectively growing latex particles become unstable and collide irreversibly with the nanoparticles which are dispersed in

the waterphase. The key to successful polymerization is that this collision process is fast with respect to the timescales of particle nucleation and growth.

Wu studied the silica nanoparticle-stabilized emulsion polymerization of vinyl acetate, with the aid of a small amount of anionic reactive surfactant, 3-allyloxy-2-hydroxy-1-propanesulfonic acid sodium salt (HAPS). They argued that hydrogen bond interactions allowed for strong adhesion and also commented on the mechanism of solids-stabilized emulsion polymerization.

Bon and coworkers carried out a study on the fate of the nanoparticles throughout solids-stabilized emulsion polymerization. [118] A quantitative method based on disk centrifugation was developed to monitor the amount of nanoparticles present in the waterphase in solids stabilized emulsion polymerizations of vinyl acetate, methyl methacrylate and *n*-butyl acrylate. The concentration profile of nanoparticles in the waterphase as function of monomer conversion agreed with theoretical models developed for the packing densities in these systems. [119] Noteworthy was that in the case of silica nanoparticle-stabilized emulsion polymerization of vinyl acetate the event of late stage limited coalescence, leading to small armored nonspherical clusters could be predicted and explained on the basis of the concentration profiles and particle size measurements. Adjusting the amount of silica nanoparticles prevented this phenomenon.

Ma and Dai[120] reported the synthesis of silica nanoparticle (10-15 nm in diameter, PA-ST silica sol, Nissan Chemicals) armored poly(styrene) latexes made via solids-stabilized emulsion polymerization. They used VA-086 (2,2′-azobis(2-methyl-N-(2-hydroxyethyl)propionamide)) as nonionic initiator. Whereas Bon and coworkers[117] found that Pickering emulsion polymerization of

styrene using Ludox TM-40 and a low flux of radicals generated from potassium persulfate did not result in an armored latex, most likely the hydroxyethyl groups enhance the wettability of the surface of the latex particles to promote silica adhesion. This was confirmed by a study undertaken by Bourgeat-Lami,[121] who showed that poly(ethylene glycol) monomethylether methacrylate (PEGMA) macromonomer aided the adhesion of silica nanoparticles in the surfactant free solids-stabilized emulsion polymerization of styrene. They also noticed a reduced overall rate of polymerization due to the presence of the nanoparticles on the surface of the growing latex particles, which was earlier observed by Bon and Colver[122] in Pickering miniemulsion polymerizations. Similar results of reduced polymerization rates were reported by Zhang and coworkers who studied the silica nanoparticle stabilized emulsion polymerization of methyl methacrylate in presence of hydroxyethyl methacrylate. [123] Song and coworkers performed photocatalytic emulsion copolymerizations of styrene and ethyleneglycoldimethacrylate with auxiliary monomers acrylic acid or sodium styrene sulfonate, and in presence of a cationic titania hydrosol. They found that the auxiliary monomers greatly promoted adhesion of the titania nanoparticles onto the polymer latexes. [124,125]

I.5. Hybrid polymer colloids through assembly of colloidal building blocks through interface-driven templating

Mixtures of polymer latexes and inorganic colloids can be assembled into supracolloidal clusters with control spatial organization of the particles via geometric or interfacial energy driven confinement.

Pine and coworkers [126] confined particles to the interface of emulsion droplets, after which the fluid was evaporated, leading to specific packing arrangement dependent on the original number of spheres per liquid droplet (see **Figure I.14**). Clusters of colloidal spheres included, doublets, triangles, tetrahedral and more exotic polyhedra. This was extended using various combinations of two different colloids with several size ratios in water-in-oil emulsions: monodisperse silica or poly(styrene) microspheres for larger particles and silica or titania nanoparticles for smaller particles. Not only the size but also the adhesion behavior of the individual colloids into the water-oil interface played an important role. Packing predictions were carried out with Surface Evolver and corresponded to the experimentally observed structures. [127] A third paper addressed formation of composite colloids in toluene-in-water emulsions in which poly(styrene) was added as macromolecular glue. [128]

Lee and Weitz showed that confinement of particles in the middle phase of double emulsion droplets and subsequent evaporation of this phase led to nanoparticle supracolloidal capsules, [129] also referred to as colloidosomes.[130]Velegol used a so-called particle lithography technique in which colloids were deposited on a flat solid surface after which on the exposed areas heterocoagulation of macromolecules and or particles could take place.[131-134] Via this route anisotropic assemblies of colloids can be manufactured.

Xia and coworkers demonstrated the assembly of colloids into well defined clusters by dewetting of aqueous dispersions of monodisperse particles across surfaces patterned with two-dimensional arrays of templates or relief structures.[135]

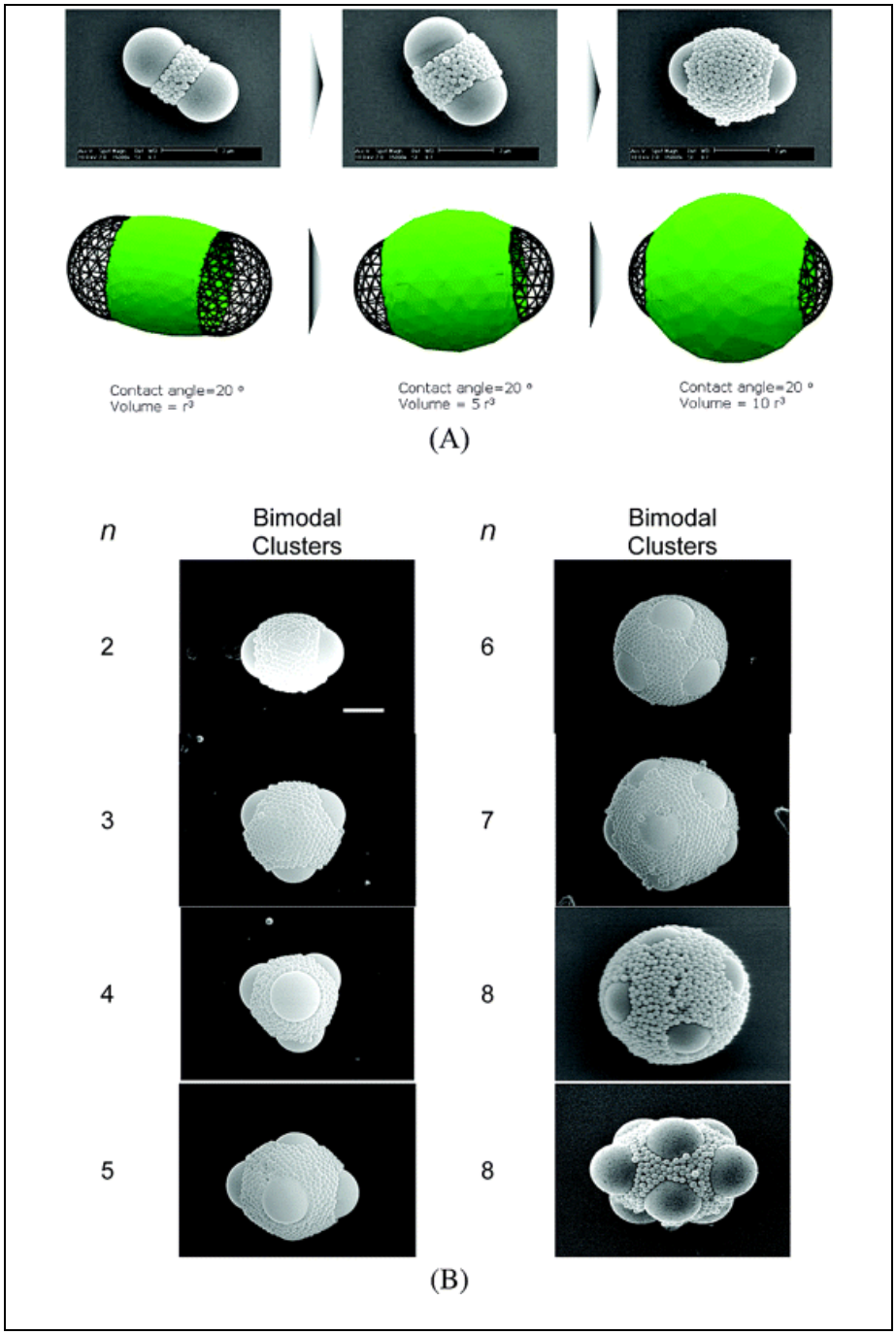

Figure I.14. Top: SEM images for the structural evolution of bimodal colloidal clusters of silica microspheres and nanospheres for n = 2. Bottom: Surface Evolver simulated structural evolution for n = 2 as a function of the amount of silica nanospheres. (B) SEM images of silica−silica composite clusters for n = 2−8. Scale bar is 2 μm. The size ratio of large and small silica

particles was fixed at 10. Figure and legend are a reproduction of Fig. 3 from ref. [127]

I.6. Outlook of the thesis

It is demonstrated above that there are a vast array of physical methods that can make use of in the design of nanocomposite polymer colloids. The classical approach of heterocoagulation can undergo a renaissance by exploring driving forces such as the hydrophobic effect and secondary molecular interactions. Self-assembly of complex anisotropic colloidal particles is already creating a whole new direction in the fabrication of supracolloidal structures.

The behavior of nanoparticles at soft interfaces and their ability to adhere to these strongly has great potential to be studied further, especially in the area of solids-stabilized emulsion polymerization. The ability to control and understand mechanistically this process will allow for design of innovative hydrid polymer colloids.

In this industrial project, sponsored by BASF (Ludwigshafen, Germany), the goal is to investigate and design innovative polymer colloids using nanoparticles as solid stabilizers then generate polymer films from these colloidal particles and investigate the water and mechanical properties.

I.6.1. A brief overview of each chapter

Chapter II. Pickering emulsion polymerization process in which silica nanoparticles are used as stabilizers for the fabrication of raspberry like particles of vinyl esters and (metha)acrylates are investigated. In addition, we address key

mechanistic features of the polymerization process by monitoring the concentration of nanoparticles in the water phase over monomer conversion.

Chapter III. Pickering emulsion polymerization process using Laponite clay nanodiscs as solid stabilizers are investigated for the fabrication of various hydrophobic (meth)acrylates. In addition, polymerization kinetics and particle size distribution are monitored over monomer conversion in order to better understand the mechanism of particle heterocoagulation. Limitations and drawbacks are also addressed.

Chapter IV. Introduction to film formation is firstly addressed. Then mechanical and thermal properties of polymer films made from poly(styrene-*co*-*n*-butyl acrylate) particles armored with Laponite clay are addressed. Particularly attention is given to the influence of clay dics on the polymer films properties.

Chapter V. In this chapter, the influence of Laponite clay on water uptake and water permeability properties of armored polymer films with a honeycomb structure is investigated. Innovative methods to analyze water properties of polymer films are addressed.

Chapter VI. In this chapter, the synthesis of core-shell particles armored with clay nanodiscs by two steps Pickering emulsion polymerization process is addressed. First, the fabrication of hard core nanoparticles is described. Then, in

a second step, the synthesis of an armored “soft” shell around the “hard” core particles is explained.

Chapter VII. Conclusions and industrial outlook of the project is reported.

I.7. References

(1) Teixeira, R. F A.; Bon, S. A. F., *Adv. Polym Sci*. **2011**; 233, 19-52.

(2) Derjaguin, B. V., *Discuss. Faraday Soc.* **1954**, *18*, 85-98.

(3) Jachowicz, J.; Berthiaume, M. D., *J. Colloid. Inter. Sci.* **1989**, *133*, 118-134.

(4) Derjaguin, B. V.; Landau, L., *Acta Physicochim. USSR* **1941**, *14*, 633-662.

(5) Verwey, E. J. W.; Overbeek, J. T. G., Theory of the Stability of Lyophobic Colloids, *Elsevier Publishing Company Inc* **1948**.

(6) Hamaker, H. C., *Phy. Rev. Lett.* **1937**, *4*, 1058-1072.

(7) J. Visser, J., *Adv. Colloid Inter. Sci* **1972**, *3*, 331-363.

(8) Hogg, R.; Healy, T. W.; Fuerstenau, D. W., *Trans. Faraday Soc.* **1966**, *62*, 1638-1651.

(9) Eytan, B.; Matijevi, E.; Wright, T. H., *J. Chem. Soc., Faraday Trans.* **1985**, *81*, 1819 - 1832.

(10) Bleier, A.; Matijevic, E., *J. Colloid Inter. Sci.* **1976**, *55*, 510-524.

(11) Luckham, P. F.; Vincent, B.; McMahon, J.; Tadros, T. F., *Colloid Surf.* **1983**, *6*, 83-95.

(12) Luckham, P. F.; Vincent, B.; Tadros, T. F., *Colloid Surf.* **1983**, *6*, 101-118.

(13) Luckham, P. F.; Vincent, B.; Tadros, T. F., *Colloid Surf.* **1983**, *6*, 119-133.

(14) Vincent, B.; Young, C. A.; Tadros, T. F., *Faraday Discuss. Chem. Soc.* **1978**, *65* 296.

(15) Vincent, B.; Jafelicci, M.; Luckham, P. F.; Tadros, T. F., *J. Chem. Soc., Faraday Trans. 1 Phys. Chem. Cond. Phas.* **1980**, *76*, 674-682.

(16) Hansen, F.N.; Matijević, E., *J. Chem. Soc., Faraday Trans. 1 Phys. Chem. Cond. Phas.* **1980,** 1240-1262**.**

(17) Barouch, E.; Matijevic, E.; Ring, T. A.; Finlan, *J. Colloid Inter. Sci.* **1978**, *67*, 1-9.

(18) Furusawa, K.; Anzai, C., *Colloid Surf.* **1992**, *63*, 103-111.

(19) Furusawa, K.; Anzai, C., *Colloid Polym. Sci.* **1987**, *265*, 882-888.

(20) Harley, S., Ph.D. dissertation thesis, University of Bristol **1990**.

(21) Harley, S.; Thompson, D. W.; Vincent, B., *Colloid Surf.* **1992**, *62*, 163-176.

(22) Ottewill, R. H.; Schofield, A. B.; Waters, J. A.; Williams, N. S. J., *Colloid Polym. Sci.* **1997**, *275*, 274-283.

(23) M. Okubo, M.; Lu, Y.; Wang, Z., *Colloid Polym. Sci* **1999**, *277* 77-82.

(24) Xu, Y.; Brittain, W. J.; Xue, C.; Eby, R. K., *Polymer* **2004**, *45*, 3735-3746.

(25) Chen, J.-H.; Dai, C.-A.; Chen, H.-J.; Chien, P.-C.; Chiu, W.-Y., *J. Colloid Inter. Sci.* **2007**, *308*, 81-92.

(26) Voorn, D. J.; Ming, W.; van Herk, A. M.; Bomans, P. H. H.; Frederik, P. M.; Gasemjit, P.; Johanssmann, D., *Langmuir* **2005**, *21*, 6950-6956.

(27) Voorn, D. J.; Ming, W.; Laven, J.; Meuldijk, J.; de With, G.; van Herk, A. M., *Colloid Surf. a-Physicochem. Eng. Asp.* **2007**, *294*, 236-246.

(28) Kauzmann, W., *Adv. Prot. Chem.* **1959**, *14*, 1-63.

(29) Chandler, D., *Nature* **2005**, *437*, 640-647.

(30) Attard, P., *Adv. Colloid Inter. Sci.* **2003**, *104*, 75-91.

(31) Eriksson, J. C.; Ljunggren, S.; Claesson, P. M. *J. Chem. Soc. Faraday Trans. 2* **1989**, *85*, 163-176.

(32) Stillinger, F. H., *J.Chem.Phys.* **1982**, *76*, 1087-1091.

(33) Yaminsky, V. V.; Yushchenko, V. S.; Amelina, E. A.; Shchukin, E. D., *J. Colloid Inter. Sci.* **1983**, *96*, 301-306.

(34) Mezger, M.; Reichert, H.; Schoeder, S.; Okasinski, J.; Schroeder, H.; Dosch, H.; Palms, D.; Ralston, J.; Honkimaeki, V., *PNAS* **2006**, *103*, 18401-18404.

(35) Lum, K.; Chandler, D.; Weeks, J. D., *J. Phys. Chem. B.* **1999**, *103*, 4570-4577.

(36) Pashley, R. M.; McGuiggan, P. M.; Ninham, B. W.; Evans, D. F., *Science* **1985**, *229*, 1088-1089.

(37) Singh, S.; Houston, J.; van Swol, F.; Brinker, C. J., *Nature* **2006**, *442*, 526.

(38) Yamaguchi, K.; Ito, M.; Taniguchi, T.; Kawaguchi, S.; Nagai, K., *Colloid Polym. Sci.* **2004**, *282*, 366-372.

(39) Yamaguchi, K.; Taniguchi, T.; Kawaguchi, S.; Nagai, K., *Chem Lett.* **2001**, *7*, 658-659.

(40) Zubarev, E. R.; Xu, J.; Sayyad, A.; Gibson. J.D., *J. Am. Chem. Soc.* **2006**, *128*, 15098-15099.

(41) Walther, A.; Mueller, A. H. E., *Soft Matter* **2008**, *4*, 663-668.

(42) Wurm, F.; Kilbinger, A. F. M., *Angew.Chem., Inter. Ed.* **2009**, *48*, 8412-8421.

(43) Erhardt, R.; Boeker, A.; Zettl, H.; Kaya, H.; Pyckhout-Hintzen, W.; Krausch, G.; Abetz, V.; Mueller, A. H. E., *Macromolecules.* **2001**, *43*, 1069-1075.

(44) Erhardt, R.; Zhang, M.; Boeker, A.; Zettl, H.; Abetz, C.; Frederik, P.; Krausch, G.; Abetz, V.; Mueller, A. H. E., *J. Am. Chem. Soc.* **2003**, *125*, 3260-3267.

(45) Nie, L.; Liu, S.; Shen, W.; Chen, D.; Jiang, M., *Angew. Chem. Int. Ed.* **2007**, *46*, 6321-6324.

(46) Hong, L.; Cacciuto, A.; Luijten, E.; Granick, S., *Langmuir* **2008**, *24*, 621-625.

(47) Miller, W.; Cacciuto, A., *Phys.Rev. E* **2009**, *80*, 21404-021406.

(48) Whitelam, S.; Bon, S. A. F., *J. Chem. Phys.* **2010**, 132, 074901.

(49) Maeda, S.; Armes, S. P., *J. Colloid Inter. Sci.* **1993**, *159*, 257-259.

(50) Maeda, S.; Armes, S. P., *J. Mater. Chem.* **1994**, *4*, 935-942.

(51) Li, R.; Yang, X.; Li, G.; Li, S.; Huang, W., *Langmuir* **2006**, *22*, 8127-8133.

(52) Li, G. L.; Song, Y. Y.; Yang, X. L.; Huang, W. Q., *J. Appl. Polym. Sci.* **2007**, *104*, 1350-1357.

(53) Jin, J.; Iyoda, T.; Cao, C.; Song, Y.; Jiang, L.; Li, T. J.; Zhui, D. B., *Angew.Chem., Inter. Ed.* **2001**, *40*, 2135-2138.

(54) Mirkin, C. A.; Letsinger, R. L.; Mucic, R. C.; Storhoff, J. J., *Nature* **1996**, *382*, 607-609.

(55) Valignat, M.-P.; Theodoly, O.; Crocker, J. C.; Russel, W. B.; Chaikin, P. M., *Proc.Nat. Ac. Sci. U. S. A.* **2005**, *102*, 4225-4229.

(56) Fleming, M. S.; Mandal, T. K.; Walt, D. R., *Chem. Mater.* **2001**, *13*, 2210-2216.

(57) Chern, C. S.; Lee, C. K.; Chen, C. Y., *Colloid. Surf. B: Biointerf.* **1996**, *7*, 55-64.

(58) Decher, G., *Science* **1997**, *277*, 1232.

(59) Stockton, W. B.; Rubner, M. F., *Macromolecules.* **1997**, *30*, 2717-2725.

(60) Wang, L.; Wang, Z.; Zhang, X.; Shen, J.; Chi, L.; Fuchs, H., *Macromolecules.Rapid Comm.* **1997**, *18*, 509-514.

(61) Zhang, H.; Wang, D.; Wang, Z.; Zhang, X., *Eur. Polym. J.* **2007**, *43*, 2784-2791.

(62) Hoshi, T.; Anzai, J.-i.; Osa, T., *Analy. Chem.* **1995**, *67*, 770-774.

(63) Anzai, J.-i.; Kobayashi, Y.; Nakamura, N.; Nishimura, M.; Hoshi, T., *Langmuir* **1998**, *15*, 221-226.

(64) Decher, G.; Lehr, B.; Lowack, K.; Lvov, Y.; Schmitt, J., *Biosen. Bioelect.* **1994**, *9*, 677-684.

(65) Sukhorukov, G. B.; Möhwald, H.; Decher, G.; Lvov, Y. M., *Thin Solid Films* **1996**, *284-285*, 220-223.

(66) Caruso, F.; Caruso, R. A.; Moehwald, H., *Science* **1998**, *282*, 1111-1114.

(67) Donath, E.; Sukhorukov, G. B.; Caruso, F.; Davis, S. A.; Mohwald, H. *Angew. Chem., Inter. Ed.* **1998**, *37*, 2202-2205.

(68) Johnston, A. P. R.; Cortez, C.; Angelatos, A. S.; Caruso, F., *Curr. Op. Colloid Interf. Sci.* **2006**, *11*, 203-209.

(69) Caruso, F.; Mohwald, H., *Langmuir* **1999**, *15*, 8276-8281.

(70) Ramsden, W., *Proc. R. Soc. Lond., Sect. A* **1903**, *72*, 156-164.

(71) Pickering, S. U., *J. Chem. Soc., Trans.* **1907**, *91*, 2001-2021.

(72) Aveyard, R.; Binks, B. P.; Clint, J. H., *Adv. Colloid Inter. Sci.* **2003**, *100-102*, 503-546.

(73) Binks, B. P., *Curr. Op. Colloid Interf. Sci.* **2002**, *7*, 21-41.

(74) Finkle, P.; Draper, H. D.; Hildebrand, J. H. *J. Am. Chem. Soc.* **1923**, *45*, 2780-2788.

(75) Pieranski, P., *Phys. Rev. Lett.* **1980**, *45*, 569-572.

(76) Aveyard, R.; Clint, J. H. *J., Chem. Soc., Faraday Trans.* **1996**, *92*, 85-89.

(77) Cheung, D. L.; Bon, S. A. F., *Phys. Rev. Lett.* **2009**, *102*, 066103.

(78) Widom, B.; Rowlinson, J. S., *J. Chem. Phys.* **1970**, *52*, 1670-1684.

(79) Madivala, B.; Fransaer, J.; Vermant, J., *Langmuir* **2009**, *25*, 2718-2728.

(80) Madivala, B.; Vandebril, S.; Fransaer, J.; Vermant, J., *Soft Matter* **2009**, *5*, 1717-1727.

(81) Lin, Y.; Skaff, H.; Emrick, T.; Dinsmore, A. D.; Russell, T. P., *Science* **2003**, *299*, 226-229.

(82) Thomson, J. J. *Philos. Mag. (1798-1977)* **1904**, *7*, 237-265.

(83) Bausch, A. R.; Bowick, M. J.; Cacciuto, A.; Dinsmore, A. D.; Hsu, M. F.; Nelson, D. R.; Nikolaides, M. G.; Travesset, A.; Weitz, D. A., *Science* **2003**, *299*, 1716-1718.

(84) Lipowsky, P.; Bowick, M. J.; Meinke, J. H.; Nelson, D. R.; Bausch, A. R., *Nat. Mater.* **2005**, *4*, 407-411.

(85) Fortuna, S.; Colard, C. A. L.; Troisi, A.; Bon, S. A. F., *Langmuir* **2009**, *25*, 399-403.

(86) Bon, S. A. F.; Colver, P. J., *Langmuir* **2007**, *23*, 8316-8322.

(87) Cauvin, S.; Colver, P. J.; Bon, S. A. F. *Macromolecules.* **2005**, *38*, 7887-7889.

(88) Hohenstein, W. P., *Polym. Bull* **1945**, *1*, 13-16.

(89) Hohenstein, W. P.; Mark, H., *J. Polym. Sci.* **1946**, *1*, 127-145.

(90) Winslow, F. H.; Matreyek, W., *J. Ind. Eng. Chem.* **1951**, *43*, 1108-1112.

(91) Wiley, R. M., *J. Colloid Sci.* **1954**, *9*, 427-437.

(92) Deslandes, Y., *J. Appl. Polym. Sci.* **1987**, *34*, 2249-2257.

(93) Bon, S. A. F.; Cauvin, S.; Colver, P. J., *Soft Matter* **2007**, *3*, 194-199.

(94) Bon Stefan, A. F.; Chen, T., *Langmuir* **2007**, *23*, 9527-9530.

(95) Chen, T.; Colver, P. J.; Bon, S. A. F., *Adv. Mater.* **2007**, *19*, 2286-2289.

(96) Colver, P. J.; Chen, T.; Bon, S. A. F., *Macromolecules. Symp.* **2006**, *245*, 34-41.

(97) Bon, S. A. F.; Chen, T., *Langmuir* **2007**, *23*, 9527-9530.

(98) Wang, C.; Zhang, C.; Li, Y.; Chen, Y.; Tong, Z., *React. Funct. Polym.* **2009**, *69*, 750-754.

(99) Hasell, T.; Yang, J.; Wang, W.; Li, J.; Brown, P. D.; Poliakoff, M.; Lester, E.; Howdle, S. M., *J. Mater. Chem.* **2007**, *17*, 4382-4386.

(100) Yang, J.; Hasell, T.; Wang, W.; Li, J.; Brown, P. D.; Poliakoff, M.; Lester, E.; Howdle, S. M., *J. Mater. Chem.* **2008**, *18*, 998-1001.

(101) Chen, K.; Yang, Y.; Sa, Q.; Shi, L.; Zhao, H., *Polymer.* **2008**, *49*, 2650-2655.

(102) Duan, L.; Chen, M.; Zhou, S.; Wu, L., *Langmuir* **2009**, *25*, 3467-3472.

(103) Gao, Q.; Wang, C.; Liu, H.; Wang, C.; Liu, X.; Tong, Z., *Polymer.* **2009**, *50*, 2587-2594.

(104) Nie, Z.; Park, J. I.; Li, W.; Bon, S. A. F.; Kumacheva, E., *J. Am. Chem. Soc.* **2008**, *130*, 16508-16509.

(105) Bon, S. A. F.; Mookhoek, S. D.; Colver, P. J.; Fischer, H. R.; van der Zwaag, S., *Eur. Polym. J.* **2007**, *43*, 4839-4842.

(106) Tiarks, F.; Landfester, K.; Antonietti, M., *Langmuir* **2001**, *17*, 5775-5780.

(107) Zhang, K.; Wu, W.; Meng, H.; Guo, K.; Chen, J. F., *Powd. Technol.* **2009**, *190*, 393-400.

(108) Zhang, Y.; Chen, H.; Shu, X.; Zou, Q.; Chen, M., *Colloid. Surf. A: Physicochem. Eng. Asp.* **2009**, *350*, 26-32.

(109) Wang, T.; Colver, P. J.; Bon, S. A. F.; Keddie, J. L., *Soft Matter* **2009**, *5*, 3842-3849.

(110) Voorn, D. J.; Ming, W.; Van Herk, A. M., *Macromolecules.* **2006**, *39*, 2137-2143.

(111) Walther, A.; Hoffmann, M.; Mueller, A. H. E., *Angew. Chem., Inter. Ed.* **2008**, *47*, 711-714.

(112) Percy, M. J.; Amalvy, J. I.; Randall, D. P.; Armes, S. P.; Greaves, S. J.; Watts, J. F., *Langmuir* **2004**, *20*, 2184-2190.

(113) Schmid, A.; Tonnar, J.; Armes, S. P., *Adv. Mater.* **2008**, *20*, 3331-3336.

(114) Schmid, A.; Armes, S. P.; Leite, C. A. P.; Galembeck, F., *Langmuir* **2009**, *25*, 2486-2494.

(115) Sacanna, S.; Philipse, A. P., *Adv. Mater.* **2007**, *19*, 3824-3826.

(116) Sacanna, S.; Kegel, W. K.; Philipse, A. P., *Phys. Rev. Lett.* **2007**, *98*, 158301.

(117) Colver, P. J.; Colard, C. A. L.; Bon, S. A. F., *J. Am. Chem. Soc.* **2008**, *130*, 16850-16851.

(118) Colard Catheline, A. L.; Teixeira, R. F. A.; Bon Stefan, A. F., *Langmuir* **2010**, 26, 7915-1921.

(119) Fortuna, S.; Colard Catheline, A. L.; Troisi, A.; Bon Stefan, A. F., *Langmuir* **2009**, *25*, 12399-12403.

(120) Ma, H.; Dai, L. L., *J. Colloid Interf. Sci.* **2009**, *333*, 807-811.

(121) Sheibat-Othman, N.; Bourgeat-Lami, E., *Langmuir* **2009**, *25*, 10121-10133.

(122) Bon Stefan, A. F.; Colver Patrick, J., *Langmuir* **2007**, *23*, 8316-8322.

(123) Yu, C.-L.; Kang, J.-S.; Zhang, F.-A., *J. Macromol. Sci., Part A Pur. Appl. Chem.* **2009**, *46*, 870-875.

(124) Song, X.; Yin, G.; Zhao, Y.; Wang, H.; Du, Q., *J. Polym. Sci., Part A Polym. Chem.* **2009**, *47*, 5728-5736.

(125) Song, X.; Zhao, Y.; Wang, H.; Du, Q., *Langmuir* **2009**, *25*, 4443-4449.

(126) Manoharan, V. N.; Elsesser, M. T.; Pine, D. J., *Science* **2003**, *301*, 483-487.

(127) Cho, Y.-S.; Yi, G.-R.; Lim, J.-M.; Kim, S.-H.; Manoharan Vinothan, N.; Pine David, J.; Yang, S.-M., *J. Am. Chem. Soc.* **2005**, *127*, 15968-15975.

(128) Cho, Y.-S.; Yi, G.-R.; Kim, S.-H.; Jeon, S.-J.; Elsesser, M. T.; Yu, H. K.; Yang, S.-M.; Pine, D. J., *Chem.Mater.* **2007**, *19*, 3183-3193.

(129) Lee, D.; Weitz, D. A., *Adv. Mater.* **2008**, *20*, 3498-3503.

(130) Dinsmore, A. D.; Hsu Ming, F.; Nikolaides, M. G.; Marquez, M.; Bausch, A. R.; Weitz, D. A., *Science* **2002**, *298*, 1006-1009.

(131) Jerri, H. A.; Dutter, R. A.; Velegol, D., *Soft Matter* **2009**, *5*, 827-834.

(132) Chaturvedi, N.; Jerri, H.; Velegol, D., *Langmuir* **2008**, *24*, 7618-7622.

(133) Yake, A. M.; Snyder, C. E.; Velegol, D., *Langmuir* **2007**, *23*, 069-9075.

(134) Snyder, C. E.; Yake, A. M.; Feick, J. D.; Velegol, D., *Langmuir* **2005**, *21*, 4813-4815.

(135) Xia, Y.; Yin, Y.; Lu, Y.; McLennan, J., *Adv. Funct. Mater.* **2003**, *13*, 907-918.

Chapter II.

Pickering Emulsion polymerizations stabilized with silica nanospheres

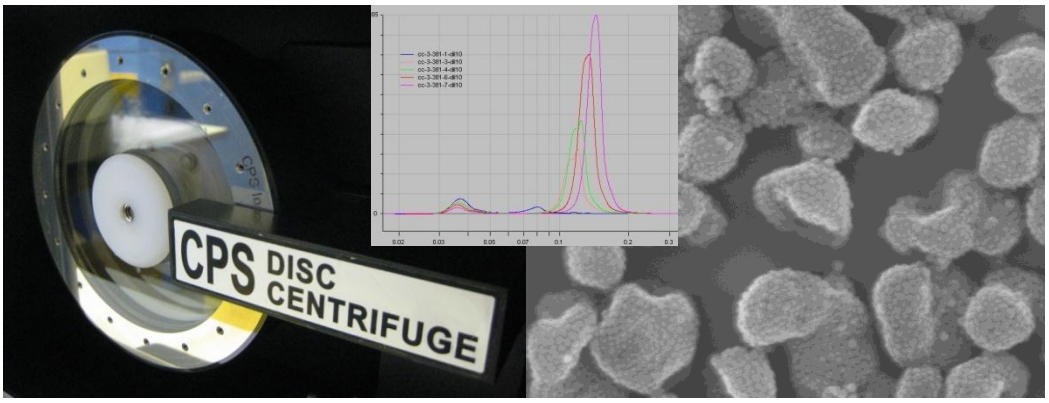

Pickering emulsion polymerization process as a convenient synthesis route in the fabrication of armored polymer latexes is investigated. This solids-stabilized emulsion polymerization process relies on the adhesion of solid particles to soft interfaces, replacing the role of surfactants. Key mechanistic features of the polymerization process by monitoring the concentration of nanoparticles in the water phase over monomer conversion are reported.

Part of this work was published

[1]Colard, C.A.L.; Teixeira, R.F.A.; Bon, S.A.F., *Langmuir* **2010**, 26(11), 7915-1921

II.1. Introduction

In order to meet the ever-increasing demand for enhanced material properties and constraints (e.g., of structural and compositional complexity), different strategies to build tailored micro- and nanomaterials have gained a lot of interest from the scientific community. The combination of organic-inorganic materials to produce hybrid nanocomposites with synergetic properties has considerable interest in a breadth of applications including waterborne coatings and adhesives. One interesting morphological class of hybrid polymer latexes is those showing an armored supracolloidal structure in which inorganic nanoparticles are assembled onto and adhere to the surface of polymer latex spheres. These armored hybrid morphologies when applied to waterborne coatings feature for example scratch resistance[2-4] and flame retardancy of the resulting films.[5] When soft polymer latexes armored with clay nanodiscs are used as an additive in waterborne pressure sensitive adhesives, profound synergistic effects are observed in the bulk mechanical properties.[6]

Pioneering work by Ramsden[7] and Pickering[8] showed that emulsions can be stabilized by solid particles that can adhere to fluid interfaces. [9-10] Numerous research works have been done based on this phenomenon of heterogeneous coagulation.[11-31] For example, Armes *et al.* described the synthesis of hybrid polymer latexes armored with silica nanoparticles using heterocoagulation based on electrostatic attraction with the aid of auxiliary monomers/initiators as assembly tool to produce the raspberry-like morphologies.[11-14] Bon and collaborators reported on the fabrication of titanium oxide armored polymer microspheres and microcapsules made *via* Pickering suspension

polymerization,[16] on Laponite clay nanodisc armored polymer latexes via Pickering miniemulsion polymerization,[17-18] and on waterborne hybrid polymer latexes armored with silica nanoparticles *via* both Pickering miniemulsion polymerization[19] and solids-stabilized emulsion polymerization

Chevalier *et al.*[23] recently carried out suspension and miniemulsion polymerizations using fumed silica as a Pickering stabilizer. Chen and coworkers[25] reported on the preparation of poly(styrene)/nano-SiO_2 composite microspheres with a raspberry morphology *via* either Pickering miniemulsion polymerization and Pickering emulsion polymerization process, using an auxiliary cationic comonomer, 2-(methacryloyl)ethyltrimethyammonium chloride, to promote adsorption of nanosilica onto growing latex particles of poly(styrene) and poly(*n*-butyl acrylate).[26] Bourgeat-Lami *et al.* reported the synthesis of poly(styrene)/silica (PS/SiO_2) and poly(styrene-co-methyl methacrylate)/SiO_2 hybrid latex particles via Pickering emulsion polymerization with the help of small amounts of of poly(ethylene glycol) monomethylether methacrylate (PEGMA) macromonomer to promote nanoparticle adhesion to the surface of the latex particles.[28] Using the same approach, they extended their work for the preparation of poly(styrene)-*co*-butyl amored with clay platelets.[21]

The presence of inorganic nanoparticles not only has a marked influence on the final mechanical and physical properties of the polymer dispersions, but also plays a key role in the kinetic events throughout the polymerization reaction. The armored layer of inorganic nanoparticles on the surface of latex particles has a pronounced effect on radical entry and exit events in (mini)emulsion polymerizations.[18,28,32] The relative amounts of nanoparticles with respect to both water and monomer used in the polymerization processes are critical

parameters. The partitioning of the nanoparticles between the water phase and their adsorbed state at the surfaces of the latex particles and monomer droplets, determines whether the synthesis of the nanocomposite armored polymer colloids is successful. Note that, it is assumed here that nanoparticles do not get encapsulated, which potentially is possible for certain systems. The presence of the nanoparticles not only influences the colloidal stability of the system but also can show a profound effect on the number of armored particles formed and thus on the average particle size and the particle size distribution of the hybrid polymer dispersion.

Monitoring the adhesion of silica nanoparticles onto the polymer latex particles throughout the emulsion polymerization process is key not only for reaction process optimization but also to tailor the composition of the final composite dispersion. For example a substantial excess of silica nanoparticles can lead to cracked or brittle polymer films. It is of great importance to develop a method to follow the adhesion of these inorganic nanoparticles onto polymer particles surface. Current techniques such as atomic force and electron microscopic techniques are labor intensive. Particle tracking using dark field microscopy is complicated by difference in scattering intensities. Dynamic light scattering suffers from its light intensity scaling with the radius of colloids to the power six, and hydrodynamic chromatography commonly uses a surfactant containing eluent phase which upon analysis would lead to detachment of nanoparticles that were adhered to the surface of the polymer latex.

In this work, it is shown that disc centrifugation can be used as a quantitative monitoring tool to measure the concentration of nanoparticles in the water phase throughout solids stabilized emulsion polymerizations. A series of emulsion

polymerizations in the presence of silica nanoparticles (Ludox TM-40, *ca.* 25 nm in diameter) were performed and showed that our developed method to quantify the amount of silica nanoparticles in the water phase throughout the polymerization process is an invaluable tool to explain features such as the packing densities of the nanoparticles on the surface of the latex particles and occasional limited coalescence of armored particles, observed in the solids-stabilized, or Pickering, emulsion polymerizations. It is also addressed the kinetics of Pickering emulsions polymerizations stabilized with silica nanoparticles using different monomers.

II.2. Experimental part

Materials: All monomers, vinyl acetate (VAc), vinyl pivalate (VPiv), methyl methacrylate (MMA), and *n*-butyl acrylate (BA), were purchased from Aldrich at 99 % or greater purity and used as received. Ludox TM-40 sol (colloidal silica, 40 wt% in water, density of silica particles ρ_{silica} = 1.75 g cm^{-3}) was purchased from Aldrich. HCl (aq. 37 wt%, reagent grade) was supplied by BDH. Potassium persulfate (KPS, 99+% p.a) was obtained from Fluka. Deionized water was used in all experiments. Poly(vinyl chloride) (PVC) standard latex (0.377 μm particle diameter) and *n*-dodecane were provided by Analytik Ltd. Sucrose (analytical reagent grade) was purchased from Aldrich and used as received.

Equipment: Emulsion polymerizations were carried out in double-walled cylindrical glass reactors (250 mL, Asynt Ltd.) equipped with an external

circulating heating bath (Julabo F-25 unit), a condenser, and a four-bladed teflon or metal overhead turbine stirrer fitted at approximately 2 cm from the bottom of the reactor vessel (Cowie Ltd.) typically running at 300 rpm. pH measurements were performed on a pH-Meter (765 calimatic, Knick). A disc centrifugation particle sizer (CPS Disc Centrifuge, Model DC24000, CPS Instruments Inc.) was used to develop our quantitative method to monitor and determine the amount of silica nanoparticles in the water phase throughout the solids-stabilized emulsion polymerizations. Average particle sizes and dispersities of the armored latexes were measured by dynamic light scattering using a Malvern Zetasizer Nano (data was analyzed using the CONTIN algorithm). SEM analyses were performed using a Zeiss Supra55VP FEGSEM with an EBSD camera and the samples were prepared on silicon wafers (kindly donated by Wacker Chemie AG) to be analyzed uncoated. TEM analyses were performed on a 1200EXII TEM with a 1K Gatan camera using Formvar-Film grids (200 Mesh Cu, Agar Sc. S138) and cryo-TEM analyses were performed on a Jeol 2011 TEM (200KV LaB6) with 2K Gatan Ultrascan camera or on a Jeol 2010F TEM (200KV FEG) with 4K Gatan Ultrascan camera using Lacey-Carbon-Film grids (300 Mesh Cu, Agar Sc. S166-3H). An Analytical Balance (Precisa XT 220A) and micropipettes Pipetman P200 (20 – 200 µL) and P1000 (200 – 1000 µL) were used for accurate measurements.

Typical solids-stabilized emulsion polymerization (for exact quantities of all polymerizations see Table II-1): A 40.0 wt% solution of Ludox TM-40 silica sol (33.0 g, 5.7 wt% overall, or 44.0 wt% based on monomer) was diluted and dispersed in 167.0 g of deionized water in a 250 mL double-walled glass reactor.

The pH of the dispersion was adjusted with conc. HCl (aq) to pH 4.5-5.5 and was placed under a nitrogen atmosphere by purging. Degassed monomer, 30.0 g (13.0 wt%) was added. The reaction mixture was heated to 65 ºC, whilst stirring at 300 rpm. The emulsion polymerization was started upon addition of 0.13 g KPS dissolved in 3.0 g of water. Monomer conversion was monitored via gravimetry by taking typically samples of 2 g by syringe (see Supporting Information for details on monomer conversion vs. time, particle size, and dynamic light scattering data).

Table II-1. Composition of the polymer latexes prepared by emulsion polymerization in presence of Ludox TM-40 silica nanoparticles.

Monomer	Overall monomer content/ wt%	Overall silica content/ wt%	Silica content in water phase/ wt%	Silica: monomer/ $g \times g^{-1}$	KPS: monomer $g \times g^{-1}$	SEM/TEM images
VPiv	9.0	8.0	9.0	0.90	0.0043	Figure II.2E
VAc	9.0	8.0	9.0	0.90	0.0043	Figure II.2D
MMA	9.0	8.1	9.0	0.90	0.0050	Figure II.2A
MMA/BA (0.67 wt/wt)	9.0	8.2	8.9	0.89	0.0048	Figure II.2C
BA	8.9	8.3	9.1	0.93	0.0052	Figure II.2B/ Figure II.7A
VPiv	13.1	5.8	6.6	0.44	0.0043	-
VAc	13.0	5.7	6.5	0.44	0.0043	Figure II.3
VAc	11.1	11.6	13.1	1.04	0.0081	-
MMA	5.1	5.7	6.0	1.12	0.0114	Figure II.7B

Typical procedure of disc centrifugation measurements: We operated the disc centrifuge at its maximum speed (24,000 rpm). A density gradient is built from 24.0 wt% to 8.0 wt% sucrose solutions in deionized water. The gradient is prepared by the subsequent injections of mixtures of a 24.0 wt% and an 8.0 wt% sucrose solution in water: (1.6 + 0) mL, (1.4 + 0.2) mL, (1.2 + 0.4) mL, (1.0 + 0.6) mL, (0.8 + 0.8) mL, (0.6 + 1.0) mL, (0.4 + 1.2) mL, (0.2 + 1.4) mL, (0 + 1.6) mL, respectively. Next we inject 0.5 mL of dodecane, this is to extend the life time of the gradient by limiting evaporation. A waiting period of 15 minutes was essential for the gradient to become linear, consistent and stable. After this, samples could be analysed. Typically the gradient remained stable for a period of 5-6 h. A typical run to determine the concentration of silica nanoparticles takes approximately 20-30 min. After this a new gradient had to be built. A calibration standard (a waterborne poly(vinyl chloride) latex of average particle diameter 377 nm) was used. The settings of the software procedure were, for the sample parameters: maximum diameter = 1 μm, minimum diameter = 0.017 μm, particle density = 1.75 $g.mL^{-1}$, particle refractive index = 1.45, particle absorption = 0.001 K, for the calibration standard parameters: peak diameter = 0.377 μm, half height peak width = 0.1 μm, particle density = 1.385 $g.mL^{-1}$ and for the fluid parameters: fluid density = 1.064 $g.mL^{-1}$, fluid refractive index = 1.357, fluid viscosity = 1.3 cP).

Each analysis consists of the injection of about 0.05 mL of PVC standard followed by the injection of about 0.1 mL of sample. The syringe was systematically weighed before and after injection of the sample to determine accurately the amount injected. Colloidal silica nanoparticles solutions of 0.39 wt%, 0.33 wt%, 0.28 wt%, 0.22 wt%, 0.21 wt%, 0.15 wt% and 0.11 wt% were

prepared by weight from the commercial Ludox TM-40 sol of 40.0 wt% and were used as quantitative calibration standards. Samples taken throughout the solids-stabilized emulsion polymerizations were diluted 10 times with deionized water, using micropipettes, before injection into the disc centrifuge.

II.3. Results and Discussion

(Mini)emulsion polymerizations stabilized by solid nanoparticles, such as silica, and titanium dioxide are an attractive route to produce armored nanocomposite polymer latexes. To unravel the mechanistic role of the nanoparticles in these polymerization processes and the related polymerization kinetics a method to measure the concentration of the nanoparticles in the water phase at a given time, or extent of monomer conversion, in the nanoparticle-stabilized (mini)emulsion polymerization process would be very useful.

Herein, it is shown that disc centrifugation could be used to calculate the concentration of nanoparticles in the water phase throughout the particle growth period in solids-stabilized emulsion polymerizations, which is based on a model for the packing of nanoparticles onto the surface of the polymer latex particles. It is also addressed polymerization kinetics of the solids-stabilized emulsion polymerizations.

II.3.1. Emulsion polymerizations carried out in presence of silica nanoparticles

Pickering emulsion polymerizations using vinyl acetate (VAc), vinyl pivalate (VPiv), *n*-butyl acrylate (BA), and methyl methacrylate (MMA) as monomers in

the presence of Ludox TM-40, using potassium persulfate as radical initiator at 0.13 g in 187.55 g of water were performed (**Table II-1**).

The Pickering emulsion polymerizations of vinyl esters were performed at pH 4.5 while the Pickering emulsions polymerizations of acrylates were done at pH 5.5 in order to minimize hydrolysis and electrostatic repulsion and favor the closely-packed pattern.[1,20] Kinetics of emulsion polymerizations were performed and are shown in **Figure II.1**.

Figure II.1 shows that vinyl esters have faster polymerizations rates in comparison with acrylates, with vinyl acetate being the fastest one (silica:monomer ratios of *ca* 0.90, see first five entries of table II-1). These differences in the polymerization rates are due to substantial differences in the coefficient propagation rates.[22] In the case of acrylate monomers, the reaction using methyl methacrylate (MMA) as monomer is faster than the reaction using *n*-butyl acrylate (BA) as monomer while the reaction using the comonomers (MMA:BA) (0.67 wt/wt) had an intermediate rate of polymerization, between pure MMA and pure BA. Initially this result seems counter-intuitive as the rate coefficient of propagation of BA is markedly higher than that of MMA. However, the solubility of MMA in water is much higher than the solubility of BA and as a result diffusion limitation of monomer transport through water phase occurs.[22]

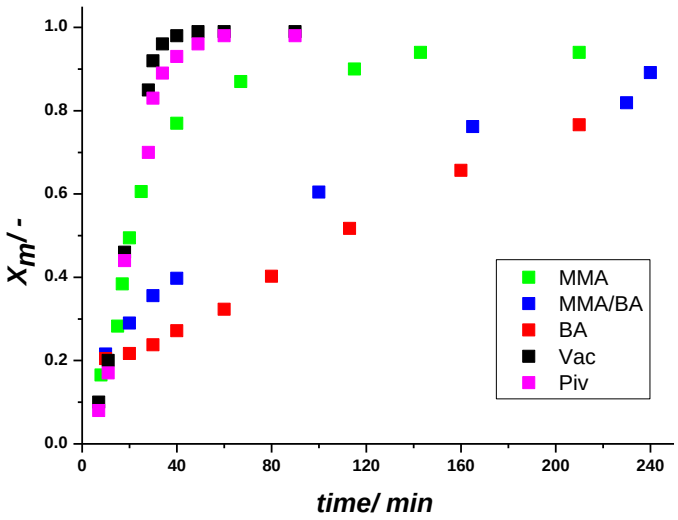

Figure II.1. Overall monomer conversion, X_m, *versus* time for Pickering emulsion (co)polymerizations of different (co)monomers. Silica:monomers ratios of *ca* 0.90. (See the first five entries of table II-1)

Cryo-TEM pictures and SEM pictures were taken to check if the silica nanoparticles were or were not on the polymer particles surface. As demonstrated in **Figure II.2**, all samples, with the exception of poly(vinyl pivalate), show adhesion of silica nanoparticles onto polymer particle surfaces. The reason for the no adhesion of silica nanoparticles onto polyvinyl pivalate particles surfaces is that poly(vinyl pivalate) is too hydrophobic and the silica nanoparticles do not wet and thus adhere to the surface of the particles. This behavior for hydrophobic monomers has previously been observed.[20, 28] This lack of adhesion can be overcome easily by either using small amounts of hydrophilic co-monomer, such as 4-vinylpyridine (4-VP),[15] 2-methacryloyl)ethyltrimethyammonium chloride,[26] poly(ethylene glycol) monomethylether methacrylate (PEGMA) macromonomer,[28] or by modifying the hydrophilicity of the nanoparticles, such as glycerol-functionalized silica.[14]

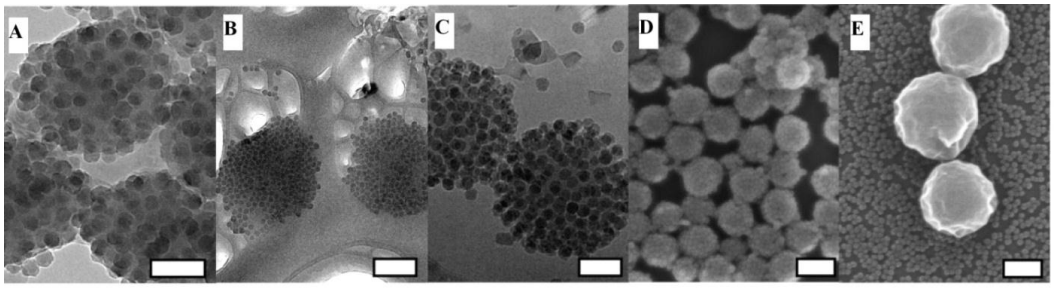

Figure II.2. From left to right: Cryo-TEM pictures of **A**: p(MMA) (scale bar: 100nm), **B:** p(BA) (scale bar: 200nm), **C**: p(MMA-co-BA) (scale bar: 100nm). SEM pictures of **D**: p(Vac) (scale bar: 200nm) and **E**: p(VPiv) (scale bar: 200nm). Silica:monomer ratios of *ca*. 0.90.

Figure II.3 shows a non-spherical shape with partial coalescence of poly(vinyl acetate) stabilized with silica nanoparticles when the silica:monomer ratio is dropped to 0.44 (this does not happen when silica:monomer ratio of p(Vac) is 0.90, as shown in **Figure II.2D**) . It is possible to see that the coalescence leads to the formation of some doublet and triplets clusters as a consequence of lack of colloidal silica stabilizer. A method to monitor the amount of inorganic particles in the water phase would be very helpful to follow the polymerization process.

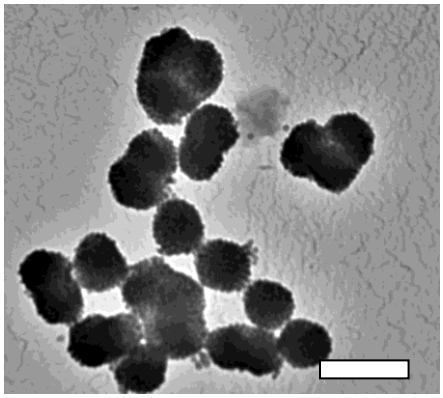

Figure II-3. TEM image of Ludox TM-40 stabilized PVAc latex with a silica:monomer ratio of 0.44. Scale bar 500 nm.

II.3.2. Quantitative Disc Centrifugation

The application of a centrifugal force on a colloidal dispersion allows either sedimentation or creaming of particles that under the normal gravitational force would remain dispersed as a direct result of their Brownian motion. The disc centrifugation technique is based on this principle and is commonly used to measure particle size distributions of colloids.[12] A combination of particle mass and shape allows separation which is detected typically using turbidity as a measure, hereby employing a laser. Turbidity can be used quantitatively in order to determine the concentration of nanoparticles present in the water phase. To correlate the intensity of the detection signal to the concentration of the nanoparticles we injected a series of calibration standards of known concentration of Ludox TM-40 silica nanoparticles dispersed in water. Note that it is important to accurately know the injected mass of the sample, as detection and thus signal intensity obviously correlates with the number of nanoparticles (see appendix for detailed explanation).

II.3.3. Theoretical model for the concentration of nanoparticles in the water phase

Our model is based on partitioning of the nanoparticles between the water phase and the surface of the latex particles. The total surface area provided by the monomer droplets is small in emulsion polymerizations, which allows us to neglect the amount of nanoparticles adhered to the surface of the monomer droplets. The amount of nanoparticles in the water phase, C, expressed in number per gram of water, depends on the initial concentration of silica nanoparticles, C_0, and correlates with the amount of silica nanoparticles that

adheres to the surface of the latex particles, C_S, expressed in the same dimensions:

$$C = \quad C_0 - C_S$$

Equation II-1

We assume that no nanoparticles are encapsulated fully into the polymer particles. When we know the number of latex particles, their shape and size, we can calculate their total surface area. Once we know the adhesion behavior of the nanoparticles and thus their packing patterns we are able to calculate the total amount of nanoparticles adhered, and thus C_S. In line with our model developed for clay-disc armored polymer particles,[18] we assume the colloidal silica and the polymer particles to be monodisperse in size, and both of spherical shape. The diameter of Ludox TM-40, d_{silica}, was measured to be 24.1 nm (+/- 3.4 nm) from TEM micrographs.[19] Values for the area which is covered by nanoparticles from the armored polymer latex particle, A_{polym}, are obtained from the average diameter for the armored-polymer composite latex particles, d_z, as determined by dynamic light scattering (DLS). When we use the value for d_z as a measure for calculating the amount of nanoparticles adhered onto the polymer latex particles, we need to keep in mind that (i) dynamic light scattering provides a hydrodynamic and higher order mean value for the diameter of the particles, (ii) the nanocomposite armored particles are of a non-smooth raspberry-type nature, whereby we assume the formation of a single armored layer. We therefore introduce a correction factor β. This leads to:

$$A_{polym} = \pi\left(\beta d_z\right)^2$$

Equation II-2

To correlate our model to experimental data, different packing patterns and packing densities have been considered. An effective area "occupied" by one silica nanoparticle, A_{silica}, can be calculated with Equation 3. We introduce a packing parameter *P* to allow for correction as a result of different packing geometries and thus packing densities of the nanospheres onto the surface of the latex particle. We define P = 1 for a 2D square packing geometry, $A_{silica-2D}$, in which the silica squares touch each other (negligible thickness of double layer). Hexagonal packing of the nanospheres is more closely packed reducing the effective area occupied by each silica nanosphere, $A_{silica-hex}$, with $P = \sqrt{3}/2$, or 0.866. Both these values of *P* do not take into account the curvature, finite dimensions, and the non-monodisperse nature of Ludox TM-40 silica nanoparticles. To accommodate for this we therefore considered the packing density obtained from our Monte Carlo simulations that predicted the packing patterns of armored Ludox TM-40-poly(styrene) latexes made via Pickering miniemulsion polymerization.[19] The packing parameter *P* is found to be 0.909 for the assembly of 206 silica nanospheres on a spherical surface of 161.58 nm in diameter.

$$A_{silica} = P\, d_{silica}^2$$

Equation II-3

The total number of polymer particles (N_{polym}) per gram of water, C_{polym}, is found using:

$$C_{polym} = \frac{N_{polym}}{m_{water}} = \frac{m_{m,0} X_m \Big/ \rho_{polym}}{m_{water} \frac{\pi}{6} (\beta d_z)^3}$$

Equation II-4

Where $m_{m,0}$ is the initial mass of monomer, m_{water} is the mass of water, X_m monomer conversion (determined by gravimetry), ρ_{polym} the density of the polymer. Note that we do not account for the swelling of the polymer particles with monomer, which could lead to volume increases up to 30 % vol.[33]

The concentration of adhered silica particles, C_S, can be calculated from $C_S A_{silica} = C_{polym} A_{polym}$, which combined with Equation II-1 leads to a final expression for C:

$$C = \frac{6}{m_{water} d_{silica}^2} \left[\frac{m_{silica}}{\pi \rho_{silica} d_{silica}} - \frac{m_{m,0} X_m}{\rho_{polym} P \beta d_z} \right]$$

Equation II-5

II.3.4. Calculation of the concentration of silica nanoparticles in water phase

Figure II.4 shows the concentration of silica nanoparticles, *C*, as function of monomer conversion, X_m, as determined by quantitative disc centrifugation for the PVAc and PVPiv reactions with a silica:monomer ratio of 0.44 (or 5.8 wt% silica nanoparticles). The data obtained from the emulsion polymerization of vinyl pivalate shows no relevant drop in nanoparticle concentration in the water phase. This is in agreement with the SEM analysis of the final polymer latex (**Figure II.2E**). Measured values exceed the value of C_0, an effect which we attribute to the non-homogeneity of the sample taken from the emulsion polymerization reactor. The data obtained for vinyl acetate shows that indeed throughout the emulsion polymerization process the silica nanoparticles concentration in the water phase, *C*, drops and thus that they adhere to the surface of the growing latex particles, as previously suggested.[20] The ability of

silica nanoparticles to stick to poly(vinyl acetate) latex particles was previously demonstrated by Wen *et al.*[27] and by Uricanu *et al.*, the latter elegantly studied the adsorption behavior of silica nanoparticles onto the surface of pre-fabricated latex spheres dispersed in water.[34]

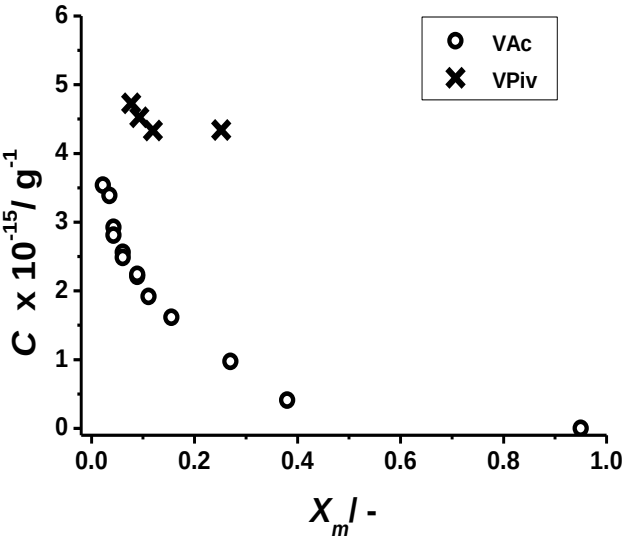

Figure II.4. The measured concentration of silica nanoparticles in the water phase, *C*, versus monomer conversion, X_m, as measured by quantitative disc centrifugation. [○] Solids-stabilized emulsion polymerization of vinyl acetate at silica:monomer ratio of 0.44. [×] Emulsion polymerization of vinyl pivalate at silica:monomer ratio of 0.44.

For the silica nanoparticle stabilized emulsion polymerization of vinyl acetate we measured the average particle diameter, d_z, and the dispersity, D_I, of the particle size distribution by dynamic light scattering (see **Figure II.5**).

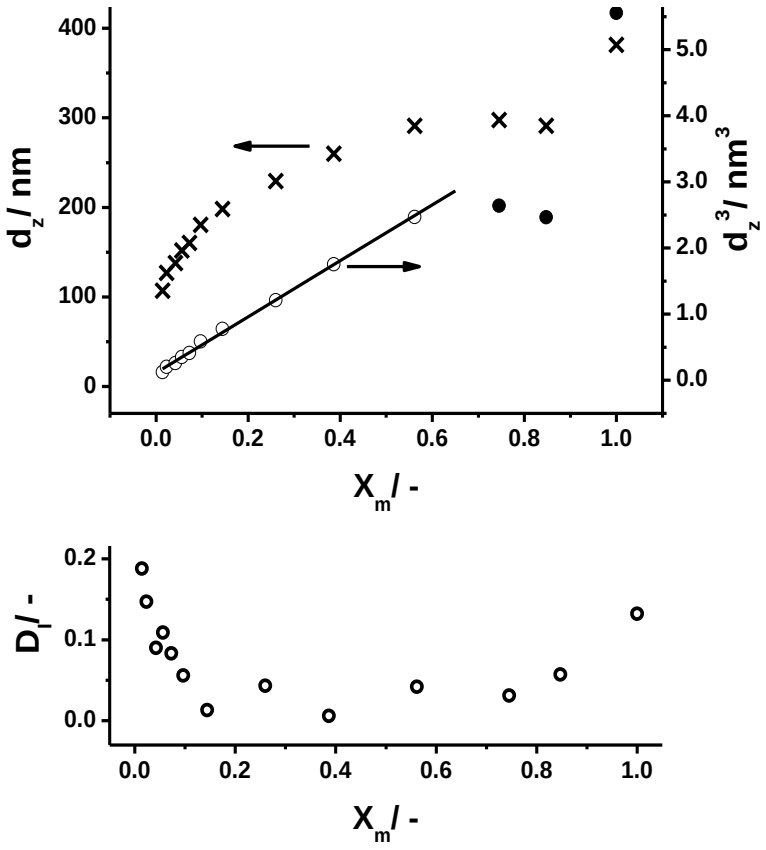

Figure II.5. Average particle diameter, d_z, and d_z^3 (top), and dispersity, D_I, (bottom) versus monomer conversion, X_m, of (Ludox TM-40)-stabilized emulsion polymerization of vinyl acetate (silica:monomer ratio of 0.44). Linear fit yields: $d_z^3 = 1.13\ (\pm 0.16) \times 10^6 + 4.23\ (\pm 0.07) \times 10^7\ X_m$ ($r^2 = 0.998$). Closed symbols were excluded in linear fit.

From experimental observations, it was found that solids-stabilized emulsion polymerizations often have a relatively narrow particle size distribution, which means that particle formation is fast comparatively to particle growth. When we assume that throughout the particle growth period the number of polymer latex particles, N_{polym}, stays constant, the average particle size, d_z, versus monomer conversion should show a 3rd order dependence (hereby ignoring monomer-swelling), as conversion scales to mass, which scales to volume, and volume

scales to d_z^3. Such behavior is indeed observed from **Figure II.5**, up to approximately 70 % monomer conversion. Noteworthy is that the dispersity of the particle size distribution goes up considerably at the later stages of the emulsion polymerization process. This coincides with undetectable low levels of remaining silica nanoparticles in the water phase (See **Figure II.4**). The lack of solid stabilizers results in coalescence of not fully covered poly(vinyl acetate) latex particles. We believe that since the coalescing particles are swollen and thus in a "soft" state, especially in the outer regions near the surface, the silica particles can migrate and rearrange. This agrees with the TEM analysis (see **Figure II.3**) in which fused armored agglomerates of non-spherical shape are observed.

Since d_z scales with $X_m^{1/3}$ for this solids stabilized emulsion polymerization, C should scale with $X_m^{2/3}$, as can be derived using Equation II-5. This is under the condition that partitioning of the silica nanoparticles remains the same throughout the particle growth period, uninfluenced by diffusion limitations of the heterocoagulation process and the nanoparticle occupancy of the surface of the armored polymer latex particle. Indeed such behavior can be observed from **Figure II.6**. The measured values at low conversion were omitted as a result of inhomogeneous sampling.

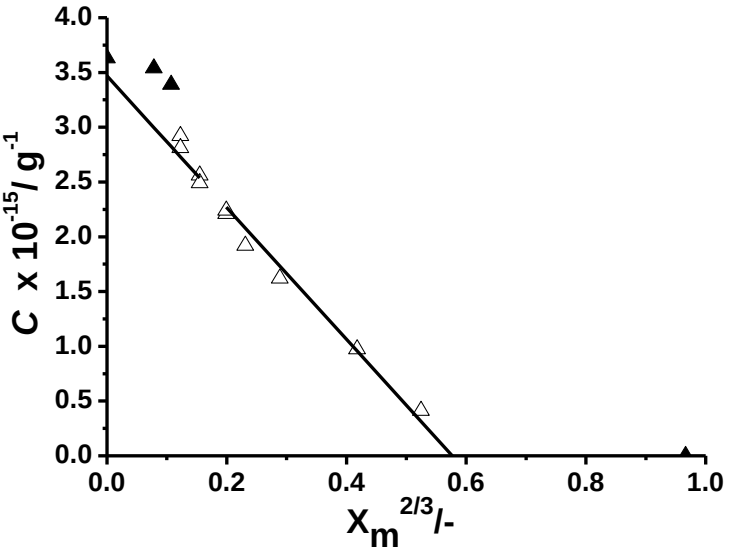

Figure II.6. The measured concentration of silica nanoparticles in the water phase, *C*, versus $X_m^{2/3}$ for the solids-stabilized emulsion polymerization of vinyl acetate (silica:monomer ratio of 0.44, see **Table II-1**). Linear fit yields: $C = 3.46\ (\pm 0.07) \times 10^{15} - 6.01\ (\pm 0.28) \times 10^{15}\ X_m^{2/3}$ ($r^2 = 0.98$). Closed symbols were excluded in linear fit due to the non-homogeneity of the sample at lower conversion stages.

Using the two linear correlations obtained for $C \propto -6.01 \times 10^{15}\ X_m^{2/3}$ and $d_z \propto \sqrt[3]{4.23 \times 10^7}\ X_m^{1/3}$ and with the aid of equation 5 we can find a value for $P\beta$ of 0.67 (using ρ_{polym} = 1.19 g cm^{-3}). For close-packed systems (the nanoparticles are in close proximity on the surface) we stated values for *P* of approximately 0.9. This means that the average values for the diameter of the particles, d_z obtained from dynamic light scattering for the armored latex particles need to be corrected with a factor β of 0.73. This is plausible when compensating for the combined effects of the non-spherical geometry of the particle, the thickness of the double layer, and the dispersity of the particle size distribution (**Figure II.5**).

Solid stabilized emulsions of methyl methacrylate (MMA) and *n*-butyl acrylate (BA) monomers were also investigated with overall MMA and silica contents of 5.1 wt% and 5.7 wt%, respectively and overall BA and silica contents of 8.9 wt% and 8.3 wt%, respectively. Cryo-TEM micrographs are displayed in **Figure II.7** clearly showing that in both cases armored polymer latexes were obtained. In the case of BA, particles deformed during deposition onto the cryo-TEM grid as a result of its low glass transition temperature with wetting of the grid by the polymer and potential rearrangement of more hydrophilic silica nanoparticles.

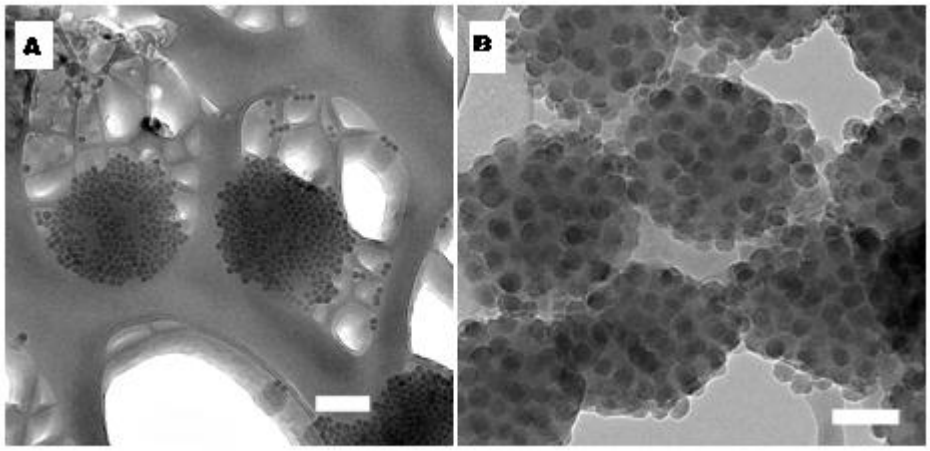

Figure II.7. On the left (**A**) Cryo-TEM images of BA and MMA on the right (**B**) latexes prepared in batch emulsion polymerization in presence of Ludox TM-40 colloidal silica. PMMA-TM40 and BA-TM40 cryo-TEM (scale bars: 200 and100 nm respectively)

Figure II.8 shows the concentration of silica nanoparticles as a function of monomer conversion, as determined by quantitative disc centrifugation for the PMMA and PBA reaction batches with a silica:monomer ratio of 1.12 and 0.93 respectively. In both cases, data obtained from the emulsion polymerization

shows a drop in nanoparticle concentration in the water phase. This concurs with cryo-TEM analysis of the final polymer latex (**Figure II.7**). (Note: we increase the silica content of pMMA to avoid micro precipitation of the latex solution)

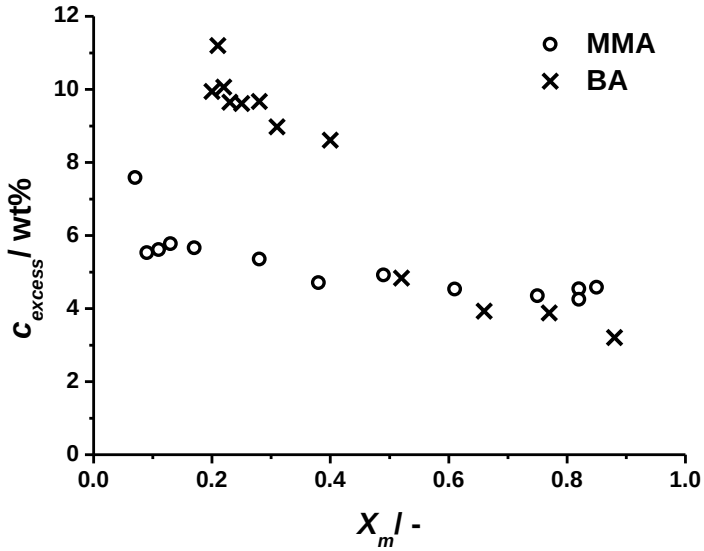

Figure II.8. Graph of the amount in silica nanoparticles, c_{excess}, versus monomer conversion, X_m. [○] Overall contents in MMA and silica are 5.1 wt% and 5.7 wt%, respectively (silica monomer ratio of 1.12). [×] Overall contents in BA and silica are 8.9 wt% and 8.3 wt%, respectively (silica:monomer ratio of 0.93).

In the case of MMA, an interestingly different packing density; a greater "interdistance" between the silica nanoparticles and holes is observed in **Figure II.7B**. This is due to the difference in the wettability between polymer/monomer and electrostatic repulsions between the silica nanoparticles and the surface of the polymer latex particle.

This inter-distance, $x_{int\text{-}d}$, between the edge of two nearby nanoparticles was evaluated from the micrograph to be ~ 10 nm. This can be taken into account in

the coverage calculations to come up with a more realistic value for *P*. When we assume that the only effect is that the particles become "larger", a value of 1.29 for *P* can be obtained using equation 3 as follows with d_{silica} = 24.1 nm:

$$P = 0.909 \frac{(d_{silica} + \mathrm{x}_{\text{int-d}})^2}{d_{silica}^2}$$

Equation II-6

Using the above calculated value of 0.73 for β, yields $P\beta$ = 0.94. We can now use Equation II-5 to calculate values for *C* using experimental values for X_m and d_z with ρ_{polym} = 1.19 g cm^{-3}. The results are presented in **Figure II.9**. An overall good agreement between measured and calculated values for the concentration of silica nanoparticles in the water phase was obtained. The measurements deviate from the calculations at low monomer conversion. At these initial stages the dispersity of the particle size distribution is relatively high (See **Figure II.10**), which has an influence on β and for very small particles also potentially on *P*. Moreover, experimental values suffer from inhomogeneous sampling, as mentioned before.

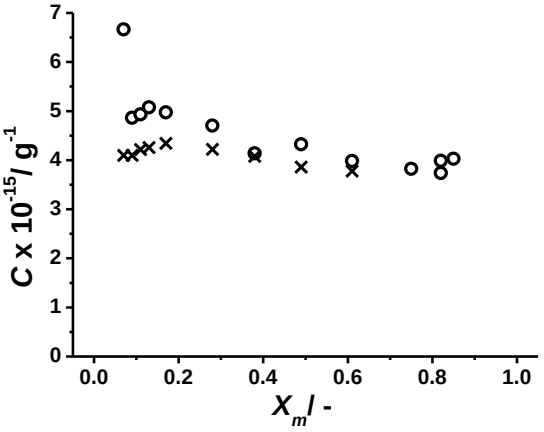

Figure II.9. [○] The measured concentration of silica nanoparticles in the water phase, *C*, versus monomer conversion, X_m, as measured by quantitative disc centrifugation for the solids stabilized emulsion polymerization of methyl methacrylate (5.1 wt% MMA and 5.7 wt% silica). [×] The calculated values for *C* using $P\beta = 0.94$ and experimental values for X_m and d_z .

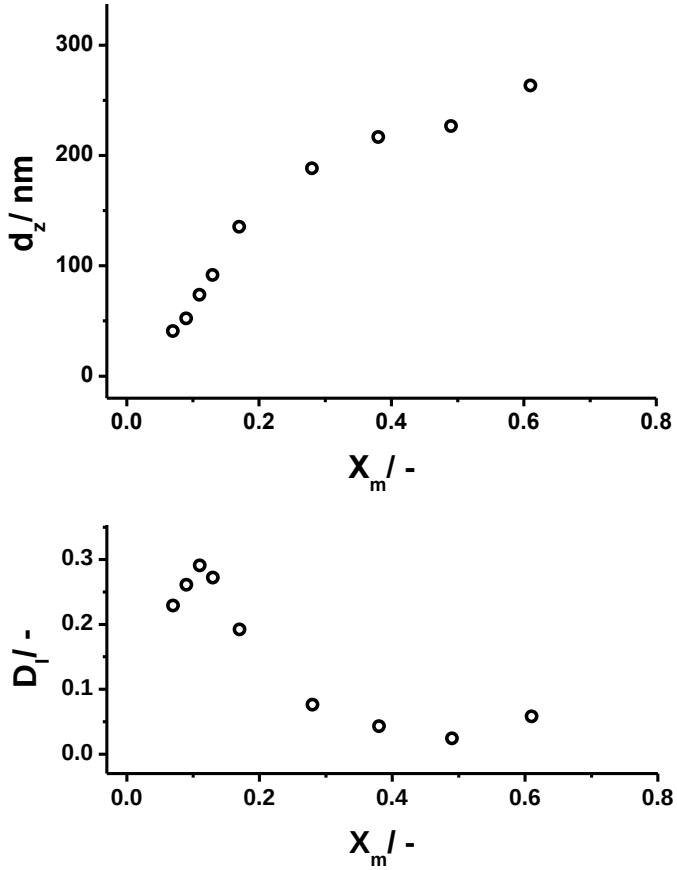

Figure II.10. Graphs of the monomer conversion, X_m, versus average particle size diameter, d_z, (top) and dispersity index, D_I, (bottom) of Ludox-stabilized PMMA polymer particles (silica:monomer ratio of 1.12).

II.4. Conclusions

In this chapter, it was shown that the rate of Pickering emulsion polymerizations stabilized by silica nanoparticles of vinyl esters are faster in comparison with the ones using acrylates as monomers. It was demonstrated that disc centrifugation can be used as a powerful tool to analyze and determine the concentration of nanoparticles in the water phase throughout the polymerization process. The obtained concentration profiles vs. monomer conversion unraveled key mechanistic features in the formation of the raspberry-like armored polymer colloids, such as potential limited coalescence of armored particles in the later stages of the solids-stabilized emulsion polymerization process leading to non-spherical structures. A good correlation was obtained between the measured concentration profiles and our theoretical model, which required a value for the average particle size of the armored latex, experimentally obtained via dynamic light scattering measurements.

II.5. References

(1) Colard, C. A. L.; Teixeira, R. F. A.; Bon, S. A. F., *Langmuir* **2010**, *26*, 7915.

(2) Xue, Z.; Wiese, H., US Patent 7094830, **2003**.

(3) Bauer, F.; Flyunt, R.; Czihal, K.; Buchmeiser, M. R.; Langguth, H.; Mehnert, R., *Macromol. Mater. Eng.* **2006,** *291*, 493-498.

(4) Tiarks, F.; Leuninger, J.; Wagner, O.; Jahns, E.; Wiese, H., *Surf. Coat. Int.* **2007,** *90*, 221-229.

(5) Porter, D.; Metcalfe, E.; Thomas, M. J. K., *Fire Mater.* **2000,** *24*, 45-52.

(6) Wang, T.; Colver, P. J.; Bon, S. A. F.; Keddie, J. L., *Soft Matter* **2009,** *5*, 3842-3849.

(7) Ramsden, W., *Proc. R. Soc. London, Sect. A* **1903,** *72*, 156-164.

(8) Pickering, S. U., *J. Chem. Soc., Trans.* **1907,** *91*, 2001-2021.

(9) Pieranski, P., *Phys. Rev. Lett.* **1980,** *45*, 569-72.

(10) Cheung, D. L.; Bon, S. A. F., *Phys. Rev. Lett.* **2009,** *102*, 066103/1-066103/4.

(11) Balmer, J. A.; Schmid, A.; Armes, S. P., *J. Mater. Chem.* **2008,** *18*, 5722-5730.

(12) Schmid, A.; Fujii, S.; Armes, S. P., *Langmuir* **2005,** *21*, 8103-8105.

(13) Schmid, A.; Fujii, S.; Armes, S. P., *Langmuir* **2006,** *22*, 4923-7.

(14) Schmid, A.; Armes, S. P.; Leite, C. A. P.; Galembeck, F., *Langmuir* **2009,** *25*, 2486-2494.

(15) Tiarks, F.; Landfester, K.; Antonietti, M., *Langmuir* **2001,** *17*, 5775-5780.

(16) Chen, T.; Colver, P. J.; Bon, S. A. F., *Adv. Mater.* **2007,** *19*, 2286-2289.

(17) Cauvin, S.; Colver, P. J.; Bon, S. A. F., *Macromolecules* **2005,** *38*, 7887-7889.

(18) Bon, S. A. F.; Colver, P. J., *Langmuir* **2007,** *23*, 8316-8322.

(19) Fortuna, S.; Colard, C. A. L.; Troisi, A.; Bon, S. A. F., *Langmuir* **2009,** *25*, 12399-12403.

(20) Colver, P. J.; Colard, C. A. L.; Bon, S. A. F., *J. Am. Chem. Soc.* **2008,** *130*, 16850-16851.

(21) Bourgeat-Lami, E., Guimaraes, T. R., Pereira, A. M. C., Alves, G. M., Moreira, J. C., Putaux, J.-L., dos Santos, A. M. *Macromol. Rapid Comm.* **2010**, *31*, 1874-1880.

(22) Sajjadi, S.; Jahanzad, F., *Chem. Eng. Sci.* **2006,** *61*, 3001-3008.

(23) Frelichowska, J.; Bolzinger, M.-A.; Chevalier, Y., *Colloid Surface A* **2009,** *343*, 70-74.

(24) Zhang, K.; Wu, W.; Meng, H.; Guo, K.; Chen, J. F., *Powder Technol.* **2009,** *190*, 393-400.

(25) Zhang, Y.; Chen, H.; Shu, X.; Zou, Q.; Chen, M., *Colloid Surface A* **2009,** *350*, 26-32.

(26) Zhang, Y.; Zou, Q.; Shu, X.; Tang, Q.; Chen, M.; Wu, L., *J. Colloid Interf. Sci.* **2009,** *336*, 544-550.

(27) Wen, N.; Tang, Q.; Chen, M.; Wu, L., *J. Colloid Interf. Sci.* **2008,** *320*, 152-158.

(28) Sheibat-Othman, N.; Bourgeat-Lami, E., *Langmuir* **2009,** *25*, 10121-10133.

(29) Akartuna, I.; Tervoort, E.; Studart, A. R.; Gauckler, L. J., *Langmuir* **2009,** *25*, 12419-12424.

(30) Wang, T.; Keddie, J. L., *Adv. Colloid Interface Sci.* **2009,** *147-148*, 319-332.

(31) Fujii, S.; Okada, M.; Sawa, H.; Furuzono, T.; Nakamura, Y., *Langmuir* **2009,** *25*, 9759-9766.

(32) Yu, C.-L.; Kang, J.-S.; Zhang, F.-A., *J. Macromol. Sci. A* **2009,** *46*, 870-875.

(33) Fitch, R. M., *Polymer Colloids: A Comprehensive Introduction*. Academic Press (1997).

(34) Uricanu, V.; Eastman, J. R.; Vincent, B., *J. Colloid Interf. Sci.* **2001,** *233*, 1-11.

Chapter III.

Pickering Emulsion Polymerization using Laponite Clay as Stabilizer to prepare Armored "Soft" Polymer Latexes

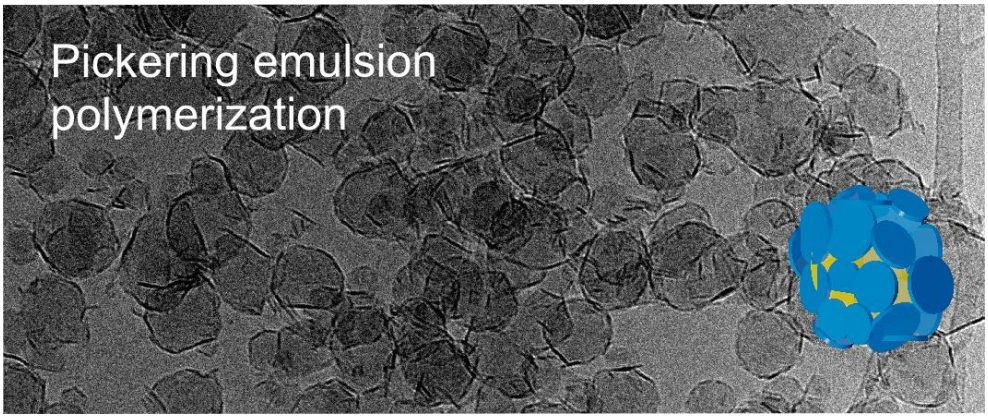

The fabrication of "soft" nanocomposite clay armored polymer latexes is described. Laponite clay XLS is used as the stabilizer in the Pickering emulsion polymerization of a variety of monomer mixtures, of methyl methacrylate and *n*-butyl acrylate, styrene and *n*-butyl acrylate, and styrene and 2-ethyl hexyl acrylate. Overall solids contents of up to 24wt% are reported under batch conditions. Key mechanistic aspects of the Pickering emulsion polymerization process are discussed. The use of monomers that have high water solubility and are prone to hydrolyze under basic conditions, for example methyl methacrylate, should be restricted. The use of small amounts of methacrylic acid as an auxiliary monomer promotes clay adhesion to the surface of the particles in the Pickering emulsion (co)polymerization of hydrophobic monomers. Detailed kinetic studies at both 60 and 80 °C of the Pickering emulsion copolymerization

of styrene and *n*-butyl acrylate (Sty:BA = 0.67 wt/wt) are reported, with varying amounts of Pickering stabilizer. The Laponite clay discs play a crucial role in the particle formation (nucleation) stage of the Pickering emulsion polymerization process. Use of increasing amounts leads to smaller average particle sizes, but inflicts longer nucleation periods hereby broadening the particle size distributions. Catastrophic coagulation phenomenon for Pickering emulsion polymerizations carried out at a low initiator (ammonium persulfate) flux at 60 °C is reported, for a small window of concentrations of Laponite clay discs.

Part of this work was published

Teixeira, R.F.A.; McKenzie, S.; Boyd, A.; Bon, S.A.F., *Macromolecules*, **2011**, 44, 7415-7422

III.1. Introduction

Waterborne nanocomposite polymer colloid formulations are of increasing interest as a base for fabrication of hybrid materials with tailored features of nanoscale dimensional characteristics that enhance material properties and performance. [1-4]A straightforward way to such formulations is to blend colloidal components into a water-based dispersion in which the individuality of the premade colloidal particles is preserved. Orientation of the colloidal components takes place at a subsequent processing or application step, for example during film formation of a waterborne polymer latex coating.[5] A more exotic example following this approach is the fabrication of a nanocomposite open cellular conductive foam to be used as a gas sensor by freeze-drying a mixture of colloidal carbon black, nanoparticles of silica, and a "soft" polymer latex.[6] Whereas a certain extent of spatial control of colloidal components can be achieved in these cases, there is a clear need for better control of nanocomposite morphology. A clear and illustrative example is the impressive enhancement of tack adhesion energy of a waterborne pressure sensitive adhesive upon addition of a small quantity of "soft" polymer latex particles which are armored with nanosized clay discs.[7] A simple blend of colloidal components did not lead to improvements, showing that the armored hybrid particle morphology was essential. Waterborne "soft" polymer latexes armored with silica or clay particles can form transparent nanocomposite polymer films, with a continuous honeycomb network of the inorganic nanoparticles.[8-10] When we restrict ourselves to binary colloidal systems, ways to achieve armored supracolloidal

structures is the assembly of small particles onto a central larger colloidal object, a process traditionally referred to as heterocoagulation.[3]

An interesting strategy towards polymer latexes armored with inorganic nanoparticles is to synthesize the polymer particle *in situ*. Not only does this approach reduce product formulation steps, it also can potentially alleviate the issue of the necessary diluted conditions of traditional heterocoagulation processes. One attractive way to achieve this goal is to make use of Pickering stabilization, the phenomenon that solid particles can adhere to soft interfaces hereby reducing the overall interfacial energy of the system. Pioneering work in the synthesis of armored polymer colloids through Pickering suspension polymerization was reported by Hohenstein and coworkers in the 1940s.[11,12] This concept was taken up and built upon in the last few years by us and others to fabricate a raft of armored micron-sized colloidal structures.[13-18] Miniaturization of this concept to polymerize Pickering stabilized emulsion droplets has lead to the development of Pickering miniemulsion polymerization as a tool to fabricate armored nanocomposite polymer latexes of submicron particle size.[19-24] Drawbacks of this technology is that a high shear emulsification step is required to fabricate the small Pickering stabilized monomer droplets. An innovation therefore is to assemble the inorganic nanoparticles onto the forming polymer latex particles employing a water-based emulsion polymerization process. Armes demonstrated the fabrication of poly(methyl methacrylate)-silica armored nanocomposite particles in aqueous alcoholic media in a single polymerization step without the need for pre-emulsification.[25] They extended their approach to a full waterborne system using a glycerol-modified silica sol as Pickering stabilizer.[26] Sacanna showed the

spontaneous emulsification of methacryloxypropyltrimethoxysilane in the presence of silica nanoparticles in water,[27] and reported seeded polymerization of methyl methacrylate onto the armored particles.[28] We reported on the Pickering emulsion polymerization using silica nanoparticles in water for a variety of monomers under batch emulsion polymerization conditions,[29] and undertook a mechanistic study on the fate of the nanoparticles measuring their concentration in the water phase throughout the Pickering emulsion polymerization process.[30] Bourgeat-Lami and coworkers demonstrated that the use of poly(ethylene glycol)methacrylate as auxiliary comonomer promoted the adhesion of silica nanoparticles in the Pickering emulsion polymerization of styrene.[31] Dos Santos and coworkers used the same auxiliary approach in the Pickering emulsion copolymerization of styrene and *n*-butyl acrylate using Laponite clay discs as stabilizer.[32]

Herein, we report on our studies on the Pickering emulsion copolymerization of a variety of monomer mixtures stabilized by Laponite XLS clay discs. Our strategy was to focus on the preparation of "soft" polymer latexes armored with clay discs for potential use in the coatings, polymer films, and adhesive industries. We take a mechanistic approach to discuss our results in order to shine a further light on the mechanism of Pickering emulsion polymerization.

III.2. Experimental part

Materials: All monomers, methyl methacrylate (MMA), *n*-butyl acrylate (BA), styrene (Sty), methacrylic acid (MA) and 2-ethyl hexyl acrylate (2-EHA) were purchased from Aldrich at 99 % or greater purity and used as received. Laponite Clay XLS (synthetic disc shaped layered silicate with 25nm in diameter and 0.92 nm in thickness), density of ρ_{clay} = 2.57 g cm^{-3} was kindly donated by Rockwood Additives Ltd. Ammonium persulfate (APS, 99+% p.a) and potassium persulfate (KPS, 99+% p.a.) were obtained from Sigma-Aldrich. Deionized water was used in all experiments.

Equipment: Emulsion polymerizations were carried out in double-walled cylindrical glass reactors (250 mL, Asynt Ltd.) equipped with an external circulating heating bath (Julabo F-25 unit), a condenser, and a four-bladed teflon or metal overhead turbine stirrer fitted at approximately 2 cm from the bottom of the reactor vessel (Cowie Ltd.) typically running at 275 rpm. Average particle sizes and dispersities of the armored latexes were measured by dynamic light scattering using a Malvern Zetasizer Nano (data was analyzed using the CONTIN algorithm). Cryo-TEM analyses were performed on a Jeol 2011 TEM (200KV LaB6) with 2K Gatan Ultrascan camera or on a Jeol 2010F TEM (200KV FEG) with 4K Gatan Ultrascan camera using Lacey-Carbon-Film grids (300 Mesh Cu, Agar Sc. S166-3H). An Analytical Balance (Precisa XT 220A) was used for gravimetry.

Typical solids-stabilized emulsion polymerization (for exact quantities of all polymerizations see Table 1): 2.0 g of Laponite Clay XLS was dispersed in

200.0 g of deionized water in a 250 mL double-walled glass reactor and placed under a nitrogen atmosphere by purging during 15 minutes. Degassed monomer, 20.0 g (10.0 wt%) was added. After 5 minutes, the reaction mixture was heated to 60 ºC, whilst stirring at 275 rpm. The emulsion polymerization was started upon addition of 0.13 g APS dissolved in 2.0 g of water. Monomer conversion was monitored via gravimetry by taking samples of approximately 2.0 g using a syringe.

Typical solids-stabilized cryo-TEM measurements: Cryo-TEM specimens were prepared by quench freezing one sample droplet on a Lacey-Carbon-Film grid (300 Mesh Cu, Agar Sc. S166-3H) in liquid ethane using a controlled humidity chamber.[33] The specimens were then mounted in dedicated cartridges for use in a Jeol 2011 TEM (200KV LaB6) with 2K Gatan Ultrascan camera or on a Jeol 2010F TEM (200KV FEG) with 4K Gatan Ultrascan. The speciments were observed in a liquid nitrogen environment.

Table III-1. Pickering emulsion copolymerizations for different ratios of MMA:BA stabilized by Laponite clay XLS.

Sample	MMA g	BA/ g	MMA: n-(BA) ratio/ -	Laponite Clay /g	Water/ g	Initiator/ g	Overall monomer content/ wt%	Clay: monomer/ $g \times g^{-1}$
RT-2-40	5.92	2.60	2.28	2.02	227.1	0.11	3.6	0.24
RT-2-41	2.52	5.95	0.42	1.99	221.8	0.11	3.6	0.24
RT-2-42	4.27	4.31	0.99	2.03	223.3	0.12	3.7	0.26
RT-2-43	3.41	5.12	0.67	2.02	224.2	0.11	3.6	0.24

Table III-2. Pickering emulsion copolymerizations of various monomers stabilized by Laponite clay XLS.

Sample	Monomers	Mo1	Mo2	Laponite Clay/ g	Water /g	Initiator /g	Overall monomer content/ wt%	Clay: monomer / g×g^{-1}
RT-2-44	Sty+BA	8.00	12.01	2.01	200.0	0.14	9.0	0.10
RT-2-25	MMA+BA	3.36	5.16	2.02	219.9	0.13	3.7	0.24
RT-2-21	Sty+2-EHA	8.08	12.16	2.07	202.5	0.13	9.0	0.10

Note: The reaction RT-2-21, an additional amount of 0.21 of MA and 0.19 of β-cyclodextrin were added.

Table III-3. Pickering emulsion colymerizations of Sty:BA using different amounts of Laponite clay XLS at 80°C.

Sample	Sty g	BA g	Sty: n-(BA) ratio/ -	Laponite Clay g	Water g	Initiator g	Overall monomer content/ wt%	Clay: monomer/ g×g^{-1}	Clay: water mg/g
RT-2-50	8.41	13.65	0.61	2.08	207.1	0.14	9.5	0.0940	10.04
RT-2-52	8.16	13.18	0.62	1.04	204.9	0.14	9.4	0.0490	5.08
RT-2-51	8.37	12.59	0.66	0.52	201.7	0.14	9.4	0.0250	2.58
RT-2-54	8.34	12.5	0.67	0.22	204.0	0.14	9.3	0.0110	1.08
RT-2-56	8.12	12.13	0.67	0.14	204.3	0.14	9.0	0.0068	0.69
RT-2-55	8.27	12.06	0.69	0.078	202.8	0.13	9.1	0.0038	0.38
RT-2-57	8.55	12.65	0.68	0.046	207.8	0.13	9.2	0.0022	0.22
RT-2-53	8.29	12.35	0.67	0	206.3	0.14	9.1	0	0

Table III-4. Pickering emulsion copolymerizations of Sty:BA using different amounts of Laponite clay XLS at 60°C.

Sample	Sty g	BA g	Sty:n-(BA) ratio/-	Laponite Clay/g	Water g	Initiator g	Overall monomer content/ wt%	Clay: monomer/ $g \times g^{-1}$	Clay: water mg/g
HM-1	8.05	12.05	0.67	0	198.4	0.14	9.2	0	0
HM-2	8.05	12.07	0.67	0.10	199.0	0.14	9.2	0.0040	0.50
HM-3	8.02	12.09	0.66	0.20	199.0	0.14	9.2	0.0090	1.01
HM-4	8.05	12.00	0.67	0.50	198.5	0.14	9.1	0.0250	2.52
HM-5	8.05	12.01	0.67	0.70	198.2	0.14	9.2	0.0350	3.53
HM-6	8.06	12.01	0.67	1.00	198.4	0.14	9.1	0.0498	5.04
HM-7	8.00	12.10	0.66	2.00	199.0	0.14	9.1	0.0994	10.05

III.3. Results and Discussion

The aim of this study was to investigate the Pickering emulsion copolymerization of mixtures of monomers, that is styrene/*n*-butyl acrylate, methyl methacrylate/*n*-butyl acrylate, and styrene/2-ethyl hexyl methacrylate, using Laponite XLS clay discs as stabilizer. The reason for these combinations of monomers is to tailor the predicted glass transition temperature of the copolymer to be below room temperature to allow for film formation under ambient conditions (using the Fox equation to calculate a predictive value for T_g). This would allow for easy fabrication of waterborne nanocomposite polymer films with potentially interesting mechanical and physical properties.[9,10] In our previous studies on Pickering emulsion polymerization we used spherical nanoparticles of silica (Ludox). Conceptually we were interested

in replacing these spherical nanoparticles with Laponite, as the clay nanoparticles were of different geometry. Laponite Clay XLS are disc-shaped crystals of specific density of ρ_{clay} = 2.57 g cm^{-3}, lateral diameter of ca. 25 nm and approximately 0.92 nm in thickness (h).[34,35] Laponite Clay XLS is a synthetic layered silicate with low heavy metal content which contains a small quantity of blended tetrasodium pyrophosphate. The added tetrasodium pyrophosphate allows for easy sol formation preserving a relatively low overall viscosity as the pyrophosphate anions associate onto the positively charged edges of the Laponite clay disc, inducing charge inversion. The difference in geometry of the Laponite clay discs with respect to spherical nanoparticles of silica (Ludox TM40 with R = 12.03 nm, and ρ_{silica} = 1.75 g cm^{-3}),[21,30] and hence the difference in surface-to-volume ratio being (3/R) for a sphere and (2/h) for a clay disc, allows for a marked reduction in the total amount required to fabricate armored hybrid polymer latex particles and nanocomposite coatings and films thereof (this despite the counter-effect of the difference in densities between the two different inorganic nanoparticles).

In our previous works on Pickering emulsion polymerization using silica nanoparticles as stabilizer we discussed that the mechanism for formation of the armored particles involved heterocoagulation between a growing latex particle and inorganic nanoparticles.[29,30] In this process the inorganic nanoparticle effectively adheres onto the surface of the growing polymer latex particle. The strength of this adhesion undoubtedly relies on the chemical nature of the polymer particle. We therefore wanted to establish first what polymer composition of the growing latex particles would warrant successful heterocoagulation throughout the Pickering emulsion polymerization process. In

other words to which particles would the Laponite clay discs adhere successfully? From our studies using Ludox silica nanoparticles in which we monitored the concentration of nanoparticles in the water phase throughout the Pickering emulsion polymerization process we found that there had to be sufficient affinity between the hydrophilic silica-based surface of the nanoparticle and the surface composition of the latex particle. The surface of the latex particle had to be relatively hydrophilic. Pickering emulsion polymerizations of hydrophobic monomers such as vinyl pivalate,[30] *n*-butyl methacrylate and styrene[29] resulted in stable effectively "bare" latexes, not having the targeted armored structure. In the Pickering emulsion polymerizations of more hydrophilic monomers, such as methyl or ethyl methacrylate and vinyl acetate, it was essential to lower the pH of the water phase. All Pickering emulsion polymerizations carried out with methyl methacrylate at pH 8-10 resulted in coagulation, the coagulum showing a mixture of "bare" latex particles and silica nanoparticles. Lowering the pH of Laponite sols to pH 5.5 or less unfortunately is not an option as the clay sol gels after about 20 min at room temperature. Pickering emulsion polymerizations in the presence of Laponite XLS without adjustment of the pH, and thus under basic conditions, of vinyl acetate and methyl methacrylate at a monomer-to-water ratio of 0.1 wt/wt, and a clay-to-monomer ratio of 0.1 wt/wt at 60 °C using 0.13 g of ammonium persulfate as initiator, resulted in complete micro-coagulation. A potential reason is the substantial hydrolysis of the monomer throughout the polymerization process, as the water solubility of both these monomers is high in conjunction with the methyl and acetate moieties being good leaving groups for base-catalyzed hydrolysis. The logic of this is

strengthened in that Pickering emulsion polymerization of ethyl methacrylate and *n*-butyl methacrylate using Laponite XLS clay discs as stabilizer under these conditions were successful. It therefore is important to restrict the use of monomers which have a relatively high water solubility and that can easily be hydrolyzed in water under basic conditions. This is further emphasized by our series of experiments in which we carried out the Pickering emulsion copolymerization of methyl methacrylate and *n*-butyl acrylate (**Table III-1**). We had to reduce the monomer-to-water ratio to values of approximately 0.038 wt/wt as all reactions carried out at higher ratios led to coagulation. Under these diluted conditions the ratio of MMA:BA was varied being 0.42, 0.67, 0.99, 2.28 wt/wt respectively. Only the two reactions with the lowest relative amount of MMA were successful, with MMA:BA of 0.42 and 0.67 respectively. **Figure III.2A** shows a cryo-TEM image for the armored polymer latex obtained by Pickering emulsion copolymerization of an MMA:BA ratio of 0.67. It is clear from this image that the Laponite clay discs are adhered to the surface of the "soft" latex particles. The overall rate of polymerization was the highest for the reaction with the higher amount of MMA. Average values for the particle sizes are of the same order of magnitude (See **Figure III.1** for monomer conversion *vs.* time plots and average particle diameter and dispersity *vs.* monomer conversion). Initially this result seems counter-intuitive as the rate coefficient of propagation of BA is markedly higher than that of MMA. The reason for the lower rate of polymerization in the BA rich Pickering emulsion polymerization is the result of diffusion limitation of monomer transport through the water phase and thus monomer entry into the latex particles.[36]

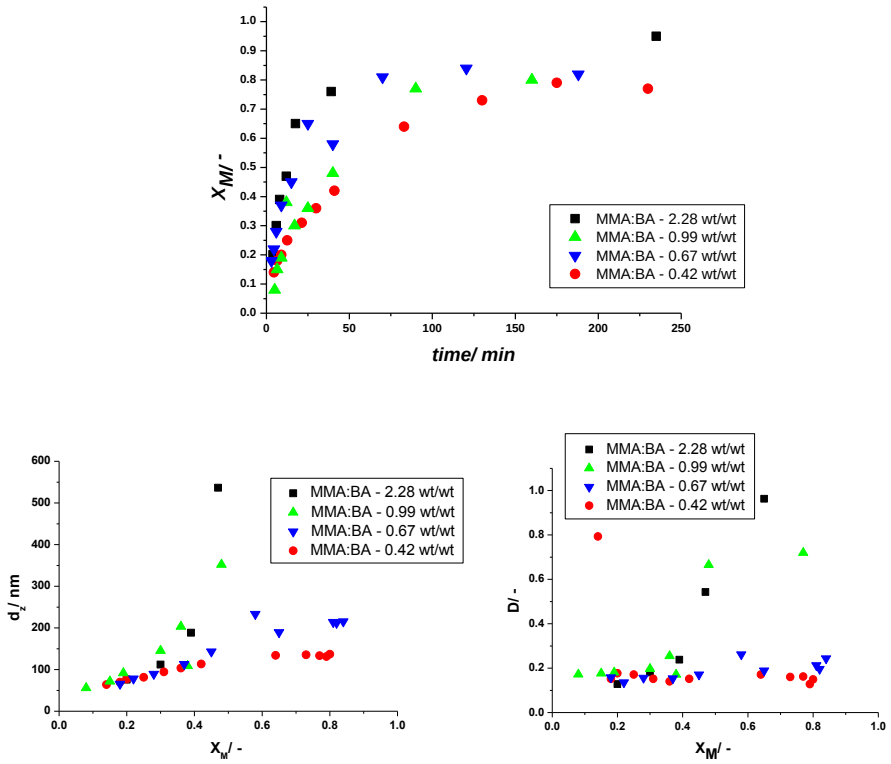

Figure III.1. Pickering emulsion polymerization of MMA:BA wt/wt ratios of 2.28, 0.99, 0.67, 0.42 stabilized with Laponite clay (clay:monomer weight ratio of *ca*. 0.11). On top: overall monomer conversion (X_M) versus time (min); bottom left: monomer conversion (X_M) versus average particle size (d_z) and right bottom: monomer conversion (X_M) versus dispersity (D). See recipes in Table 2.

The issues and polymerization restrictions faced with using MMA led us to investigate alternative monomer combinations, replacing MMA with styrene. Pickering emulsion copolymerization of styrene and *n*-butyl acrylate (Sty:BA = 0.67 wt/wt) were successful up to 24 wt% overall solids under batch conditions at 80 °C (200.0 g water, 60.0 g monomer, 2.00 g clay, 0.12 g APS), all leading to the formation of the targeted Laponite clay armored "soft" polymer latex

particles (See **Figure III.2**B for a cryo-TEM image). The Pickering emulsion copolymerization of styrene and 2-ethyl hexyl acrylate (Sty:EHA = 0.67 wt/wt) was also investigated at 60 °C. As observed also in the Pickering emulsion polymerizations stabilized with Ludox silica nanospheres,[29,30] these hydrophobic monomers did not lead to substantial adhesion of the clay platelets on the surface of the particles. This is clearly evident from the cryo-TEM analysis (**Figure III.2**C), which shows that the majority of latex particles do not have any clay discs stuck onto their surface. To overcome this restriction and promote adhesion onto the surface of the latex particles a small amount of methacrylic acid (1.04 wt% based on total amount of monomer) was added as functional hydrophilic comonomer, as part of the Pickering emulsion polymerization recipe. Cryo-TEM analysis now undoubtedly shows the desired clay armored supracolloidal morphology (**Figure III.2**D). This approach is in line with the one reported by Bourgeat-Lami who employed poly(ethylene glycol) methacrylate as an auxiliary monomer the promote the adhesion of Pickering stabilizers in the emulsion polymerization of styrene.[31] To facilitate transport of the hydrophobic monomers through the water phase during the Pickering emulsion polymerization process β-cyclodextrin was used as a carrier.[37,38] Auxiliary monomers, such as poly(ethylene glycol) methacrylate and methacrylic acid, may promote adhesion of clays (and other silicates and metal oxides) through hydrogen bond interaction. On the other hand, the depth of the energy well as accomplished through minimization of the total interfacial free energy (following the classical description of Pickering stabilization) potentially is lowered as the interfacial tension between the latex particle and the water drops substantially when higher amounts of these hydrophilic monomers are

used. Note that *in situ* hydrolysis of monomer (see before in case of Laponite clay stabilized Pickering emulsion polymerizations using MMA) or polymer during or after polymerization can also contribute in changing the chemical composition of the surface of the latex particles. The obvious unanswered question that remains is how much of these auxiliary monomers or better functional auxiliary surface functional groups is needed to optimize the fabrication of the armored nanocomposite latexes?

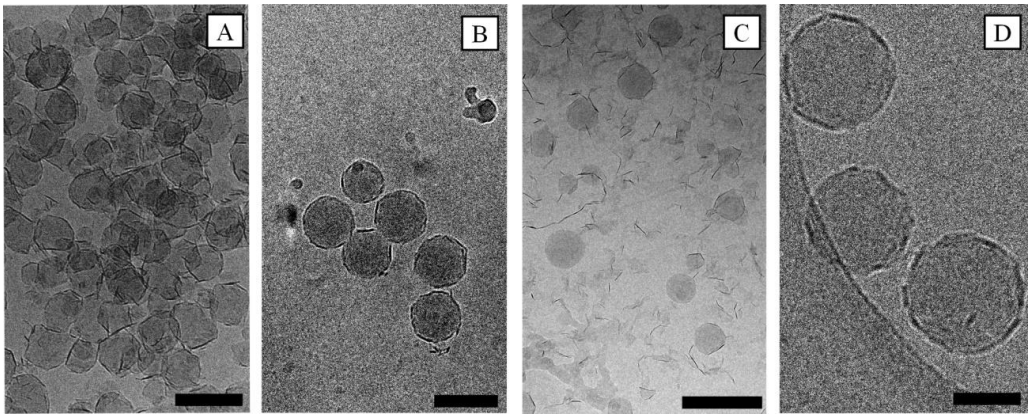

Figure III.2. Cryo-TEM images of polymer latex particles. **A**: poly(MMA-*co*-n-(BA)/Laponite, **B**: poly(Sty-*co*-BA)/Laponite, **C**: poly(Sty-*co*-2-EHA)/Laponite, **D**: poly(Sty-*co*-2-EHA)/Laponite with methacrylic acid. Scales bars of 100nm, 100nm, 200nm and 50 nm respectively.

Next we wanted to investigate whether the heterocoagulation process not only occurred during the growth stage of the polymer latex particles, but also if it played a role in the nucleation phase of the Pickering emulsion polymerization process, as we suggested in our earlier work.[29] If affirmative, varying the amount of Laponite clay would have a pronounced effect on the particle size distribution of the hybrid latexes obtained by the Pickering emulsion polymerization process. We previously demonstrated that in the case of

Pickering miniemulsion polymerizations indeed the particle size distribution was influenced by the total amount of Laponite clay used and that the average particle size could be predicted theoretically.[20] To probe the effect of the amount of Laponite clay discs used in Pickering emulsion polymerization we carried out two series of copolymerizations of styrene and *n*-butyl acrylate, at Sty:BA ratio of *ca.* 0.67, at both 60 °C and 80 °C in which we varied the relative amounts of Laponite clay. For the clarity of the discussion of the results we will first addressed the reactions performed at 80 °C.

Figure III.3 displays the results of overall monomer conversion, X_M, as function of time as measured using gravimetry (for the data see appendix of Chapter III). From a qualitative viewpoint the overall rate of polymerization (obtained from the 1st derivative of this plot) is increased when larger amounts of clay are employed as Pickering stabilizer, though the effect was not big. The enhancement in overall polymerization rate upon increasing amounts of clay suggests an increase in the total amount of particles, and hence smaller particles at the same value for X_M, as the rate in emulsion polymerization systems is proportional to the total amount of particles, as a direct result of compartmentalization.

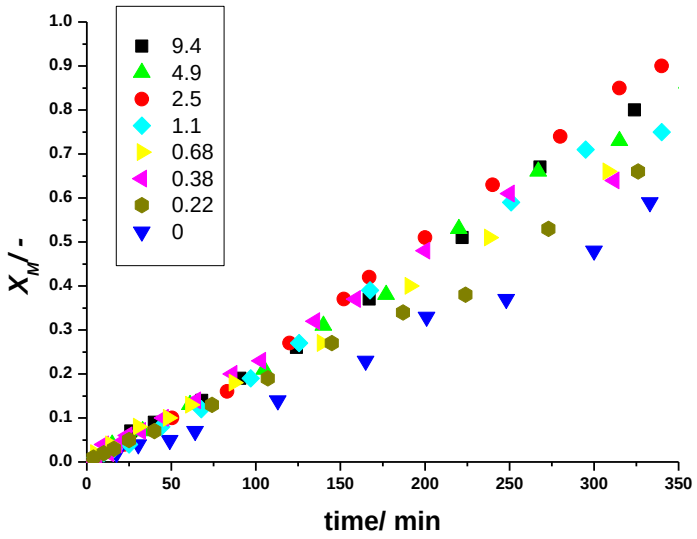

Figure III.3. Overall monomer conversion, X_M, *versus* time for Pickering emulsion copolymerizations of styrene and *n*-butyl acrylate (at Sty:BA weight ratio of *ca.* 0.67) at 80 °C for varying amounts of Laponite XLS clay discs used as Pickering stabilizer (clay:monomer weight ratios ($\times 10^2$) of 9.4, 4.9, 2.5, 1.1, 0.68, 0.38, 0.22, 0)

The average particle diameter, d_z, and the corresponding dispersity of the particle size distribution, D, were measured by dynamic light scattering (DLS) as a function of monomer conversion (X_M) (See **Figure III.4** and **Figure III.5**, respectively). Substantial effects of varying the amount of Laponite XLS clay as Pickering stabilizer were found.

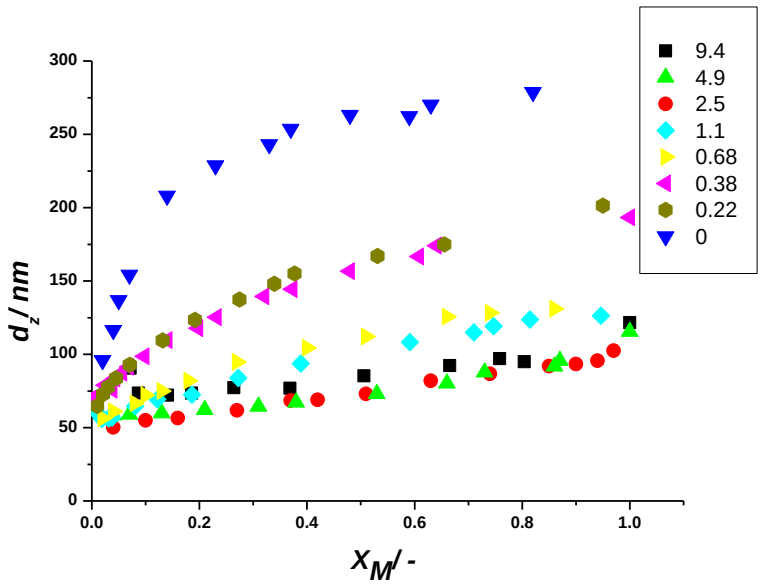

Figure III.4. Average particle size diameter, d_z, versus overall monomer conversion, X_M, measured with dynamic light scattering (DLS) throughout the Pickering emulsion copolymerization of styrene and *n*-butyl acrylate (at Sty:BA weight ratio of *ca.* 0.67) at 80 °C for varying amounts of Laponite XLS clay discs used as Pickering stabilizer (clay:monomer weight ratios ($\times 10^2$) of 9.4, 4.9, 2.5, 1.1, 0.68, 0.38, 0.22, 0)

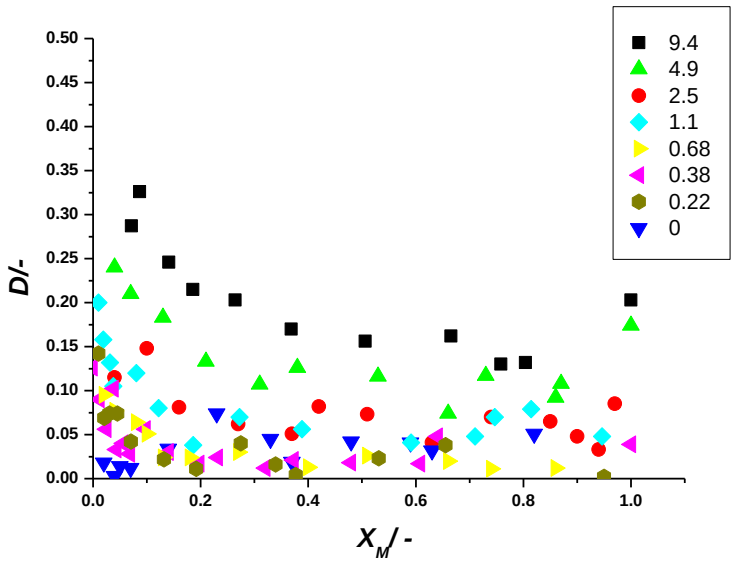

Figure III.5. Dispersity of the particle size distributions, *D*, versus overall monomer conversion, X_M, measured with dynamic light scattering (DLS) throughout the Pickering emulsion copolymerization of styrene and *n*-butyl acrylate (at Sty:BA weight ratio of *ca.* 0.67) at 80 °C for varying amounts of Laponite XLS clay discs used as Pickering stabilizer (clay:monomer weight ratios ($\times 10^2$) of 9.4, 4.9, 2.5, 1.1, 0.68, 0.38, 0.22, 0)

Use of relatively small amounts of clay already led to marked reductions in the particle diameters, in other words addition of clay as a Pickering stabilizer led to a greater number of latex particles. This not only supports the results found on the increase in overall polymerization rates upon increase of the amounts of Pickering stabilizer (See **Figure III.4**), but also it is clear evidence that clay plays an important role in the particle formation stage of the Pickering emulsion polymerization process. Two important observations can be made from **Figure III.4** and **Figure III.5**. One is that reduction in particle size upon increase of the amounts of Laponite clay as Pickering stabilizer does not correlate in a straightforward manner. This becomes more evident when we plot the final average particle size of the polymer latexes as a function of the weight ratio of clay:monomer (see **Figure III.6**). From this Figure it is apparent that the influence of the amounts of clay used on the average particle size phases out rapidly to a approximate lower values of 120 nm (0.094 of clay:monomer weight ratio). From **Figure III.5** it can be observed that the dispersity of the particle size distributions increases upon greater amounts of clay as Pickering stabilizer used in the emulsion polymerizations. The values for *D* gradually decrease upon increase in X_M, which is logical. The increase in values for *D*

upon increasing the amount of clay Pickering stabilizer suggests a prolongation of the nucleation period (particle formation) in these emulsion polymerization reactions. This is plausible as a greater number of Pickering nanoparticles in the water phase would lead to an increase in probability for the events of heterocoagulation of a clay disc with a precipitating oligomer of critical chain-length from the waterphase or with a colloidally unstable primary latex particle. If it is assume a short nucleation period leading to rapid formation of a stable and constant number of growing latex particles, plotting the data of **Figure III.4** as d_z^3 versus X_M must show a linear behavior. **Figure III.7** clearly shows this is the case (up to intermediate values for X_M) for the emulsion copolymerizations in absence of clay and those with a weight ratio of clay:monomer of 0.0022 and 0.0038. Looking more closely at the data convex deviations are found for Pickering emulsion polymerizations operated at higher amounts of Laponite clay. Continuous generation of particles leads to a slower growth rate per particle. The particle formation process slows down and eventually ceases, which does explain the convex trend observed for d_z^3 versus X_M. From **Figure III.7** it can be seen that this behavior extends to higher values of X_M when more Laponite clay discs are used as Pickering stabilizer. This reaffirms that indeed longer nucleation periods occur in Pickering emulsions polymerizations using larger amounts of Laponite clay as stabilizer, with broader particle size distributions of the latexes as a consequence (as observed in **Figure III.5**).

One question we could ask is how much Laponite clay discs remain in the water phase after the armored polymer latexes have been fabricated? Whereas for Pickering stabilizers such as Ludox silica nanospheres this can be measured directly through quantitative disc centrifugation.[30] This technique was

unfortunately not successful for clay nanodiscs because the clay discs did not have sufficient gravitational drag. Nevertheless we can get an idea by taking the ratio of the total effective surface area provided by the Laponite clay discs (assuming monodisperse discs, and a square packing geometry) and the total surface area of the latex particles made (assuming monodisperse spherical particles). This ratio can be calculated from: [20]

$$\frac{A_{clay}^{eff}}{A_{part}} = \frac{2}{3\pi}\left(\frac{d_z}{h}\right)\left(\frac{m_{clay}}{m_{pol}}\right)\left(\frac{\rho_{pol}}{\rho_{clay}}\right)$$

Equation III -1

we further assume complete conversion of monomer so that $m_{pol} = m_{Sty} + m_{BA}$ and use a value of 1.06 g cm^{-3} for the density of the copolymer. The values of the surface ratios are plotted in **Figure III.6**. From this graph it can be seen that complete armored structure of the hybrid polymer "soft" latexes is achieved at a first approximate value of 0.08 for the clay:monomer weight ratio. Use of higher weight ratios will lead to excess of Laponite clay discs in the water phase. This is undesirable as it could have a detrimental effect on the properties of polymer films made from the armored latexes, such as lower transparency, increased brittleness and cracking.

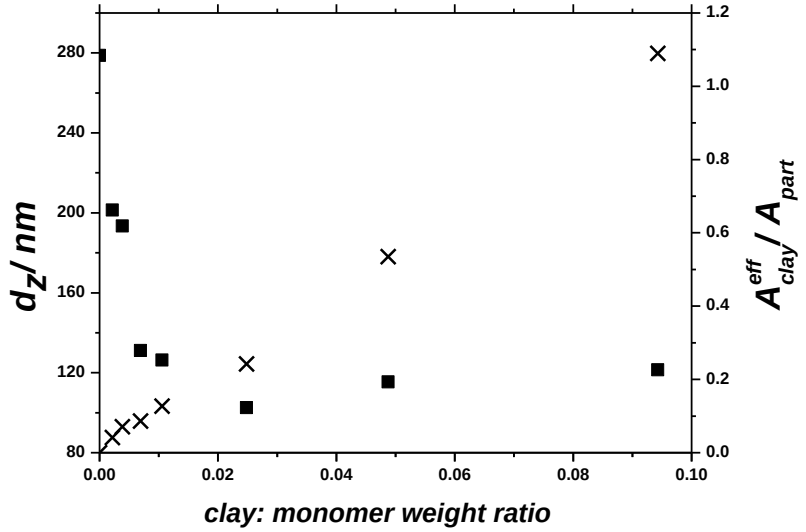

Figure III.6. Average particle size d_z, and ratio of the total effective surface area provided by the Laponite clay discs and the total surface area of the polymer latexes *versus* the weight ratio of clay:monomer for the Pickering emulsion copolymerization of styrene and *n*-butyl acrylate (at Sty:BA weight ratio of *ca.* 0.67) at 80 °C for varying amounts of Laponite XLS clay discs used as Pickering stabilizer (clay:monomer weight ratios ($\times 10^2$) of 9.4, 4.9, 2.5, 1.1, 0.68, 0.38, 0.22, 0)

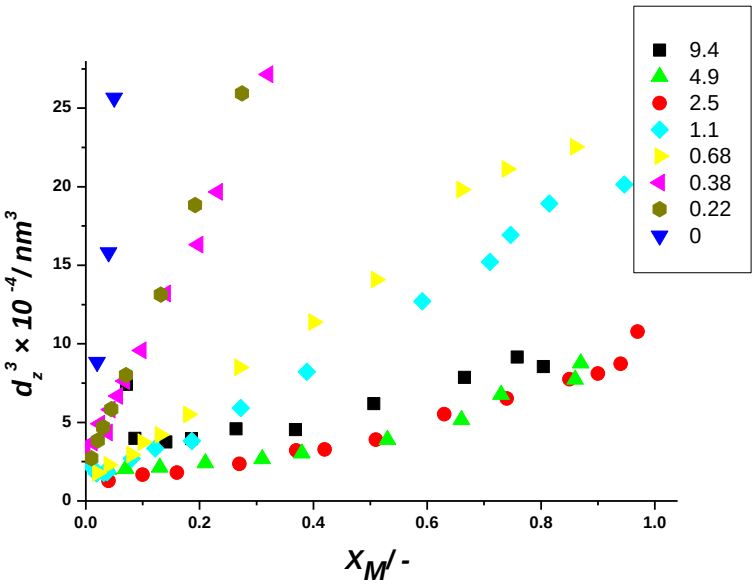

Figure III.7. d_z^3 versus X_M measured with dynamic light scattering (DLS) throughout the Pickering emulsion copolymerization of styrene and *n*-butyl acrylate (at Sty:BA weight ratio of *ca.* 0.67) at 80 °C for varying amounts of Laponite XLS clay discs used as Pickering stabilizer (clay:monomer weight ratios ($\times 10^2$) of 9.4, 4.9, 2.5, 1.1, 0.68, 0.38, 0.22, 0)

Pickering emulsion copolymerizations of styrene and *n*-butyl acrylate (at Sty:BA weight ratio of *ca.* 0.67) at 60 °C using various amounts of Laponite XLS clay discs used as Pickering stabilizer (clay:monomer weight ratios ($\times 10^2$) of 0.4, 0.9, 2.5, 3.5, 5.0, 9.9) showed in general similar behavior in that faster polymerization rates were observed, with smaller particle sizes and broader dispersities in particle size distributions, upon increasing amounts of Laponite clay used (**Figure III.8**).

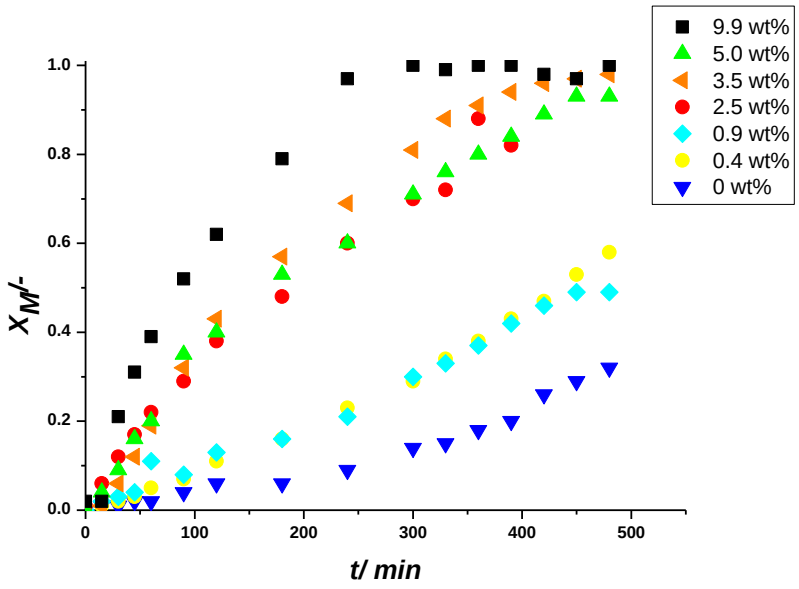

Figure III.8. Overall monomer conversion, X_M, *versus* time for Pickering emulsion copolymerizations of styrene and *n*-butyl acrylate (at Sty:BA weight ratio of *ca.* 0.67) at 60 °C for varying amounts of Laponite XLS clay discs used as Pickering stabilizer (clay:monomer weight % ratios of 0.4, 0.9, 2.5, 3.5, 5.0, 9.9).

There was, however, one drastic difference which becomes apparent from the average particle diameter, d_z, and the corresponding dispersity of the particle size distribution, D, data as measured measured by dynamic light scattering (DLS) as a function of monomer conversion (X_M) (See **Figure III.9** and **Figure III.10**, respectively).

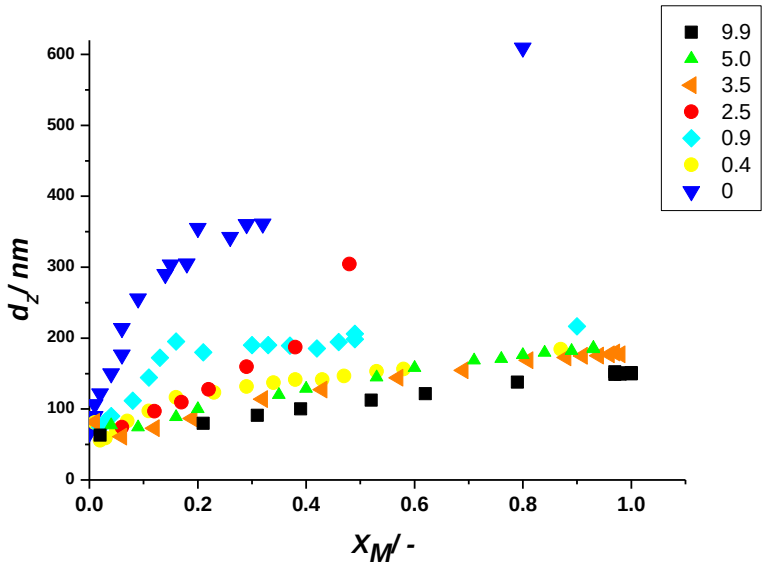

Figure III.9. Average particle size diameter, d_z, versus overall monomer conversion, X_M, measured with dynamic light scattering (DLS) throughout the Pickering emulsion copolymerization of styrene and *n*-butyl acrylate (at Sty:BA weight ratio of *ca.* 0.67) at 60 °C for varying amounts of Laponite XLS clay discs used as Pickering stabilizer (clay:monomer weight ratios ($\times 10^2$) of 0.4, 0.9, 2.5, 3.5, 5.0, 9.9)

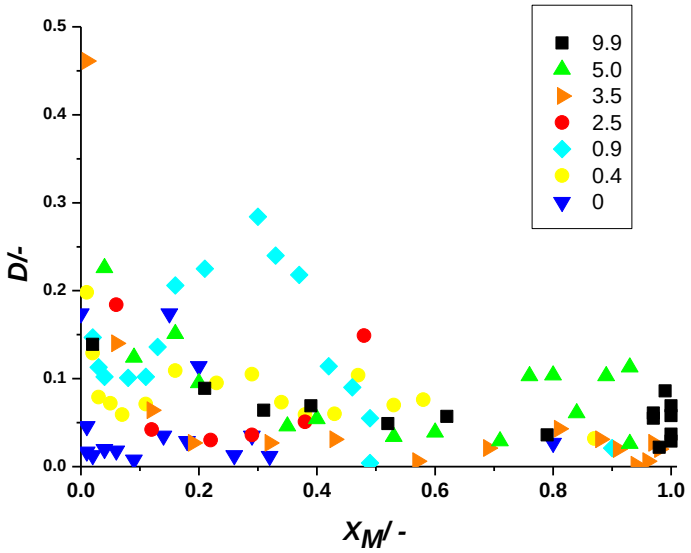

Figure III.10. Dispersity of the particle size distributions, *D*, versus overall monomer conversion, X_M, measured with dynamic light scattering (DLS) throughout the Pickering emulsion copolymerization of styrene and *n*-butyl acrylate (at Sty:BA weight ratio of *ca.* 0.67) at 60 °C for varying amounts of Laponite XLS clay discs used as Pickering stabilizer (clay:monomer weight ratios ($\times 10^2$) of 0.4, 0.9, 2.5, 3.5, 5.0, 9.9)

When intermediate amounts of clay were used, that is clay:monomer weight ratios of 0.009 and 0.025, colloidal instabilities during the emulsion polymerization process occurred. In the latter case this lead to full coagulation of the reaction at an onset of approximately 40% overall monomer conversion. From **Figure III.9** this is seen as a rapid increase in the average measured values of d_z. The case of 0.009 is more interesting. Limited coagulation throughout the early stages of polymerization was observed up to approximately 30% monomer conversion, after which the system regained colloidal stability. In (**Figure III.9**) this is reflected by the initial higher values for d_z than would be expected, on the basis of the data obtained for the experiment in the case the lower 0.004 value for the clay:monomer ratio. After regaining colloidal stability the particle growth proceeds as normal, with a final value of d_z in line with the other stable Pickering emulsion polymerizations. From the dispersity data of the particle size distributions as function of monomer conversion (**Figure III.10**) an increase in *D* can indeed be observed up to approximately 30% monomer conversion which falls in line with partial coagulation of the growing latex particles. After colloidal stability is recuperated values for *D* drop, as expected.

At the current stage we do not have a detailed explanation for the exact nature of this rather catastrophic colloidal instability in these Pickering emulsion polymerizations. What we do know is that the average particle sizes get influenced greatly by using Laponite clay, and do not correlate clearly with the initiator concentration and decomposition, as known for traditional emulsion polymerizations. The flux of radicals generated at 60 °C is about 16-20 times smaller than that at 80 °C.[39,40] It could be that the number of initiator derived hydrophilic end groups, that is sulfate and hydroxy groups, linked to polymer chains play a crucial role in providing sufficient colloidal stability. When a particle grows and creates additional hydrophobic surface it can either gain stability through entry of such an end-capped growing oligomer, through heterocoagulation with a Laponite clay disc serving as Pickering stabilizer, or through coagulation with another growing latex particle. A fine balance exists between these events, and one can envisage that indeed for certain experiments with a low initiator flux and not high concentrations of Laponite clay discs colloidal instabilities can arise. This indeed falls in line with our observations from all our experiments. To test this hypothesis, we carried out two additional Pickering emulsion copolymerizations at clay:monomer weight ratio of 0.025 at increased initiator radical flux. In the first we used 5 times the amount of initiator; in the second we fed a 1 mol equiv of sodium metabisulfite in relation to the amount of ammonium persulfate during the first hour of polymerization. Both polymerizations lead to a reduction in the catastrophic coagulation phenomenon, both showing microcoagulation (the system remained liquid). This indicates that optimization of the initiator flux potentially may alleviate the problem.

III.4. Conclusions

In this chapter, it was shown that hybrid "soft" polymer latexes armored with Laponite XLS clay discs can be prepared by Pickering emulsion polymerization using a variety of monomer mixtures. It is highlighted that it is important to restrict the use of monomers which have a relatively high water solubility and which can easily be hydrolyzed in water under basic conditions, such as methyl methacrylate. It was shown that when hydrophobic monomers are selected, such as in the case of the copolymerization of styrene and 2-ethylhexyl acrylate, the use of small amounts of methacrylic acid as auxiliary monomer promotes clay adhesion to the surface of the particles. In our detailed mechanistic studies of the pickering emulsion copolymerization of styrene and *n*-butyl acrylate (Sty:BA = 0.67 w/w) we showed that overall solids contents of 24 wt % could easily be achieved under batch conditions. We demonstrated that Laponite clay discs as Pickering stabilization played a crucial role in the particle formation (nucleation) stage of the Pickering emulsion polymerization process. Use of increasing amounts of Pickering stabilizer led to smaller average particle sizes but inflicted longer nucleation periods, hereby broadening the particle size distributions. Finally, it was shown that the fine balance which exists between events occurring in the nucleation period could lead to catastrophic colloidal instabilities and thus coagulation for Pickering emulsion polymerizations for a small window of concentrations of Laponite clay discs when carried out at a low initiator flux.

III.5. References

(1) Biswas, M.; Ray, S. S., *Adv. Polym. Sci.* **2001**, *155*, 167-221.

(2) Sanchez, C.; Julián, B.; Belleville, P.; Popall, M., *J. Mater. Chem.* **2005**, *15*, 3559–3592.

(3) Teixeira, R. F. A.; Bon, S. A. F., *Adv. Polym. Sci.* **2010**, *233*, 19-52.

(4) Zou, H.; Wu, S.; Shen, J., *Chem. Rev.* **2008**, *108*, 3893-3957.

(5) Patel, M. J.; Gundabala, V. R.; Routh, A. F., *Langmuir* **2010**, *26*, 3962-3971.

(6) Colard, C. A. L.; Cave, R. A.; Grossiord, N.; Covington, J. A.; Bon, S. A. F., *Adv. Mater.* **2009**, *21*, 2894-2898.

(7) Wang, T.; Colver, P. J.; Bon, S. A. F.; Keddie, J. L., *Soft Matter* **2009**, *5*, 3842-3849.

(8) Amalvy, J. I.; Percy, M. J.; Armes, S. P., *Langmuir* **2001**, *17*, 4770-4778.

(9) Schmid, A.; Scherl, P.; Armes, S. P.; Leite, C. A. P.; Galembeck, F., *Macromolecules* **2009**, *42*, 3721-3728.

(10) Negrete-Herrera, N.; Putaux, J-.L.; David, L.; de Haas, F.; Bourgeat-Lami, E., *Macromol. Rapid Comm.* **2007**, *28*, 1567-1573.

(11) Hohenstein, W. P., *Polym. Bull.* **1945**, *1*, 13−16.

(12) Hohenstein, W. P.; Mark, H., *J. Polym. Sci.* **1946**, *1*, 127−145.

(13) Bon, S. A. F.; Chen, T., *Langmuir* **2007**, *23*, 9527-9530.

(14) Bon, S. A. F.; Cauvin, S.; Colver, P. J., *Soft Matter* **2007**, *3*, 194-199.

(15) Yang, Y.; Zhang, J.; Liu, L.; Li, C.; Zhao, H., *J. Polym. Sci., Part A: Polym. Chem.* **2007**, *45*, 5759-5769.

(16) Duan, L.; Chen, M.; Zhou, S.; Wu, L., *Langmuir* **2009**, *25*, 3467-3472.

(17) Gao, Q.; Wang, C.; Liu, H.; Chen, Y.; Tong, Z., *Polym. Chem.* **2010**, *1*, 75-77.

(18) Salari, J. W. O.; van Heck, J.; Klumperman, B., *Langmuir* **2010**, *26*, 14929-14936.

(19) Cauvin, S.; Colver, P. J.; Bon, S. A. F., *Macromolecules* **2005**, *38*, 7887-7889.

(20) Bon, S. A. F.; Colver, P. J., *Langmuir* **2007**, *23*, 8316-8322.

(21) Fortuna, S.; Colard, C. A. L.; Troisi, A.; Bon S. A. F., *Langmuir* **2009**, *25*, 12399-12403.

(22) Voorn, D. J.; Ming, W.; van Herk, A. M., *Macromolecules* **2006**, *39,* 2137-2143.

(23) Tiarks, F.; Landfester, K.; Antonietti, M., *Langmuir* **2001**, *17*, 5775–5780.

(24) Cao, Z.; Schrade, A.; Landfester, K.; Ziener, U., *J. Polym. Sci., Part A: Polym. Chem.* **2011**, *49*, 2382-2394.

(25) Percy, M. J.; Amalvy, J. I.; Randall, D. P.; Armes, S. P.; Greaves, S. J.; Watts, J. F., *Langmuir* **2004**, *20*, 2184-2190.

(26) Schmid, A.; Tonnar, J.; Armes, S. P., *Adv. Mater.* **2008**, *20*, 3331-3336.

(27) Sacanna, S.; Kegel, W. K.; Philipse, A. P., *Phys. Rev. Lett.* **2007**, *98*, 158301.

(28) Sacanna, S.; Philipse, A. P., *Adv. Mater.* **2007**, *19*, 3824-3826.

(29) Colver, P. J.; Colard, C. A. L.; Bon, S. A. F., *J. Am. Chem. Soc.* **2008**, *130*, 16850-16851.

(30) Colard, C. A. L.; Teixeira, R. F. A.; Bon, S. A. F., *Langmuir* **2010**, *26*, 7915-7921.

(31) Sheibat-Otman, N.; Bourgeat-Lami, E., *Langmuir* **2009**, *25*, 10121-10133.

(32) Bourgeat-Lami, E.; Guimaraes, T. R.; Pereira, A. M. C.; Alves, G. M.; Moreira, J. C.; Putaux, J.-L.; dos Santos, A. M., *Macromol. Rapid Comm.* **2010**, *31*, 1874-1880.

(33) Harris, J.R.; Negative Staining and Cryoelectron Microscopy: The Thin Film Tecniques. Bios Scientific Publishers, Oxford, 1997.

(34) Mongondry, P.; Tassin, J. F.; Nicolai, T., *J. Colloid Interface Sci*. **2005**, *283*, 397-405.

(35) Balnois, E.; Durand-Vidal, S.; Levitz, P., *Langmuir* **2003**, *19*, 6633-6637.

(36) Sajjadi, S.; Jahanzad, F., *Chem. Eng. Sci.* **2006**, *61*, 3001-3008.

(37) Lau, W., US Patent Number 5521266, May 28, **1996**.

(38) Lau, W., *Macromol. Symp.* **2002**, *182*, 283-289.

(39) Kolthoff, I. M.; Miller, I. K., *J. Am. Chem. Soc.* **1951**, *73*, 3055-3059.

(40) Beylerian, N. M.; Vardanyan, L. R.; Harutyunyan, R. S.; Vardanyan, R. L., *Macromol. Chem. Phys.* **2002**, *203*, 212-218.

Chapter IV.

Mechanical, thermal and surface analysis of polymer films made from poly(styrene-*co*-*n*-butyl acrylate) latexes armored with clay nanodiscs

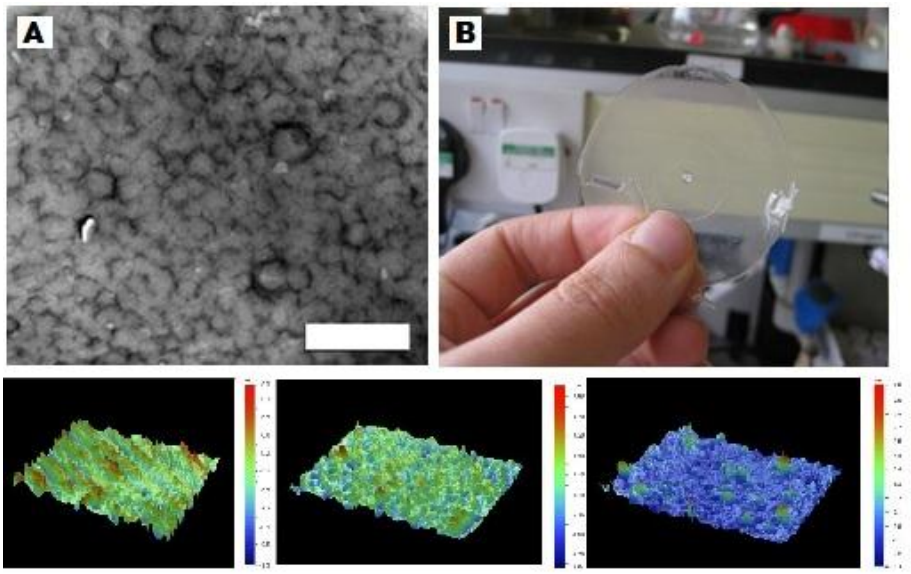

The influence of the presence of Laponite clay XLS in poly(styrene-*co*-*n*-butyl acrylate) polymer films, made by Pickering emulsion polymerization, is described. Mechanical, thermal and surface analysis is performed. Improvements on mechanical properties as a result of clay presence are reported. In addition, thermogravimentric analysis suggests that Laponite clay improves the thermal decomposition compared to a conventional polymer film without inorganic particles. Finally it is shown that the clay also plays an active role on the polymer films surface, leading to smoother surfaces.

Part of this work was performed by Gareth Davies, master student working in the lab of Prof. Joseph Keddie, Dept. of Physics, Surrey University, UK.

IV.1. Introduction

In the previous chapters, we focused on the fabrication of "soft" polymer latexes armored with inorganic nanoparticles through Pickering emulsion polymerization. In this chapter, we discuss mechanical and physical properties of the nanocomposite polymer films formed from these waterborne latexes. We will focus on surface topography, thermal properties, and mechanical characteristics. Prior to this we will elucidate the basics of the film formation process.

The interest of studying latex dispersions dates back to ancient mesoamerican people around 1600 BC.[1] It took until the 19th century AD when the term "colloid" was coined by Thomas Graham.[2] IUPAC states that the term colloidal implies that molecules or polymolecular particles dispersed in a medium have at least in one direction a dimension roughly between 1 nm and 1µm, or that in a system discontinuities are found at distances of that order.[3] The majority of polymer colloid dispersions, whether natural or synthetic, have water as the dispersion medium. When water evaporates, colloidal dispersions can transform themselves into polymer films, if the latex particles are "soft" and have the ability to deform. This process is referred as "latex film formation". The film formation process of "soft" polymer latexes is used in a variety of applications such as paints, coatings, adhesives, varnishes *etc*..[4,5]

The process of film formation is conventionally divided into three main steps: drying, particle deformation, and diffusion.[3,6-8]

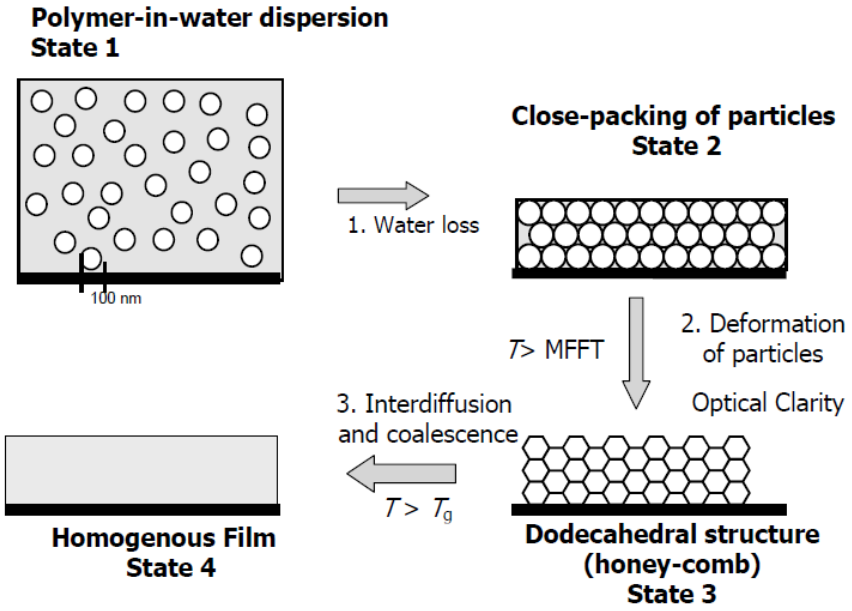

Figure IV.1. Schematic representation of the film formation process. Figure reproduced from Fig 1.8 of ref. 3.

Stage I. *Drying stage* – Water is evaporated leading to a higher concentration of particles; it forces particles into close packed structures driven by convective assembly.

Stage II. *Particle deformation* – Particles start to deform filling the space voids and lose their spherical shape. Deformation is driven by capillary under-pressure. With the interstitial spaces being filled, light scattering due to a difference in refractive index is faded out and the sample gains in optical clarity. Key parameters in this deformation process are the temperature difference between the temperature at which film formation takes place and the minimum film formation temperature of the waterborne dispersion, the latter related to the glass transition temperature of the polymer particles (can be estimated using the Fox equation or an improved estimate taking into account hydropastization as

reported by Tsavalas).[9] Other factors include the chemistry of the surface of the particles, and their average diameter and size distribution. For monodisperse particles, the ideal packing configuration is ideally face-centred-cubic (*fcc*), or the closely related but less ideal hexagonally closed packed (*hcp*) structure. In both these configurations each central particle will have twelve neighboring particles. Stage II ends when no more deformation is visible, as reported by for example, Vanderhoff.[10] In the case of low temperatures (below the minimum film formation temperature MFFT) or hard particles (particles with high glass transition temperature), the particles will not deform on the timescale required, leading to cracks and/or opaque films, which are brittle. Highly monodisperse spheres, such as silica nanoparticles or hard polymer particles, can form periodic crystalline arrays, [11,12] commonly called colloidal crystals, with fascinating optical and thermodynamic properties.[11,13-15]

Stage III. *Polymer interdiffusion* – Once the particles have deformed adopting a polyhedral-like cellular morphology, their individual identity and thus particle boundaries are slowly faded out by a process called polymer interdiffusion. Effectively polymer chains originated from individual particles in contact with each other will start to diffuse across the original boundary. The end result is a homogeneous polymer film with enhanced mechanical properties.

Obviously, the film formation process as described above for "soft" polymer latexes dispersed in water, can be altered by for example introduction of multiple colloidal entities. Especially the use of colloidal inorganic hard matter such as clays, carbon black, metal oxides continues to have great interest in the

search for synergy in physical and mechanical properties of such nanocomposite polymer films as a result of interaction between the "soft" polymer latex component and the hard inorganic material. Polymer films resulting from "soft" polymer latexes particles have good flexibility and malleability, but have poor mechanical and chemical resistance. On the other hand, polymer films from hard colloidal entities have strong mechanical and chemical resistance, but have low flexibility and malleability. Combining these two kinds of colloidal particles, we aim to combine their properties, in order to fabricate flexible/malleable and at the same time mechanical/chemical resistant polymer films.

Attractive routes towards such hybrid waterborne films are: 1.) blending of two or more colloidal dispersions, where one contains the "soft" polymeric particles and the other(s) contain(s) other colloidal components such as inorganic particles. 2.) Fabrication of hybrid or nanocomposite particles, where the polymer particle has two phases, for example a polymer phase and an inorganic phase (See Chapter I-III).

In order to improve mechanical, thermal and physical properties, the uses of inorganic materials in waterborne blends of polymeric dispersions has gained a lot of interest.[16-24] For example, Shen *et al.*,[19] showed that the combination of inorganic particles with organic polymers leads to improvements in physical and mechanical properties of the resultant polymer films. The use of fillers increases the total interfacial area of blend mixtures increasing the volume fraction of interfacial polymer, providing synergetic properties between the "hard" particles and the "soft" polymer particles.[25] Popall *et.al.*,[18] also demonstrated that the presence of organosilicates in organic polymer dispersions leads to remarkable

improvements in the mechanical and physical properties of polymer films. Drozdov *et al*.,[26] reported that the presence of 1wt.% of clay in polypropylene latex solution, improves the creep resistance of polypropylene. Vazquez and coworkers[27] also showed improvements on the creep resistance when organo-modified nanoclay is used on the preparation of starch/polycaprolactone. Similar results were obtained by Frontini[28] on the preparation of polyamide/clay films.

Waterborne polymer dispersion blends containing "hard" and "soft" particles do not necessarily have to have inorganics as the hard component. For example Winnik[29] and coworkers reported the preparation of blend mixtures of "hard" P(MMA) polymer particles with "soft" P(BMA-*co*-BA) polymer particles. They showed that when a uniform distribution of "hard" particles is achieved and a certain minimum amount of "soft" latexes particles (used as plasticizers) is used, transparent polymer films can be obtained.

However, using blends means that there is little spatial control of arrangement of the individual colloidal components. The random distribution of hard matter fillers in film forming hybrid polymer dispersions, can lead to cracks and/or opaque films. Therefore, different strategies to pre-arrange the packing of the hard and soft components have been investigated to obtain uniform distribution of fillers in the colloidal dispersions. For example encapsulation of inorganic materials with a polymer layer, or the fabrication of polymer particles armored on the surface with inorganic materials will achieve such control. Different morphologies of these more complex particles, such as core-shell/armored,[30] peanut,[31] hollow particles[32] and multilobed particles[33] have

been fabricated , depending of the fillers shape and techniques used (see chapter I).

There are numerous examples which demonstrate that fabrication of hybrid particles with a specific morphology provides enhanced physical and mechanical properties of polymer films. Wang *et al.*,[34] reported work where they compared a blend of two latexes one being polyurethane the other an acrylic copolymer, with a hybrid latex containing the same copolymers. He observed that the hybrid polymer film had a higher yield stress in comparison to the film formed from the blend. Wiese and coworkers,[35] showed that hybrid core-shell particles of acrylic polymer armored with silica nanoparticles have better scratch resistance than the same films made from a waterborne binary blend. In the latter case substantial amounts of silica nanoparticles appear in clusters, leading to cracks and brittle films. Landfester and collaborators[36] showed that hybrid polymer films of P(MMA-*co*-BA)/polyurethane have better mechanical resistance than polymer films resultant of the same composition in a blend mixture.

Polymer films prepared from armored or core-shell polymer particles with a layer of silicates on the surface of the polymeric particles, lead to the formation of a honeycomb structure in the hybrid polymer films. This normally results in a good homogeneous distribution of inorganic particles in the polymer matrix avoiding the appearance of cracks and resulting in transparency of the polymer films. For example, Bourgeat-Lami *et al.*,[37] reported the fabrication of flexible and transparent hybrid nancomposites films of poly(styrene-*co*-buyl acrylate) reinforced with clay claiming better thermal properties. Armes and coworkers[38] showed that poly(4-vinylpyridine) functionalized polymer particles armored

with silica nanoparticles led to the formation of transparent hybrid polymer films with improved abrasion and water resistance.

Herein, polymer films made from Laponite clay armored "soft" poly(styrene-*co*-*n*-butyl acrylate) latexes made via Pickering emulsion polymerization (See Chapter III) are investigated. Creep resistance of the nanocomposite films at 30°C and 60°C using DMA (dynamic mechanical analysis) analysis was evaluated. Thermal properties using thermal gravimetric analysis (TGA) were also analyzed. Moreover the surface topography of the films were measured using a profilometer..

Homogeneous distributions in the form of a polyhedral honeycomb structure of the clay throughout the polymer films was obtained, as shown in TEM analysis of a thin polymer film (**Figure IV.2**A). The nanocomposite films showed good transparency(**Figure IV.2**B).

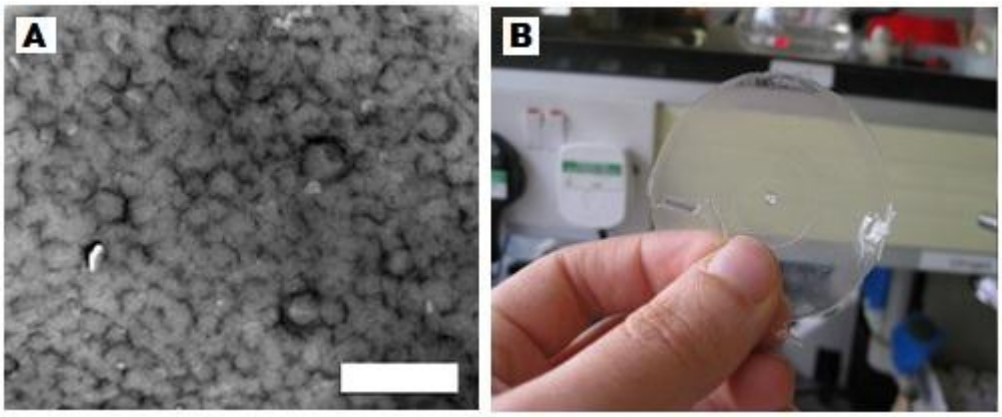

Figure IV.2. A: TEM picture of a cross section of a polymer film formed from a "soft" poly(styrene-*co*-*n*-butyl acrylate) latex armored with Laponite clay XLS. **B**: Digital picture of polymer film obtained from "soft" poly(styrene-*co*-*n*-butyl acrylate) latex armored with Laponite clay XLS at room temperature.

IV.2. Experimental part

Polymer latexes: "Soft" polymer latexes of poly(styrene-*co*-*n*-butyl acrylate) (Sty:BA = 0.67) armored with different amounts of Laponite clay XLS were prepared through Pickering emulsion polymerization process (experimental details are presented in chapter III). The clay content in each waterborne polymer dispersion are presented in **Table IV-1**.

Table IV-1. Percentage of Laponite clay XLS used in different latexes solutions and dry polymer-clay nanocomposites.

Sample	% Clay weight (latex solution)	% clay weight (polymer film)
RT-2-53	0	0
RT-2-55	0.038	0.39
RT-2-54	0.110	1.09
RT-2-51	0.250	2.53
RT-2-52	0.490	4.76
RT-3-66	0.625	5.91
RT-3-65	0.750	7.00
RT-2-50	0.940	8.90

Note: The polymer film resulting from the sample RT-2-50 showed the presence of cracks.

Polymer films preparation: 5 mL of latex solution was deposited onto a PTFE substrate mould with a 3x3 cm area. The latex was then left to dry at room temperature. Due to the low solids content of the latex solutions, typically 10

wt%, the films obtained had small thicknesses of around 0.2 mm. Therefore, subsequent polymer film layers were deposited on the top of the dry film. The final thickness was measured using digital calipers (Fowler PRO-MAX 0-6“”) with a precision of 0.01 mm.

Small-strain measurements: small strain extension of (0.05%) was investigated using a Texture Analyzer. The temperature was kept constant at 30°C.

Dynamic mechanical analysis (DMA): the DMA analysis was performed using a TA Instruments Q800. A fixed strain of 0.1% was used at a rate of 1Hz. The storage and loss modules were measured over a temperature range of -50°C to 100°C with increments of 2°C/min. An attached oven was used.

Creep Measurements: the creep measurements were performed using the Texture Analyser at a fixed temperature of 30°C (using an attached oven). A stress of 0.1 MPa was applied, over time, and the strain was recorded.

Microscopy analysis: SEM analyses were performed using a Zeiss Supra55VP FEGSEM with an EBSD camera and the samples were prepared on silicon wafers (kindly donated by Wacker Chemie AG) to be analyzed uncoated. TEM analyses were performed on a 1200EXII TEM with a 1K Gatan camera using Formvar-Film grids (200 Mesh Cu, Agar Sc. S138).

Thermogravimetric analysis: Thermogravimetric analysis were performed using a Mettler Toledo DSC1-400 equipment with a resolution of 0.1 μg and a

range of temperatures between 20 – 1600 °C, ± 0.3 °C. A pan of aluminum was used to contain the samples.

Polymer surface analysis: A Wyco Vertical Scanning Interferometer with 20 nm of resolution was used to measure the surface roughness. A vertical scanning mode was chosen and optical physical snapshots were obtained of the polymer surface. No physical contact with the polymer surface was undertaken.

IV.3. Results and discussion

The presence of clay dispersed through a polymer film enhances its mechanical resistance, but also makes the material more stiff[20,39] and more brittle.[24,40] A fine balance between flexibility provided by "soft" latex particles and mechanical reinforcement provided by "hard" inorganic particles should be taking into account. Herein, we explored the influence of Laponite clay content in polymer films made from poly(styrene-*co*-*n*-butyl acrylate) particles. Our results showed that the samples with higher clay contents fractured at lower strain values. This was clearly observed in the sample with the highest amount of clay (8.9 wt% of clay content) where the formed film showed the presence of cracks, feasibly due to a too high excess of free Laponite clay discs, and it was impossible to plot a stress-strain curve. All other samples are shown in **Figure IV.3**

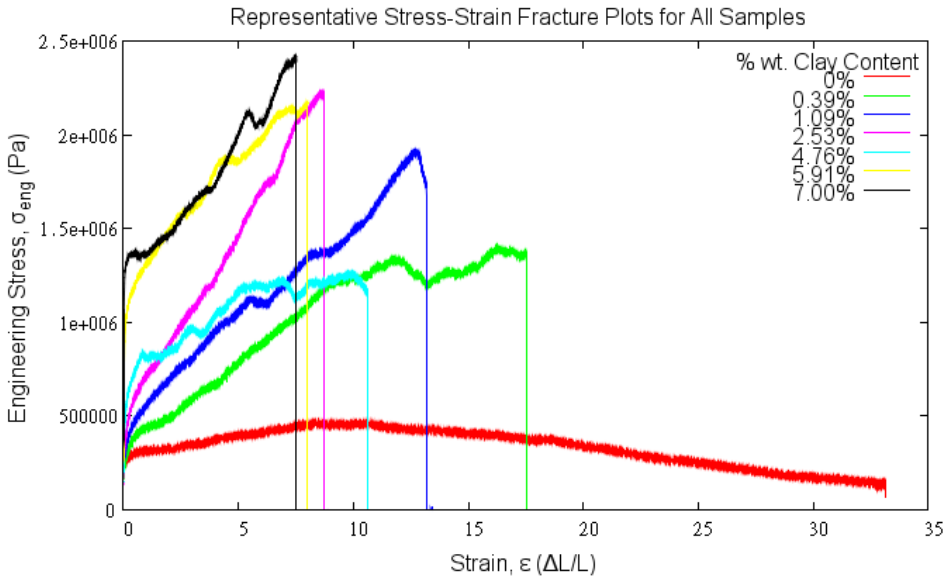

Figure IV.3. Stress-strain curves of polymer films with different amounts of Laponite clay XLS at 30°C.

The dynamic mechanical analysis (DMA) versus temperature showed that Laponite clay XLS clearly increases the storage modulus. This difference is visible at low temperatures; however, for temperatures above the T_g, the difference in the Young's modulus storage between samples with low and high amounts of clay became more pronounced (see **Figure IV.4**). At low temperatures, in a glassy state, the polymer chains cannot rearrange,[41] while at high temperatures, in a melt stage, rearrangement of polymer chains can occur provoking a sharp decrease on the storage modulus. The presence of Laponite clay improves the mechanical resistance of the films at higher temperatures as can be seen in **Figure IV.4**, especially for samples with or above 4.76 wt% in clay content.

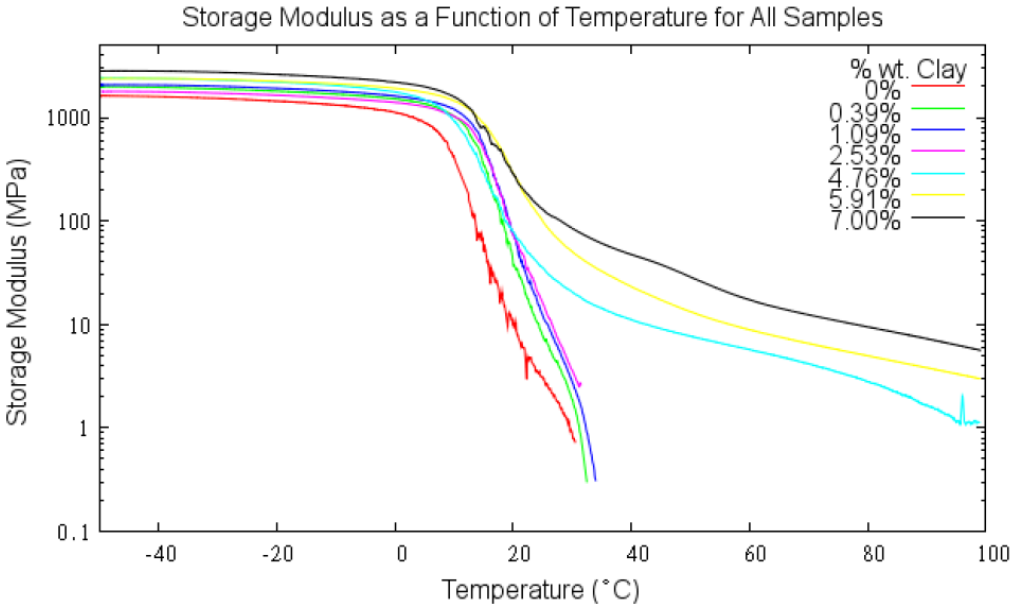

Figure IV.4. Storage modulus versus temperature of poly(styrene-*co*-*n*-butyl acrylate) films with different amounts of Laponite clay.

Interestingly, with high amounts of clay, samples showed a very nice recovery after an applied deformation of 0.05%, suggesting improvements on the elastic behavior (see **Figure IV.5**) (the recovery curves retraced the extension ones). The samples with low amounts of clay showed very low stress values, not showing viscoleastic behavior.

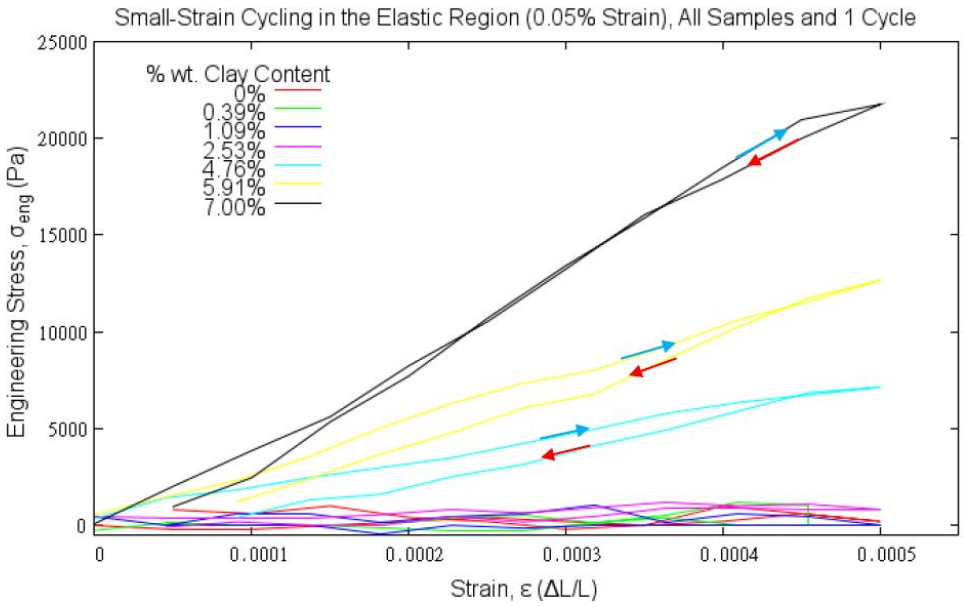

Figure IV.5. Small-strain cycling (strain and recovery) of polymer films with different amounts of Laponite clay XLS. The maximum strain applied was of 0.05%.

Similar results were obtained for creep measurements at a fixed temperature (30° C) (**Figure IV.6**) where the strain value decreases with increasing Laponite clay amount. The samples with more clay content show less deformation as a result of the presence of more "solid" material and consequent increase in viscosity. The small difference observed between the samples with 0.39 and 1.09% wt. clay are probably a result of the presence of some impurities in the film formation process or polymerization process.

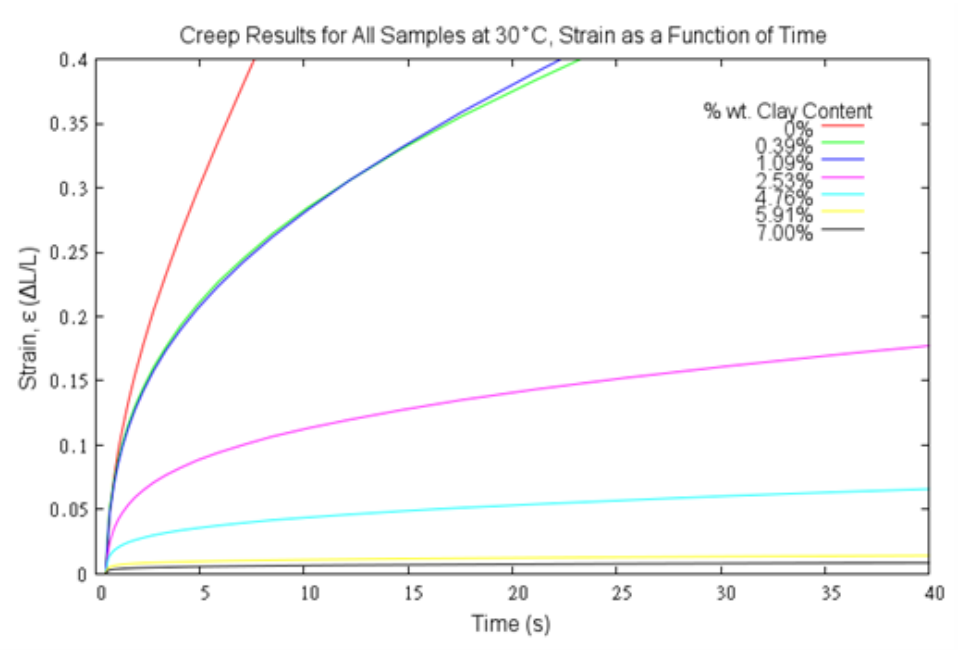

Figure IV.6. Creep measurements of polymer films with different amounts of Laponite clay XLS at 30°C.

In order to analyze the importance of the honeycomb structure and consequent homogeneous distribution of fillers in a polymer film matrix, we compared the creep resistance between a nanocomposite polymer film and a blend mixture of polymeric particles and clay platelets with the same composition. At 60 °C, temperature far above the glass transition temperature of the polymer, the nanocomposite polymer films with high amounts of clay, showed strains below 0.25. The corresponding blend polymer films showed a liquid-like behavior and the creep measurements could not be recorded for a long time. This is clear evidence that the presence of honeycomb structure is very important to improve creep resistance.

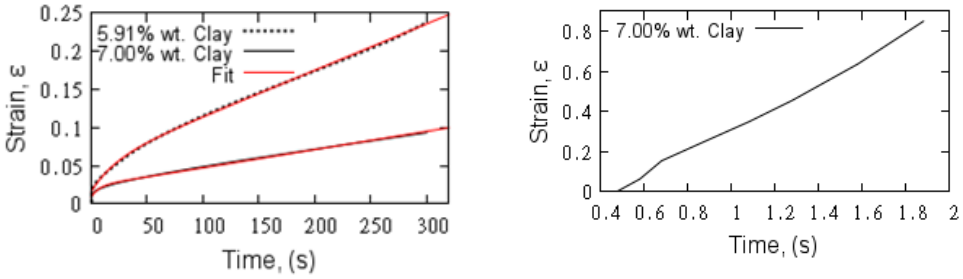

Figure IV.7. Creep measurements for polymer/clay **nanocomposites** on left, and polymer/clay **blend** on the right at at 60°C.

IV.3.1. Thermogravimetric analysis

It is known that the presence of clay in polymer materials can increase thermal and flammability properties.[42] The thin layer of clay retards the burning/oxidation of the polymer material through insulation (note this is not thermal insulation as the heat capacity of clay is considerably lower than that of the polymer) and potentially lowers the oxygen permeability.[43] Gilman and coworkers[44] reported that the clay migrates to the polymer surface when polymer films are exposed to high temperatures. In our case, a continuous protective barrier is in place as a direct result of the armored structure of the polymer latex particles. Meneghett *et al.*,[45] showed through TGA analysis that the presence of montmorillonite clay retards the thermal decomposition temperature of poly(methyl methacrylate). Bourgeat-Lami and *coworkers*[37] also demonstrated improvements on thermal decomposition when clay platelets are used in polymer films of poly(styrene-*co*-*n*-butyl acrylate). (In the cases of these last two authors, the improvement on the thermal composition temperature is related to the temperature at which the thermal degradation finishes). Here, the influence of Laponite clay XLS and its relative amount in polymer films

prepared from poly(styrene-*co*-*n*-butyl acrylate) armored latexes made by Pickering emulsion polymerization were investigated. A series of clay hybrid poly(styrene-*co*-*n*-butyl acrylate) films with different amounts of clay were analyzed by TGA.

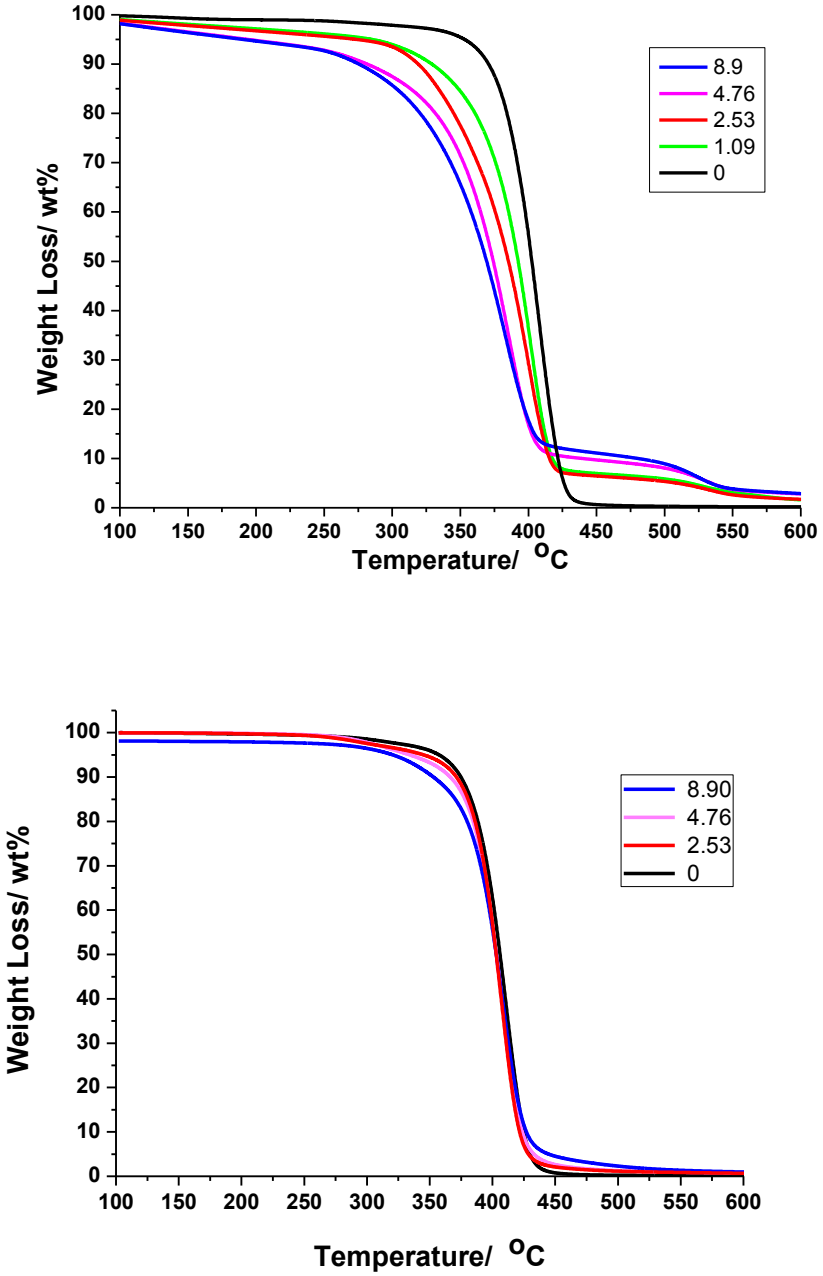

Figure IV.8. Thermogravimetric analysis of polymer films of poly(styrene-*co*-*n*-butyl acrylate) with different amounts of Laponite Clay XLS (wt% clay) in air atmosphere(top) and under nitrogen (bottom).

From the TGA analysis performed in an air atmosphere **(Figure IV.8**), we can observe that the thermal decomposition of the samples with higher quantities of clay start early. This early decomposition in comparison with a non-clay sample may happen, in the first stage, due to water evaporation. The honeycomb structure provided by clay platelets has strong affinity with water, trapping the water molecules inside of the channels, where the pressure is higher (see chapter V). But most likely, this early decomposition is due to the lower heat capacity of silicates in comparison with the most polymer matrixes (e.g. silica=0.70 $J.g.^{-1}k.^{-1}$; styrene=1.79 $J.g.^{-1}k.^{-1}$). The presence of clay will promote faster heat transfer to the polymer particles resulting in a slightly early decomposition.

However, after 400 °C the thermal degradation is slower for samples with more clay content, and a plateau region is observed. This plateau is bigger for higher loads of clay. The layer of these silicates around the polymer particles gives high thermal stability as they protect the polymer against burning/oxidation. In nitrogen atmosphere, this plateau region is not observed as a consequence of the absence of oxygen, one fundamental fire agent.

The presence of a honeycomb structure of clay discs plays an active role on the polymer films thermal and flammability properties, being particularly interesting its fire resistance behavior at higher temperatures.

IV.3.2. Polymer Surface Analysis

All of the polymer-clay films samples showed a remarkable transparency (except the one with 8.9 wt% of clay content in the dry polymer film), without any cracks while the mechanical and thermal properties were enhanced. It is

clear that the presence of clay in polymer films modifies the polymer properties, changing the mechanical, thermal, and optical properties. However does it influence the surface of the polymer films? Various approaches to study the polymer surface have been reported, especially using SEM[46-48] and XPS.[46,49,50] Here, an alternative method to analyze the influence of Laponite clay on the nanocomposite polymer surface is presented. We used a *Wyco Vertical Scanning Interferometer*, an optical non contact measurement to analyze the polymer surface. The results are showed in **Figure IV.9**

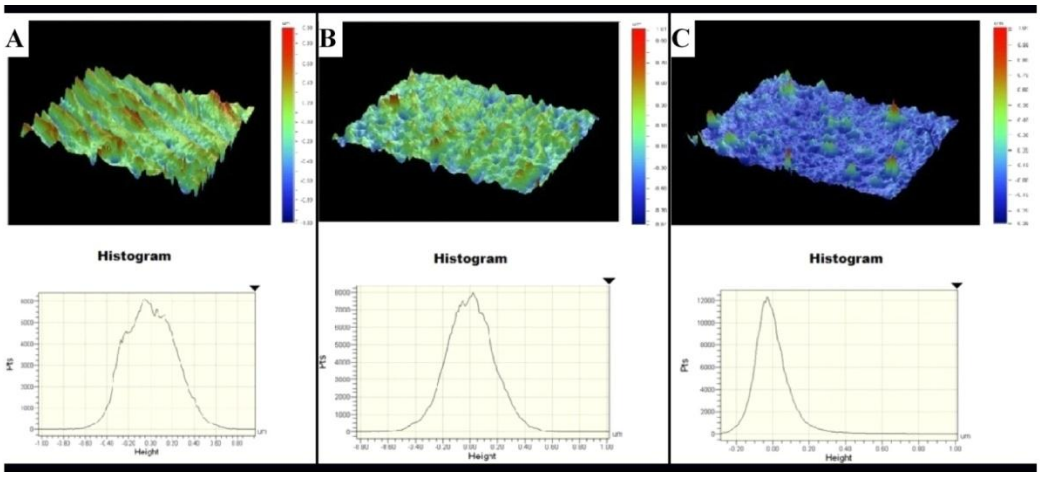

Figure IV.9. *Vertical scanning Interforometer* analysis of three polymer films of poly(styrene-*co*-*n*-butyl acrylate). **A**: polymer film without clay; **B**: polymer film with 2.53 wt% of clay; **C**: polymer film with 8.9wt% of clay.

It can be seen that the sample without Laponite clay (**Figure IV.9**.A), has a rougher surface in comparison with the other two samples. The picture shows the presence of big "mountains" and "valleys" and the corresponding histogram below shows a broader curve that corresponds to major differences between the highest and the lowest points. When a small amount of clay was added (**Figure IV.9**.B), the buckling effect was reduced and when more clay was added, a very

smooth polymer-clay film was obtained (**Figure IV.9**.C). A plausible explanation for this event is that the absence of clay, during the film formation, wrinkles the film because of side dry effects.[6,51] On the other hand, the presence of clay, even in small amounts, reinforces the polymer strength and the wrinkle behavior is reduced. Also, an excess of clay during the film formation may cover the polymer surface, filling the gaps between the "mountains" and "valleys". In the next SEM picture (**Figure IV.10**A), we can see accumulation of Laponite clay on the top polymer surface (sample with 8.9 wt% of clay). This "clay skin" is an undesired effect as excess of clay leads to brighter polymer films and crack formation. To prevent this skin formation, a balance of the clay content is necessary; while an armored structure to obtain a homogeneous distribution of ceramic compounds (such as clay) is essential to obtain, flexible, transparent and high strength polymer films(**Figure IV.10** B.).

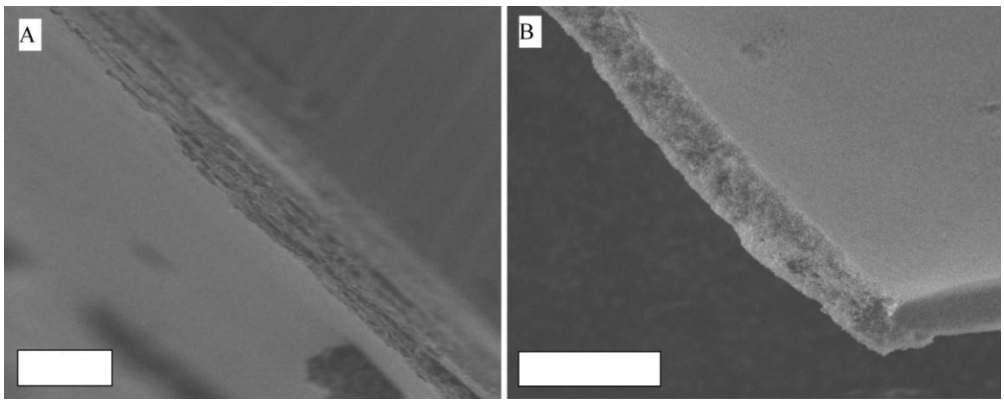

Figure IV.10. Cross-section SEM picture of poly(styrene-*co*-*n*-butyl acrylate) burnt film with 8.90 wt% of clay (**A**) and 2.53 wt% of clay (**B**). (Scale bars of 10 μm)

IV.4. Conclusions

In this chapter we have shown that the presence of Laponite clay XLS in poly(styrene-*co*-*n*-butyl acrylate) polymer films, prepared through Pickering emulsion polymerization, leads to significant improvements in its mechanical and thermal properties. We highlighted that the storage modulus increases with the amount of clay, and this behavior is particularly evidenced at higher temperatures. In addition, it was shown that the clay-polymer films demonstrate a good recovery after deformation, suggesting elastic behavior. It was also demonstrated, that the presence of a ceramic honeycomb structure in polymer films improves the creep resistance in comparison of a blend mixture with the same composition. From thermogravimetric analysis, it was verified that the presence of clay plays an important role on the polymer film thermal and flammability properties. Polymer/clay films showed the presence of plateau region at high temperatures. This slower degradation period is a consequence of burning/oxidation resistance provided by clay discs, giving to these nanocomposites films interesting fire resistance properties. Finally, we showed that the presence of Laponite clay XLS leads to the formation of much smoother polymer films in comparison with a conventional polymer film.

IV.5. References

(1) Hosler, D.; Burkett, S. L.; Tarkanian, M. J., *Science* **1999**, *284*, 1988-1989.

(2) Graham, T., *Philosophical Transactions* **1833**, *123*, 253–284.

(3) Routh, A. F.; Keddie, J. L., Fundamentals of Latex Film Formation: Processes and Properties, *Spring. Lab.* **2010**.

(4) Finch, C. A., *Polym. Int.* **2003**, *52*, 1553-1553.

(5) Fitch, R. M., *Aca. Press.* **1997**.

(6) Keddie, J. L., *Mater. Sc. Eng.: R: Rep.* **1997**, *21*, 101-170.

(7) Fitch, R. M., Polymer Colloids, A Comprehensive Introduction, *Aca. Press. 1997* **1997**.

(8) Blackley, D. C., Polymer Latices-Science and Technology, *Spring. 2nd ed.* **1997**.

(9) Tsavalas, J. G.; Sundberg, D. C., *Langmuir* **2010**, *26*, 6960-6966.

(10) Vanderhoff J.W.; Tarkowski H.L.; Jenkins M.C.; Bradford E. B., *J. Macromol. Chem.* **1966**, *1*, 361-397.

(11) Pieranski, P., *Contemp. Phys.* **1983**, *24*, 25-73.

(12) Jones, J. B.; Sanders, J. V.; Segnit, E. R., *Nature* **1964**, *204*, 990-991.

(13) Pieranski, P. *Phys. Rev. Lett.* **1980**, *45*, 569.

(14) Jiang, P.; Bertone, J. F.; Hwang, K. S.; Colvin, V. L., *Chem. Mater.* **1999**, *11*, 2132-2140.

(15) Sanders, J. V., *Act. Cryst.* **1968**, *A24*, 427.

(16) Teixeira, R. F. A.; Bon, S. A. F., *Adv. Polym. Sci*. **2011**, 233, 19-52.

(17) Biswas, M.; Ray, S. S., *Adv. Polym. Sci.* **2001**, *155*, 167-221.

(18) Sanchez, C.; Julián, B.; Belleville, P.; Popall, M., *J. Mater. Chem.* **2005**, 3559-3592.

(19) Zou, H.; Wu, S.; Shen, J., *J. Chem. Rev.* **2008**, *108*, 3893-3957.

(20) Negrete-Herrara, N.; Putaux, J.-L.; David, L.; De Haas F.; Bourgeat.-Lami, E., *Macromol. Rapid Comm.* **2007**, *28*, 1567-1573.

(21) Faucheu, J.; Gauthier, C.; Chazeau, L.; Cavaille, J.-Y.; Mellon, V.; Bourgeat-Lami, E., *Polymer* **2010**, *51*, 6-17.

(22) Diaconu, G.; Paulis, M.; Leiza, J. R. *Polymer* **2008**, *49*, 2444-2454.

(23) Diaconu, G.; Paulis, M.; Leiza, J. R., *Macromol. React. Eng.* **2008**, *2*, 80-89.

(24) Agag, T.; Koga, T.; Takeichi, T., *Polymer* **2001**, *42*, 3399-3408.

(25) Balazs, A. C.; Emrick, T.; Russell, T. P., *Science* **2006**, *314*, 1107-1110.

(26) Drozdov, A. D.; Høg Lejre, A.-L.; Christiansen, J., *Comp. Sci. Tech.* **2009**, *69*, 2596-2603.

(27) Pérez, C. J.; Alvarez, V. A.; Vázquez, A., *Mater. Sci. Eng. A* **2008**, *480*, 259-265.

(28) Seltzer, R.; Mai, Y.-W.; Frontini, P. M., *Comp. B. Eng.* **2011**, 32, 345-348.

(29) Feng, J.; Winnik, M. A.; Shivers, R. R.; Clubb, B., *Macromol.* **1995**, *28*, 7671-7682.

(30) Hergeth, W. D.; Schmutzler, K.; Wartewig, S., *Makromol. Chem.,.* **1990**, *31*, 123-142.

(31) Mock, E. B.; Bruyn, H. D.; Hawkett, B. S.; Gilbert, R. G.; Zukoski, C. F., *Langmuir* **2006**, *22*, 4037-4043.

(32) McDonald, C. J.; Devon, M. J., *Adv. Colloid Interf. Sci.* **2002**, *99*, 181-213.

(33) Okubo, M.; Kanaida, K.; Matsumoto, T., *Colloid Polym. Sci.* **1987**, *265*, 876-881.

(34) Wang, C.; Chu, F.; Graillat, C.; Guyot, A.; Gauthier, C.; Chapel, J. P., *Polymer*. **2005**, *46*, 1113-1124.

(35) Tiarks, F.; Leuninger, J.; Wagner, O.; Jahns E.; Wiese, H., *Surf Coat. Intern.* **2007**, *5*, 221-229.

(36) Guyot, A.; Landfester, K.; Joseph Schork, F.; Wang, C., *Progr. Polym. Sci.* **2007**, *32*, 1439-1461.

(37) Negrete-Herrera, N.; Putaux, J. L.; David, L.; De Haas, F.; Bourgeat-Lami, E., *Macromol. Rapid Comm.* **2007**, *28*, 1567-1573.

(38) Balmer, J. A.; Schmid, A.; Armes, S. P., *J. Mater. Chem.* **2008**, *18*, 5722-5730.

(39) Faucheu, J.; Gauthier, C.; Chazeau, L.; Cavaillé, J.-Y.; Mellon, V.; Bourgeat-Lami, E., *Polymer.* **2010**, *51*, 6-17.

(40) Haraguchi, K.; Ebato, M.; Takehisa, T., *Adv. Mater.* **2006**, *18*, 2250-2254.

(41) Plummer, C. J. G.; Ruggerone, R.; Bourgeat-Lami, E.; E., Manson, J.-A. E., *Polymer*, **2011**, *52*, 2009-2015.

(42) Gilman, J. W., *Appl. Clay Sci.* **1999**, *15*, 31-49.

(43) Inan, G.; Patra, P. K.; Kim, Y. K.; Warner, S. B., *Mater. Res. Soc. Symp. Proc.* **2003**, *708*, 289-295.

(44) Gilman, J. W.; Jackson, C. L.; Morgan, A. B.; Harris, R.; Manias, E.; Giannelis, E. P.; Wuthenow, M.; Hilton, D.; Phillips, S. H., *Chem. Mater.* **2000**, *12*, 1866-1873.

(45) Meneghetti, P.; Qutubuddin, S., *Thermochim. Act.* **2006**, *442*, 74-77.

(46) Yan, L.; Huck, W. T. S.; Zhao, X.-M.; Whitesides, G. M., *Langmuir* **1999**, *15*, 1208-1214.

(47) Southward, R. E.; Boggs, C. M.; Thompson, D. W.; St. Clair, A. K., *Chem. Mater.* **1998**, *10*, 1408-1421.

(48) Seto, F.; Tahara, K.; Kishida, A.; Muraoka, Y.; Akashi, M., *J. Appl. Polym. Sci.* **1999**, *74*, 1516-1523.

(49) Vazquez-Rodriguez, S.; Sánchez-Valdes, S.; Rodríguez-GonzáLez, F.; Castillón-Barraza, F. F.; Gonzalez-Gonzalez, V. A.; González-Cantú, M. C., *J. Appl. Polym. Sci.* **2011**, *119*, 336-342.

(50) Seto, F.; Fukuyama, K.; Muraoka, Y.; Kishida, A.; Akashi, M., *J. Appl. Polym. Sci.* **1998**, *68*, 1773-1779.

(51) Salamanca, J. M.; Ciampi, E.; Faux, D. A.; Glover, P. M.; McDonald, P. J.; Routh, A. F.; Peters, A. C. I. A.; Satguru, R.; Keddie, J. L., *Langmuir* **2001**, *17*, 3202-3207.

Chapter V.

Influence of Laponite clay on the adsorption/desorption and barrier properties of cellular nanocomposite "soft" polymer films

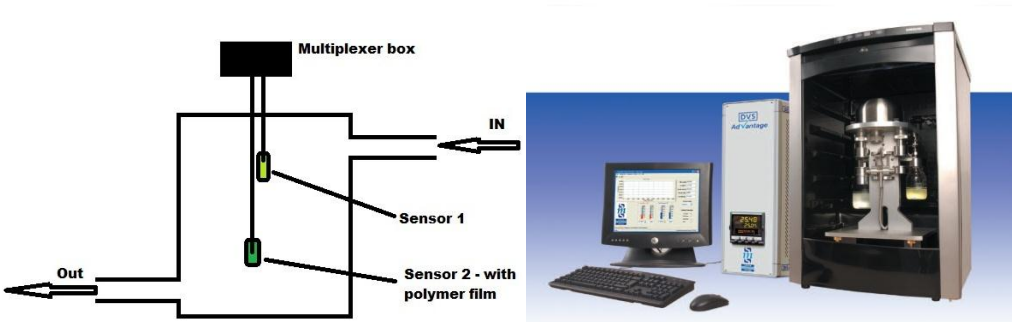

In this chapter, the influence of Laponite clay XLS on water vapor uptake/release properties of cellular nanocomposite poly(styrene-*co*-*n*-butyl acrylate) films originating from a Laponite clay armored polymer waterborne dispersion is investigated. It is shown that the presence of clay increases the water storage capacity of the polymer films. A quantitative analysis of the amount of water adsorbed/desorbed at various values of the relative humidity at atmospheric pressure values is undertaken. The nanocomposite cellular polymer films were post-modified chemically through hydrophobization by covalent bond formation with hexamethyldisiloxane (HDMS) as a reagent through sublimation, as well as physically through curing/dehydration of the polyhedral clay network through freeze-drying. Gas adsorption/desorption properties of

these nanocomposites were also investigated. Different approaches to alter the films water uptake/release properties were undertaken, in order to obtain more hydrophobic polymer films. In addition, an innovative method to study water vapor permeability properties of the hybrid cellular polymer films was developed.

V.1. Introduction

The fabrication of submicron-sized composite materials has gained a lot of interest in recent years, due to tunability of, and often synergy in, physical, mechanical[1-5] and thermal[6-8] properties. In previous chapters (chapter II and III), different strategies to build tailored micro- and nano-materials were reported. Bulk mechanical and thermal decomposition properties of nanocomposite cellular "soft" polymer films made from poly(styrene-*co*-*n*-butyl acrylate) latex particles armored with Laponite clay discs were reported in chapter IV.

In this chapter, the water uptake and release characteristics and thus the barrier properties of poly(styrene-*co*-*n*-butyl acrylate) /clay films are investigated. One key parameter in these studies is the relative amount of Laponite clay in the cellular nanocomposite films. Its influence on the water vapor barrier properties is discussed.

Barrier properties of polymer films originating from waterborne polymer dispersions are of great interest for a variety of industrial applications. Understanding the behavior of polymer films when exposed to a wet environment is of great importance, because key properties of the films may drastically change, depending of the chemical composition. Cabane *et al*., [9,10] showed that polymer films made from latex particles with a hydrophobic core of poly(styrene-*co*-*n*-butyl acrylate) and a hydrophilic shell containing acrylic acid copolymerized with P(Sty-*co*-BA) formed an interconnected cellular membrane that had great capacity to adsorb water when the waterborne polymer film was

exposed to a wet environment. Upon water uptake the polymer film, however, lost its mechanical strength and became brittle. When the hydrophilic polyhedral cellular network, the interstitial spaces between individual particles, swells with water, it weakens the integrity of the film. Eckersley and Rudin[11] also showed that polymer films made of P(MMA-*co*-BA) particles with a thin layer of P(MAA) (1 wt%, based on monomer content) decreased their mechanical strength when immersed in water in comparison with the mechanical properties in a dry environment. They ascribed the reduction in mechanical strength to water plasticization (lowering of polymer T_g). The presence of water in the interstitial spaces decreases the polymer contact leading to a decrease in the film rigidity. Winnik[12] showed that the presence of water in hydrophilic polymer films made from P(MMA-*co*-BMA) markedly increased the polymer interdiffusion. This effect was not observed for hydrophobic P(BMA) polymer films where the presence of water did not influence the polymer diffusion rate. They also demonstrated that the presence of water considerably altered the transparency of the P(BMA) film, but it did not make appreciable changes in the P(MMA-*co*-BMA) polymer film transparency. The inhomogeneity of water distribution in the hydrophobic polymer film led to the formation of cracks while the even water distribution in the hydrophilic polymer film kept the transparency of the film. They related this effect to the uniform distribution of polar groups (mainly carboxylic acids) along each polymer chain of the P(MMA-*co*-BMA) film. The water in the P(BMA) film was concentrated in the polar groups ($-OSO_3H$) of the particles boundary regions.

Polymer films with a silica-based honeycomb (continuous) structure are particularly attractive to a variety of industrial applications. [13] We and others showed that the presence of these silicates improve mechanical and thermal properties (see chapter IV) of waterborne polymer films.

Herein, we are interested in studying the influence of a honeycomb structure of Laponite clay discs on the water barrier properties of the nanocomposite polymer films made from poly(styrene-*co*-*n*-butyl acrylate) latex particles armored with the clay discs. The advantage of using armored particles is that the thin layer of silicates is pre-positioned around the polymer particles, hereby enforcing the formation of a continuous silicate network. This control of arrangement of the Laponite discs throughout the nanocomposite "soft" poly(styrene-*co*-*n*-butyl acrylate) films will potentially show intriguing effects on both the water vapor adsorption/release profiles, and also the water vapor barrier properties. An important property of this silica-based ceramic material is its capacity to retain and adsorb water molecules and its potential barrier toward oxygen permeability.[14] These two factors are of key importance for example for the food packing industry. In our study we try to understand the phenomenon of water adsorption/desorption in waterborne hybrid polymer films. In addition water vapor barrier properties through the hybrid polymer nancomposites are investigated.

Pioneering work by Irving Langmuir,[15] in 1916, described that the adsorption of molecules onto solid surfaces is related to gas pressure or concentration in the medium above the solid surface. Later, Lowry and Kohman[16] reported work where the adsorption of water by natural rubber sheets followed Henry's law, where the amount of water adsorbed is proportional to vapor pressure, where the

water adsorption correlates to the true solubility of water in the polymer film. The same behavior was also demonstrated for many other polymers. [17] Stephen **B**runauer, Paul Hugh **E**mmett, and Edward **T**eller reported a theory called the BET theory (BET consists of the first initials of their last names), [18] where they extended the work done by Langmuir. Whereas Langmuir considered the scenario of monolayer adsorption, the BET theory adds a multilayer scenario of adsorption of molecules to this in a linear algebraic fashion, with identical characteristics for layers 2 to *n* and no interaction between layers. The BET equation can be expressed by:

$$\frac{1}{Vt[(P_0/P)-1]} = \frac{C-1}{V_m C}\frac{P}{P_0} + \frac{1}{V_m C}$$

Equation V-1

*P (*Pascal) and P_0 (Pascal) are the partial and saturation pressure of vapor, where (P/P_0) is the relative humidity (RH) (%). Vt (m^3) is the total volume of vapor molecules adsorbed at one specific humidity pressure (RH), V_m (m^3) corresponding to the volume of a monolayer adsorption of vapor molecules on the surface of the substrate, and C is the BET constant. This expression is the BET adsorption isotherm and can be linearized by plotting $[1/Vt[(P_0/P)-1]$ versus P/P_0. The relationship agrees with Ficks's law[19] in which the flux between two phases will occur from the highly concentrated phase to the less concentrated phase by diffusion. Above a certain intermediate relative humidity (typical values of *ca*. 40 %), experimental values on systems for adsorption of water rise sharply, so that the model used in BET theory is no longer adequate to describe the process. At higher values for RH, capillary condensation occurs which accounts and explains the experimental observations in water

uptake/release. This more complex behavior of water sorption is modeled in an empirical fashion.[20]

Capillary condensation is an important phenomenon which can occur and therefore has to be taken into consideration, upon vapor sorption by porous materials. The transport of water in porous nanochannels can be up to 3 orders of magnitude more than the transport by vapor diffusion.[21] Capillary condensation and thus the dramatic increase in water uptake occurs at a threshold relative humidity and is linked directly to the geometry and wettability of the porous network.[22] The condensation of vapor occurs below the saturation pressure, P, of the pure liquid[23] due to an increase in van der Waals interactions between the vapor molecules inside the porous channels. In an experiment where increase the relative humidity during a sorption phase is increased, the capillary channels will become filled with vapor and the equilibrium is reached when the larger pore radius are filled. In a desorption phase, water or other solvents will remain in the larger pores sizes until the equilibrium vapor pressure satisfies the smaller pore radius.[23] This difference in the sorption/desorption isotherms originates the hysteresis behavior that is less extensive for higher temperatures.[24]

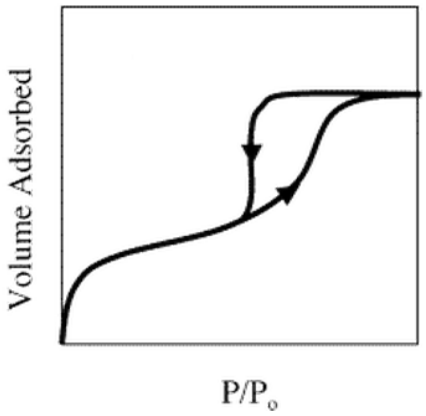

Figure V.1. Adsorption/desorption hysteresis of mesoporous molecular sieve. Figure reproduced from fig 1 of reference 25.[25]

In this porous network, capillary underpressure is applied during water evaporation, decreasing the capacity of polymer films to release solvent molecules. Our specific hydrophilic honeycomb clay network will also have strong affinity with water, trapping the water in the interstitial spaces of the polymer film

Herein, the water and octane vapor uptake/release properties of polymer films with a honeycomb structure obtained after film formation of poly(styrene-*co*-*n*-butyl acrylate) particles armored with Laponite clay XLS using dynamic vapor sorption are investigated. In addition we show an innovative method to analyze water vapor barrier properties for waterborne hybrid polymer films.

V.2. Experimental part

V.2.1. Preparation of the polymer latexes

Materials: The monomers *n*-butyl acrylate (BA) and styrene (Sty) were purchased from Aldrich at 99 % or greater purity and used as received. Laponite Clay XLS, density of ρ_{clay} = 2.57 g cm^{-3} was purchased from Rockwood Additives Ltd. Ammonium persulfate (APS, 99+% p.a) and potassium persulfate (KPS, 99+% p.a.) were obtained from Sigma-Aldrich. Deionized water was used in all experiments.

Equipment: Emulsion polymerizations were carried out in double-walled cylindrical glass reactors (250 mL, Asynt Ltd.) equipped with an external circulating heating bath (Julabo F-25 unit), a condenser, and a four-bladed teflon or metal overhead turbine stirrer fitted at approximately 2 cm from the bottom of the reactor vessel (Cowie Ltd.) typically running at 275 rpm. Average particle sizes and dispersities of the armored latexes were measured by dynamic light scattering using a Malvern Zetasizer Nano (data was analyzed using the CONTIN algorithm). Cryo-TEM analyses were performed on a Jeol 2011 TEM (200KV LaB6) with 2K Gatan Ultrascan camera or on a Jeol 2010F TEM (200KV FEG) with 4K Gatan Ultrascan camera using Lacey-Carbon-Film grids (300 Mesh Cu, Agar Sc. S166-3H). An Analytical Balance (Precisa XT 220A) was used for accurate measurements.

Typical solids-stabilized emulsion polymerization: 2 g of Laponite Clay XLS was dispersed in 200.0 g of deionized water in a 250 mL double-walled glass reactor and purged with nitrogen for 15 minutes. Degassed monomer, 20.0 g (10.0 wt%) was added. After 5 minutes, the reaction mixture was heated to 80 ºC, whilst stirring at 300 rpm. The emulsion polymerization was started upon addition of 0.13 g APS dissolved in 2.0 g of water. Monomer conversion was monitored via gravimetry by taking typically samples of 2 g by syringe.

V.2.2. Preparation of the polymer films

Typical preparation of polymer films: 5 g of a polymer latex solution was gently (to prevent air bubbles) spread on a polyethylene circular surface with 5.4cm in

diameter. Subsequently, when all polyethylene surface was covered with latex and no air bubbles were observed the sample was put in an oven at 60°C and left to dry during approximately two days.

V.2.3. Dynamic vapor sorption (DVS) sample preparation

Dynamic vapor sorption (DVS) Apparatus: The dynamic vapor sorption measurements were performed in a DVSA-STD Dynamic Vapor Sorption Advantage from Surface Measurement Systems. The machine has an active control of the RH and organic vapors (containing two organic/water solutions reservoirs), sample pre-heating and a Cahn- D200 ultra-microbalance. The microbalance allows gravimetric analysis up to 0.05 µg of resolution. The temperature range is from 5 to 60°C. The samples are allocated into two suspended pans inside two closed chambers (independently) connected to the microbalance.

Typical preparation of polymer films: Two suspended pans from the DVS apparatus (one as reference) were carefully removed from it and washed with ethanol and left to dry for approximately 5 minutes. Once dried, the pans were placed again in the DVS. Here, each pan is suspended in a different chamber (one pan for the reference). To prevent the influence of any humidity present on the pans, compressed dry air at a 200 mPa pressure was flown over the two closed chambers for approximately 10 minutes. The balance was then tarred. Then, a circular polymer film, one centimeter in diameter was cut with a mold and placed inside one pan, while the other pan was left as a reference. An initial mass of the sample was recorded. Finally, an experimental method was chosen.

Typical DVS method definitions: To eliminate all moisture present in polymer films and/or pan chambers, a first drying step was applied. 4 hours of compressed dry air at 200 mPa pressure was flown inside the two chambers. After 4 hours, the mass of the sample was weighed again, and defined as M_0 (initial mass). Different humidities pressures from 0-90% RH and 90-0% RH were then applied to the sample and reference in steps from 10% of relative humidity pressure. Note that the temperature was set at 293.15 K for all experiments. In each step, a constant vapor pressure was applied on the suspended sample and reference and the sample weight was recorded by the Cahn- D200 ultra-microbalance. The time that each sample was exposed to each vapor pressure step was the minimum time needed for the sample to reach an equilibrium with the vapor pressure. In these experiments it was defined the equilibrium point when the derivative of mass change over time was less than 0.002.

V.2.4. Permeability Experiments

Equipment: Two humidity sensors, SHT21 from Sensirion were used. The data was analyzed using a EK-H4 multiplexer box connected to a computer where the data was recorded using the EK-H4 viewer standard software program provided by Sensirion.

SHT21 humidity sensor features:

Dimensions:

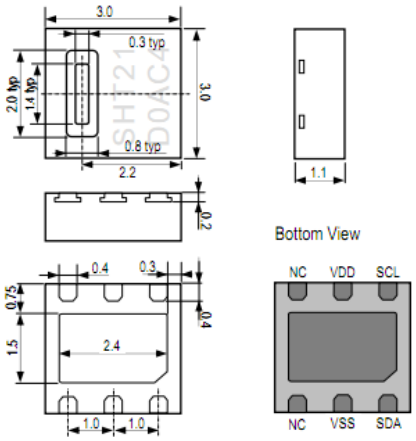

Figure V.2. Drawing of SHT21 sensor package, dimensions are given in mm, tolerances are ±0.1 mm. Information obtained from the STH21 sensor datasheet from Sensirion.

Performance

Relative Humidity

Parameter	Condition	min	typ	max	Units
Resolution [1]	12 bit		0.04		%RH
	8 bit		0.7		%RH
Accuracy tolerance [2]	typ		±2.0		%RH
	max		see Figure 2		%RH
Repeatability			±0.1		%RH
Hysteresis			±1		%RH
Nonlinearity			<0.1		%RH
Response time [3]	τ 63%		8		s
Operating Range	extended [4]	0		100	%RH
Long Term Drift [5]	normal		< 0.5		%RH/yr

Temperature

Parameter	Condition	min	typ	max	Units
Resolution [1]	14 bit		0.01		°C
	12 bit		0.04		°C
Accuracy tolerance [2]	typ		±0.3		°C
	max		see Figure 3		°C
Repeatability			±0.1		°C
Operating Range	extended [4]	-40		125	°C
Response Time [7]	τ 63%	5		30	s
Long Term Drift			< 0.04		°C/yr

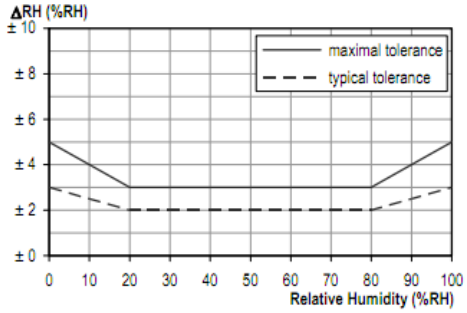

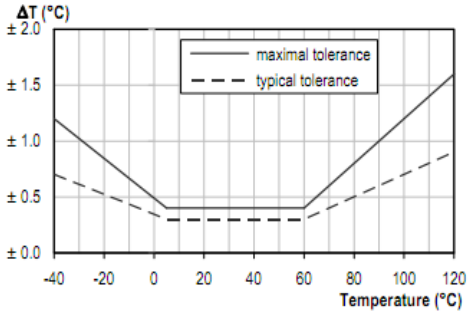

Figure V.3. On Left: Typical and maximal tolerance at 25°C for relative humidity. On right: Typical and maximal tolerance for temperature sensor in °C. Information obtained from the STH21 sensor datasheet from Sensirion.

Typical sensor preparation: A square centimeter polymer film was cut from the previously prepared polymer films. A drop of toluene was then put on the surface. Very gently, the wet region of the polymer film was put on the surface of the humidity sensor SHT21 (provided by Sensirion) covering the measuring component of the sensor. The polymer films on the sensors were left to dry for approximately one hour. After one hour, the toluene had evaporated and the polymer film was adhered onto the humidity sensors surface.

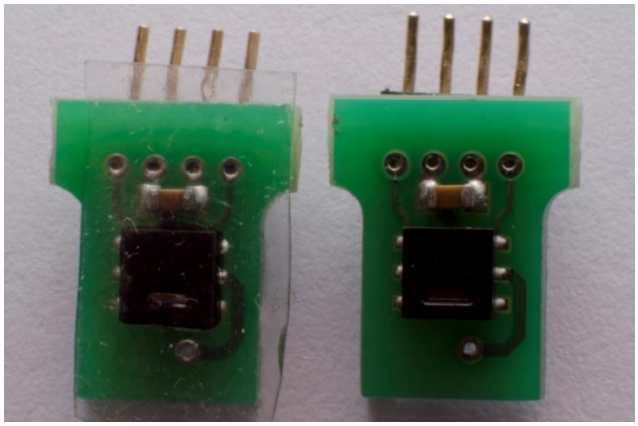

Figure V.4. Pictures of SHT21 humidity sensors (sensirion) with a polymer film (left) and without a polymer film (right).

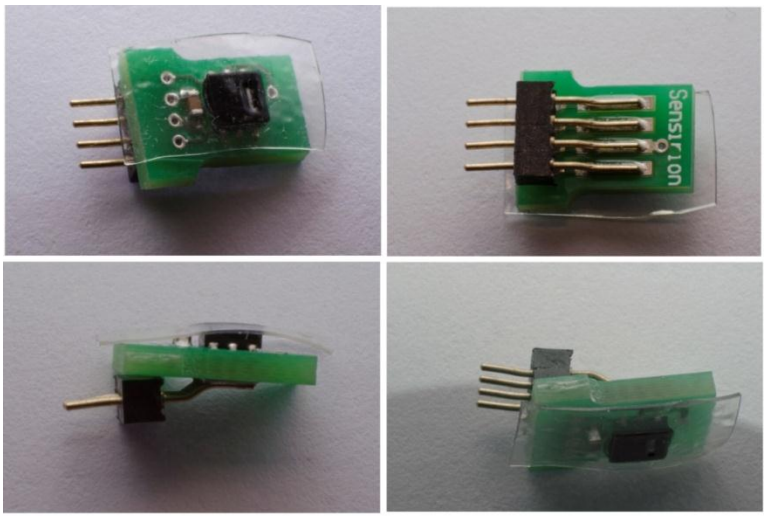

Figure V.5. Pictures of SHT21 humidity sensor with a pasted polymer film

Typical permeability measurements: Two sensors, one with the sample and other as a reference were connected to EK-H4 multiplexer box obtained from Sensirion. The sensors were allocated inside of a closed chamber with an in and out entry air. Two different experiments were undertaken, one from 90 % to 0% of relative humidity and other from 0% to 90% relative humidity. Before each experiment the samples were stabilized at 90% RH or 0% RH applying compressed air or humid air to the chamber until a stable value of humidity was observed in the sample sensor. Then, compressed dry air or humid air was applied to change the chamber humidity from 90% to 0% or from 0% to 90%. Air flow was kept constant using a gas flowmeter (Aluminum 65-mm flowmeter, RZ-32463-20). Humid air was obtained by bubbling compressed dry air in a round bottomed flask filled with water. The relative humidities over time in both sensors was measured by the EK-H4 multiplexer box and recorded on a computer using the EK-H4 viewer standard software program provided by Sensirion.

V.3. Results and Discussion

The hybrid polymer films analyzed in this work were made from waterborne poly(styrene-*co*-*n*-butyl acrylate) latex particles armored with different amounts of Laponite clay discs. The armored latex particles were prepared by soap-free Pickering emulsion polymerization (see chapter III for details of their synthesis). The clay nanodiscs are present on the polymer latex particle surfaces forming a

honeycomb structure after film formation, as evidenced by the monolayer of P(Sty-*co*-BA)/clay film TEM picture of **Figure V.6**.

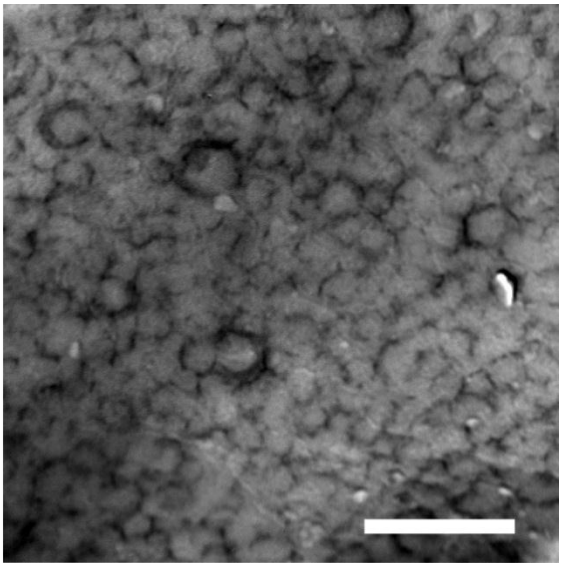

Figure V.6. TEM picture of a monolayer polymer film latex made of poly(styrene-*co*-*n*-butyl acrylate) latex particles armored with Laponite clay XLS (black "lines") (scale bar: 500 nm).

V.3.1. Water adsorption/desorption properties of clay-polymer films

V.3.1.1. Influence of Laponite clay on water adsorption/desorption properties of hybrid polymer films

It is demonstrated in chapter IV that the use of fillers leads to remarkable improvements in mechanical,[1-5] and thermal[7,8,26,27] properties of polymer films. Herein, this work focus on studying the influence of clay in water/vapor uptake and release of polymer films made from poly(styrene-*co*-*n*-butyl acrylate) latex particles armored with clay platelets. Previous work in this area showed that the presence of fillers improved the capacity of polymer films to retain water. For

example, Ragosta[28] showed using FTIR analysis that the presence of silica in polyimide films increased the water uptake as a result of an increase in hydrogen-bonding interactions with water molecules. Similar work performed by Vautrin et al.,[29] also illustrated that the presence of silica in polyimide films improved the capacity for water sorption. Sammon and coworkers[30] demonstrated that montmorillonite clay can improve the capacity of poly(vinyl alcohol) to adsorb water by diffusion onto the surface of exfoliated clay.

Herein, dynamic vapor sorption (DVS) is used to measure and quantify water uptake/release properties of waterborne hybrid polymer films. A series of poly(styrene-co-n-butyl acrylate) films containing different amounts of Laponite clay were studied. The sorption/desorption isotherms are shown in **Figure V.7**.

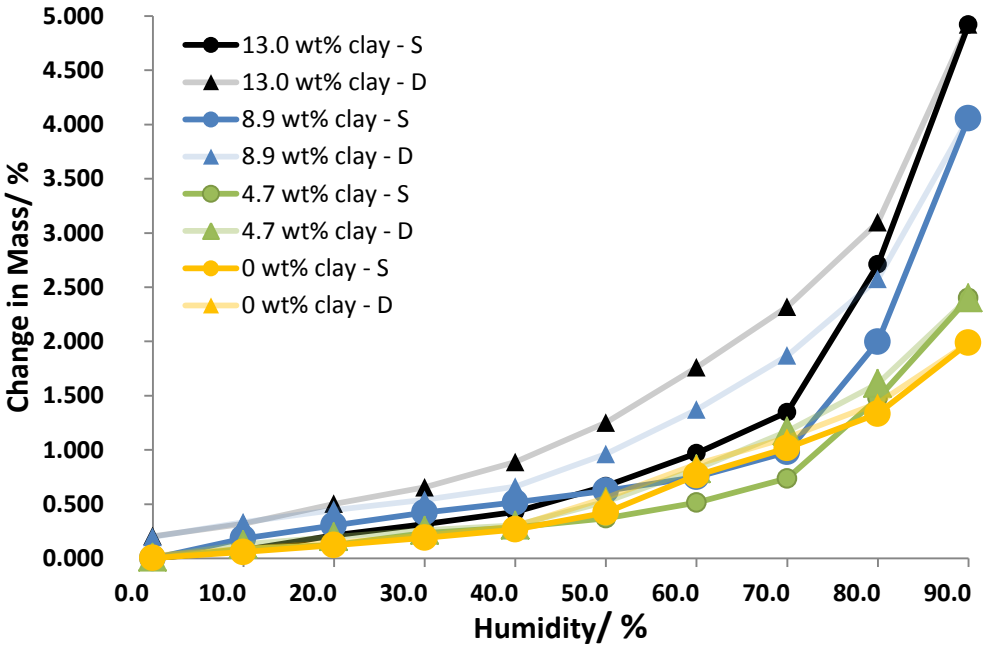

Figure V.7. Isotherm plots (from 0% to 90% RH) of hybrid polymer films made from poly(styrene-*co*-*n*-butyl acrylate) latex particles amored with different amounts of Laponite clay XLS (based on monomer content). The darker lines are the sorption isotherms (S) and the lighter liner are the desorption isotherms (D).

From the results showed in **Figure V.7**, we can clearly observe that for 90% of relative humidity (RH), the polymer films with higher amounts of Laponite clay take up a greater amount of water in comparison with polymer films with lower amounts of clay. Until 40% of RH, water adsorption is relative linear with the humidity pressure as predicted by the BET theory, accounting for multilayer adsorption of water molecules from the penetrated vapor phase. For higher values of RH, especially for values exceeding 60% of RH the increase in water uptake is substantial and can no longer be explained with the BET model. The reason for the increase can be ascribed to the phenomenon of capillary condensation in the honeycomb clay network. The interstitial spaces between the clay discs are of nanometer dimensions, causing a substantial capillary under pressure leading to condensation of water vapor, hereby forming a liquid phase, obviously allowing for higher amounts of water to be stored within the clay network. For illustration: The capillary under pressure in an open cylindrical capillary can be calculated from:

$$\Delta P = \frac{\gamma \cos\theta}{a}$$

Equation V-2

With γ being the air-liquid interfacial tension (J m^{-2}), θ the contact angle and a the diameter of the cylindrical capillary.

As discussed before, during an adsorption isotherm, capillary condensation in porous materials occurs until vapor equilibrium is reached which in a sorption isotherm satisfies the larger pore size. During the evaporation phase, this equilibrium is reached when the water in the smaller pore size is evaporated. In our case discrepancies in variation of the pore size due to a non perfect

homogeneous distribution of Laponite clay in the hybrid polymer films justifies the hysteresis observed on the adsorption/desorption curves of **Figure V.7.** It is clear that for higher amounts of clay, the hysteresis is more pronounced compared to the samples with lower amounts of clay. The sample with no Laponite, for example, shows very little difference on the adsorption/desorption isotherms as a result of the absence of a clay nanochannels.

Figure V.8 shows a correlation between water uptake/release with time for the different samples analyzed. The polymer film is exposed to different RHs in a stepwise manner, starting at 0% RH, with a stepwise of 10% RH. After a step-change the response in change in mass over time is monitored until equilibrium between the sample and the relative humidity under atmospheric overall pressure is reached, after which the next step is applied. This process repeated until a RH value of 90% after which the process is reversed until eventually dry conditions are reached again. It is clear that the samples with higher clay content adsorbed more water but also need more time to absorb it. Between the sample with 4.7 wt% of clay content and the sample without any amount of clay, we can observe a small increase in the water adsorption. This increase is due to the formation of a honeycomb structure in the polymer film that allows the water adsorption by capillary condensation. With the increase of clay content and, taking into account that all polymer-clay latexes are formed of polymer particles with the same size (*ca*. 115 nm) and therefore the total surface area of the clay network is kept approximately constant, the increase in water adsorption is likely due to the increase of the interstitial spaces between clay and polymer particles where water molecules can be stored. The capillary under pressure in

the interstitial spaces is higher with increase of clay content and water release became more difficult, as demonstrated in **Figure V.8** for samples with 13.0 wt% and 8.9 wt% of clay content.

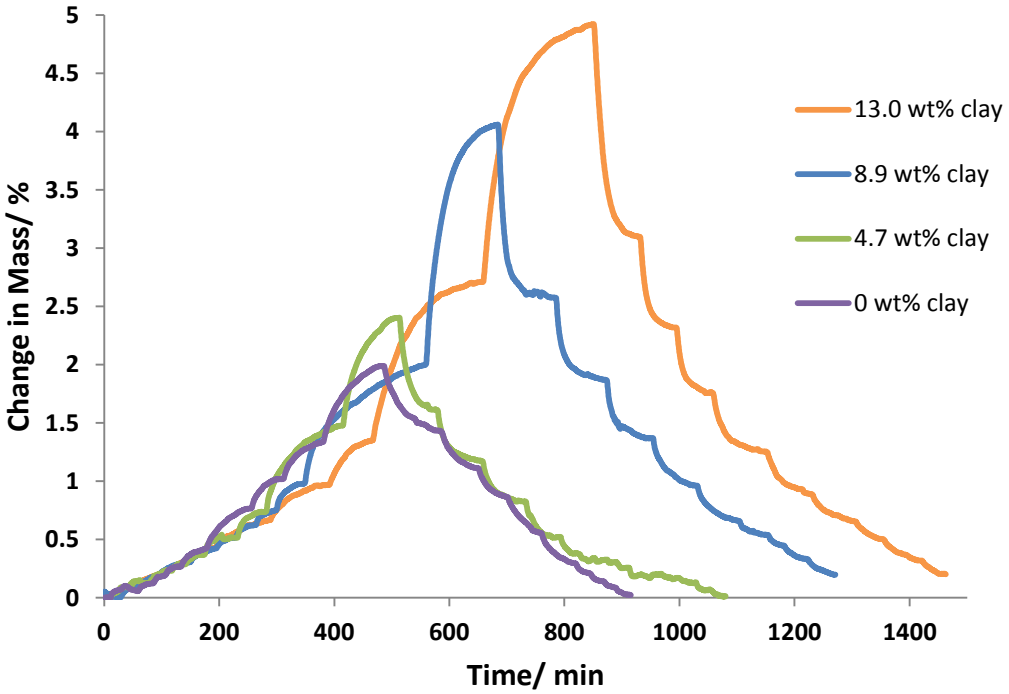

Figure V.8. Dynamic vapor sorption measurements (from 0% to 90% RH) of hybrid polymer films made from poly(styrene-*co*-*n*-butyl acrylate) latex particles armored with different amounts of Laponite clay XLS (based on monomer content).

V.3.1.2. Comparison of water and octane adsorption/desorption isotherms of a polymer film with clay and a polymer film without clay

In order to study the sorption behavior of these hybrid polymer films when exposed to vapors different from water, we ran two experiments where we compared the adsorption of octane vapor in a polymer film made by P(Sty-*co*-BA) with and without Laponite clay. One could hypothesize that if the clay

network would fully shield the polymer, the uptake in octane would be very little. This was not the case, which meant that the polymer could be exposed to octane vapor. This indirectly has to be expected as some polymer polymer interdiffusion must have occurred during film formation as coherent flexible films were obtained. In **Figure V.9**, we show that the sample with Laponite clay had a higher capacity to adsorb not only more water vapor, but also more octane vapor. A plausible reason for these results relies on the fact that besides the Laponite clay being more hydrophilic, the clay network and its channels network create "free spaces/gaps" in the polymer films where molecules can be adsorbed and stored. However, during the evaporation phase, the clay network with interstitial spaces facilitates diffusion out of the polymer film and thus speeds up the evaporation process.

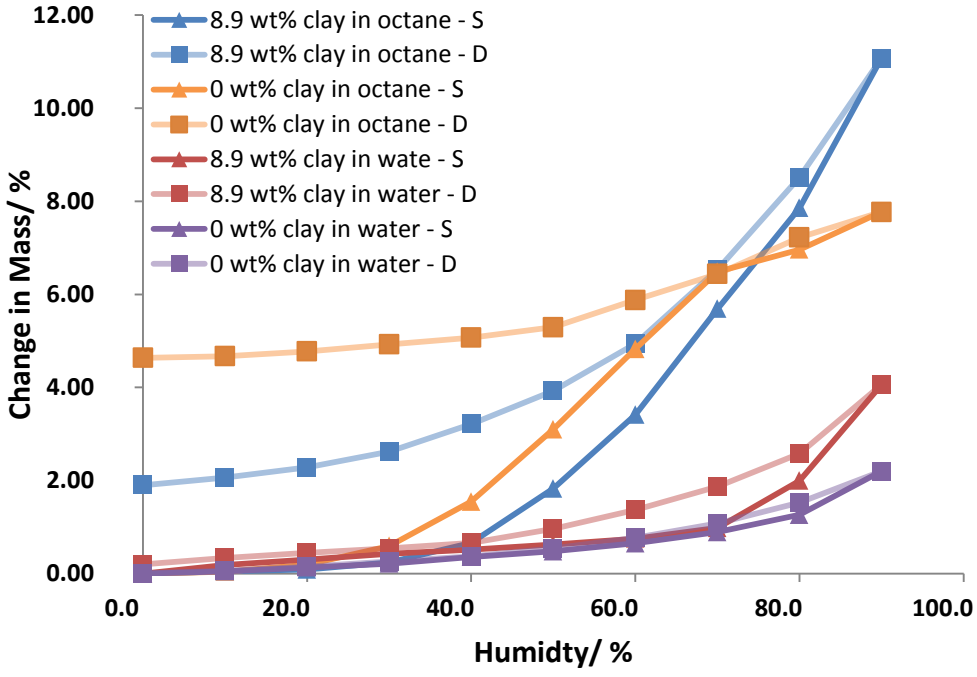

Figure V.9. Isotherms plots (from 0% to 90% of RH) of poly(styrene-*co*-*n*-butyl acrylate) polymer films with and without Laponite clay XLS (based on

monomer content) under water moisture and octane vapor. The darker lines are the sorption isotherms (S) and the lighter liner are the desorption isotherms (D).

V.3.1.3. Comparison of water adsorption/desorption isotherms between a hybrid polymer film and a blend latex film of hybrid polymer particles and polymer particles without any amount of clay discs

It was discussed above that the presence of honeycomb clay network into polymer films of poly(styrene-*co*-*n*-butyl acrylate) increases the water uptake capacity of the waterborne polymer films. However there is no proof that a simple blend mixture of P(Sty-*co*-BA) particles with Laponite clay would have the sample result. Herein, we compared the isotherms of an hybrid polymer film with a honeycomb structure, with a blend polymer film made of P(Sty-*co*-BA)/clay particles and P(Sty-*co*-BA) particles. Interestingly, **Figure V.10** shows that the blend latex film adsorbed roughly the same amount of water as a sample without any clay. In this blend mixture the honeycomb structure is broken by the "naked" particles and a continuous porous clay network is not present anymore. This means that capillary condensation of water molecules in the clay porous nanochannels will not occur or will occur to a less extent, leading to much less water adsorption.

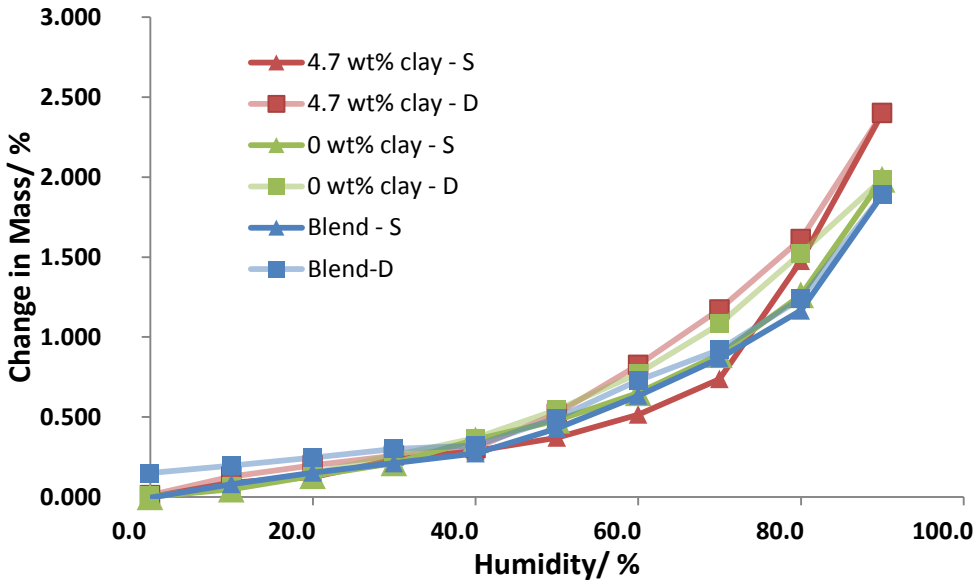

Figure V.10. Isotherms plots (from 0% to 90% RH) of poly(styrene-co-n-butylacrylate) polymer films with and without Laponite clay XLS (based on monomer content) and a blend mixture of both latexes. The darker lines are the sorption isotherms (S) and the lighter liner are the desorption isotherms (D).

V.3.1.4. Comparison of water adsorption/desorption isotherms of a hybrid polymer film with the same polymer film after HDMS or freeze dry treatment

For some applications, such as protective coatings, it would be highly useful to combine the strength of hybrid nanocomposites with good hydrophobic properties. Therefore, hydrophobic treatments of sol-gel silica based polymer films, such as tetraethylstannane, hexabutyldistannoxane, trimethylchlorosilane and hexamethyldisiloxane (HDMS) methods have been already reported.[31-33] To improve hydrophobicity of our polymer films, we exposed a waterborne hybrid polymer film to HDMS via sublimation. Alternatively, freeze drying technique,

used to prepare porous materials,[34-36] was used to fuse the clay network by dehydration and reduce the interfacial spaces created by the honeycomb structure. Figure V.11 shows the differences obtained in the water adsorption/desorption isotherms of a hybrid polymer film and the same polymer film after HDMS or freeze drying treatment (The HDMS treatment consisted in a simple exposition of the polymer film to a saturated HDMS air in a closed flask with two drops of HDMS (during one night). The freeze drying exposition was performed with the sample in a round bound flask under vacuum at -50°C during one night).

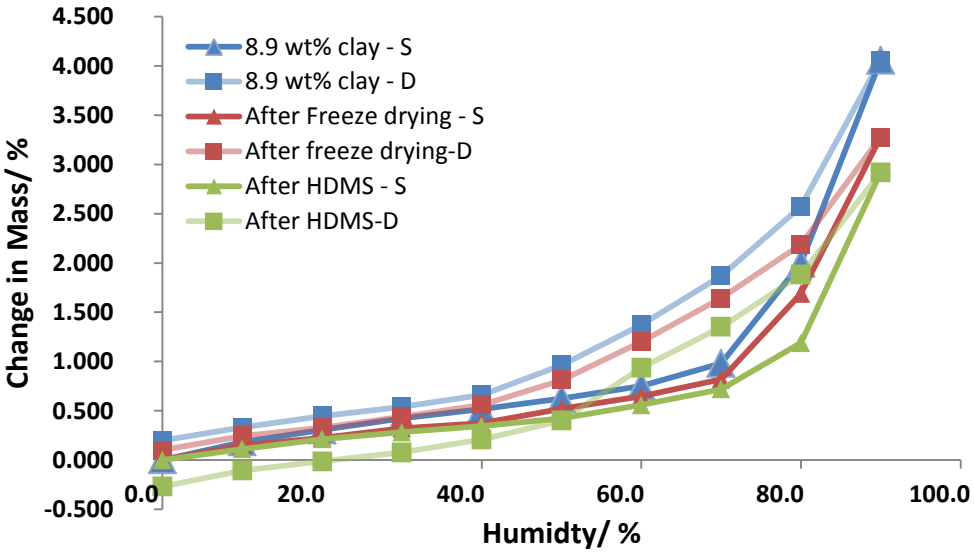

Figure V.11. Isotherms plots (from 0% to 90% RH) of poly(styrene-co-butylacrylate) polymer film with Laponite clay XLS (based on monomer content) and the same sample after freeze drying treatment or HDMS treatment. The darker lines are the sorption isotherms (S) and the lighter liner are the desorption isotherms (D).

The HDMS or freeze drying treatments considerably reduced the water uptake capacity of the hybrid polymer film. These improvements on the

hydrophobic behavior are more obvious at 90% of RH, where the amount of water adsorbed is reduced from *ca* 4 wt% to *ca* 3 wt% (freeze drying) and 2.5 wt% (HDMS). After freeze drying, the clay network fuses, becoming more rigid and strong, reducing the free/open spaces where the water molecules can be stored. The HDMS treatment was the most efficient in turning the relatively hydrophilic hybrid film into a relative hydrophobic polymer film. The negative mass observed after desorption for the sample treated with HDMS is probable due to dissolved HDMS present on the polymer films on the beginning of the experiment.

The reduction in water uptake after HMDS/freeze drying treatment led to similar water uptake results in comparison with the pure polymer film (**Figure V.11**), but potentially keeping the mechanical strengthen provided by the presence of Laponite clay.

V.3.2. Barrier properties of clay-polymer films

In the previous section, water uptake and water release properties of polymer films made from poly(styrene-*co*-*n*-butyl acrylate) latex particles armored with different quantities clay platelets were discussed. Herein, we focus on studying barrier/permeability properties of these waterborne hybrid polymer films. Some previous works, suggests that the presence of silicates have a dramatically influence on polymer films barrier properties. De Kee and coworkers[37] showed that the presence of organoclay in poly(ethylene vinyl acetate) films improves its oxygen barrier properties. The effect was more pronounced with increasing

organoclay content. Dubois *et al.*,[38] demonstrated that the presence of montmorillonite clay in poly(ε-caprolactone) films prepared by *in situ* polymerization improved the gas barrier properties of poly(ε-caprolactone) in comparison with the same polymer without any montmorillonite clay. Grunlan[39] and collaborators demonstrated that the presence of clay in polyethylenimine (PEI) and poly(acrylic acid) films markedly improved the oxygen barrier properties of PEI. In their work, a layer-by-layer technique was used to incorporate silicates into polymer films. Marais and coworkers[40] reported that water permeability and diffusivity decreases when the volume fraction of organoclay in polyamide nancomposite increases. Ha,[41] using gravimetric analysis, showed that the presence of natural unmodified (Cloisite 30B) nanoclay increases the water permeability properties of poly(l-lactide) films. However, when they used organo modified clay (Cloisite 20A and 30B) the water permeability decreased. This difference is explained with the different hydrophobicities of organo modified and unmodified clay used.

Here, water vapor permeability properties of polymer films made from poly(styrene-*co*-*n*-butyl acrylate) latex particles armored with Laponite clay XLS are investigated. We present an innovative method to analyze vapor permeability properties of waterborne polymer films (see diagram of **Figure V.12**).

In a closed chamber two humidity sensors (sensirion SHT21) connected to EK-H4 multiplexer box measure the humidity over time that is recorded on a computer using the EK-H4 viewer standard software provided by Sensirion (see diagram of **Figure V.12**). The sensor 1 is left without any sample and used as a

reference. On sensor 2, a thin waterborne polymer film is pasted on the sensor surface. To avoid any air leaks between the inside of the sensor (that real measures the humidity) and the outside (chamber), a drop of toluene was deposited on the polymer film surface before pasting it on the sensor surface. This was a crucial "trick" to completely isolate the sensor from the chamber (toluene dissolves a small amount of polymer that is then pasted on the sensor). Assuming complete isolation of the humidity sensor by the pasted polymer film, the humidity changes verified in the sensor over time are directly related to the water vapor transport across the polymer film. To make comparisons between samples, all polymer films used were cut with the same dimensions. Also, a gas flowmeter was used to control the flux rate of either humid air or compressed dry air to the humidity chamber.

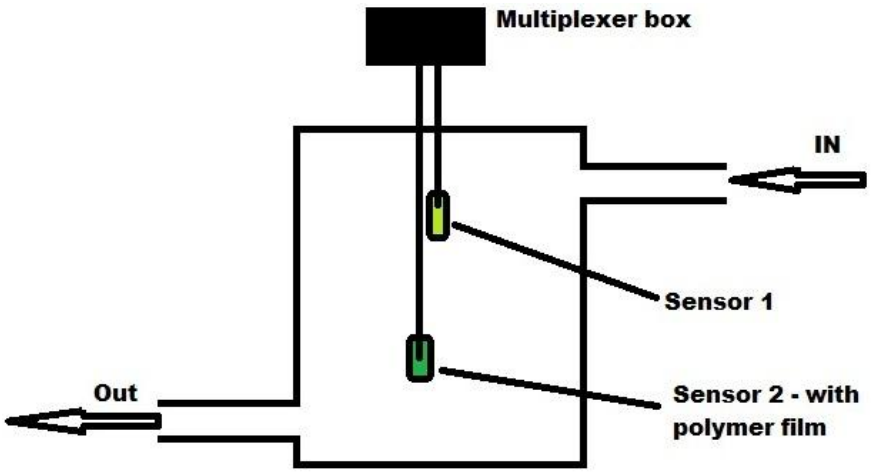

Figure V.12 Diagram of humidity chamber with two humidity sensors inside. Sensor 1 is a reference sensor and Sensor 2 is the sensor with a polymer film to analyze.

Figure V.13. Pictures of the humidity chamber designed and multiplexer box (EK-H4).

V.3.2.1. Study of the influence of Laponite clay XLS on the barrier properties of waterborne hybrid polymer films

In a first series of experiments, P(Sty-*co*-BA) films with a Laponite clay honeycomb structure using different amounts of clay were investigated. The thickness of all polymer films and their relative surface area was kept constant. In each experiment, the reference sensor was left without any polymer film on it while the sensor 2 had the sample to analyze. Humid air was passed into the closed chamber, and values of 90% of relative humidity were immediately measured by sensor 1, while a period of 10-15 hours was needed to have a similar humidity value in the sensor 2. After this equilibration period, compressed dry air was passed. The first point was considered as time zero and the end of each experiment was considered when an almost constant value of

relative humidity was observed in sensor 2. These experiments, where we monitored the humidity from high values of RH% to low RH% values are shown as the desorption curves. The opposite, sorption curves, were also investigated.

From the top graph of **Figure V.14**, it is clear that the samples with higher clay contents, take more time to transport the dry air from outside of sensor 2 to inside, or to transport water moisture from inside to outside. It was shown in the first section of this chapter that higher loads of clay means more capacity to adsorb water but also more difficulties in releasing it. Here the same behavior is observed for water vapor transport across the polymer films: the release of humidity content took more time in the samples with more clay content. As before, this behavior is justified by the strong interaction of Laponite clay with water molecules, retaining these molecules inside of the interstitial spaces of the polymer films. A second observation of the top graph of **Figure V.14** is the presence of different phases on the desorption curves. This difference in the desorption rates are more clear by observation of the first derivative of the desorption isotherm (bottom graph of **Figure V.14**). When we have a closer look at the values of RH versus time and its first derivative we can observe different regions. Initially there seems to be an inertial phase in which the sensor does not respond to a drop in RH on the outside. In other words the polymer film acts as a perfect insulator. This plateau region extends over longer time periods for the nanocomposite films with more clay (see appendix, top graph of **Figure A. V-1**, where it is clear that the time of the 1st derivative maximum is bigger for higher loads of clay). After this plateau region, we can observe a

decrease in the RH values over time. From both plots it is interesting to note that a first order drop and thus a linear response is achieved, which extends in all cases to approximate RH values of ca. 62%. We believe that throughout this region the clay network is filled with water. The next region shows an acceleration in loss of humidity in the sensor chamber, and occurs down to values of approximately 50% of RH. We think that during this period the water inside the capillary network evaporates, the end result being the loss of the internal liquid phase of water. The following step, that is very clear in both graphs of **Figure V.14**, corresponds to the transport of water mainly through diffusion. This transport happens following the BET theory until *ca* 15% of RH. A final step is observed where the RH decrease slows down. In this stage, the polymer film is almost dry. Some water may be trapped in the interstitial spaces of the hybrid polymer film and have difficulties leaving the polymer film. In the sorption curves (**Figure V.15**), the same stages are also followed. Samples with higher loads of Laponite clay, take more time to transport water vapor from one side, to other side of the hybrid polymer films. After an initial small stabilization period (see also bottom graph of **Figure A. V-1** in appendix), the sorption curves follow the BET theory until *ca* 50 % of RH (**Figure V.15**). After this period, we can observe on the first derivative graph of **Figure V.15** the presence of a flat region (until ca 62 % of RH), which is bigger for higher loads of clay. This may correspond to the period in which the water fills the clay network pores. The following step, clear in both graphs of **Figure V.15**, corresponds to a linear increase in the humidity until values *ca* 78 % of RH. Finally, like in the desorption curves, the sorption slows down and the polymer film is saturated with water.

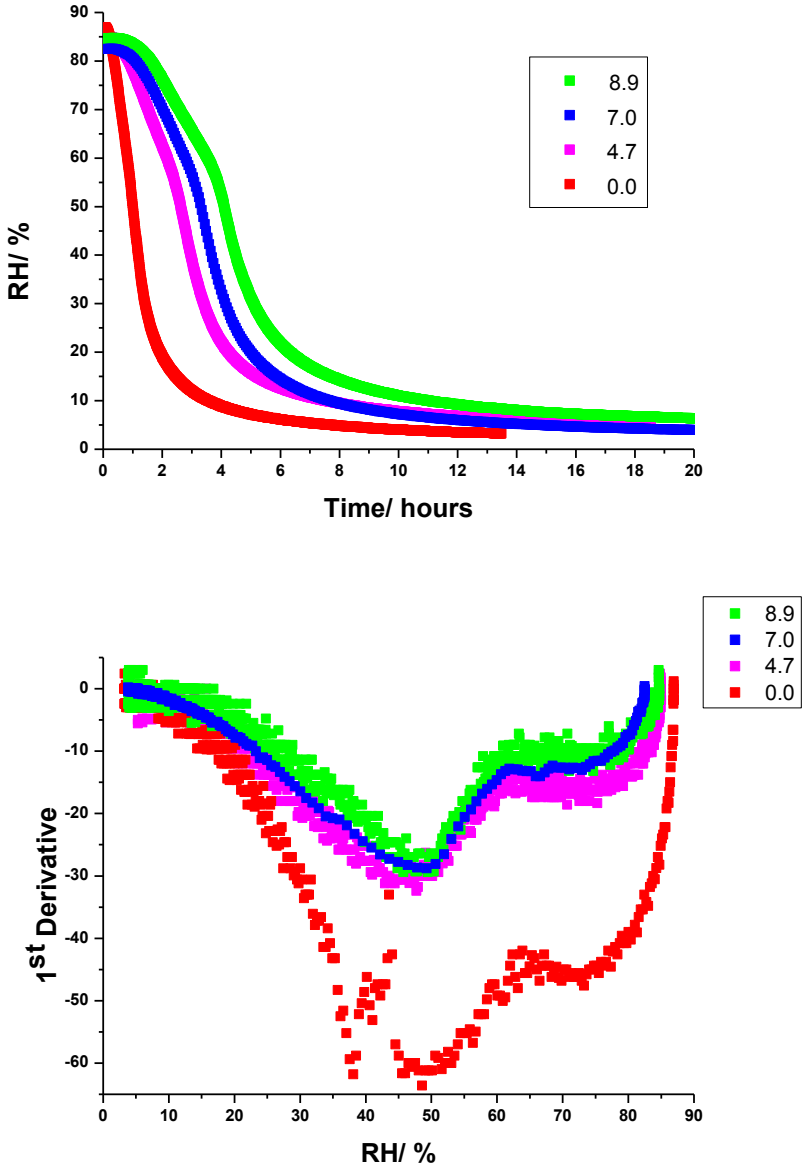

Figure V.14. On top: Desorption isotherm of relative humidity (RH %) versus time of poly(styrene-*co*-*n*-butyl acrylate)/clay films with 8.9, 7.0, 4.7, 0.0 weight % in clay content and 220 μm in thickness. On bottom: First derivative versus RH% of the top graph.

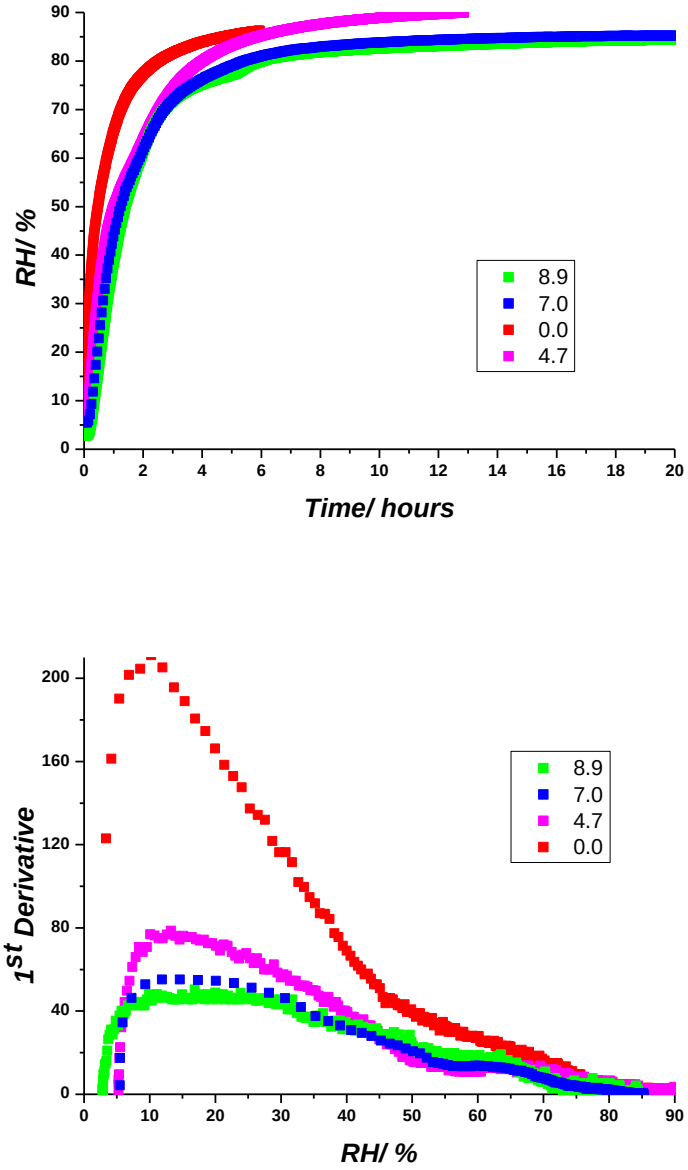

Figure V.15. On top: Sorption isotherm of relative humidity (RH %) versus time of poly(styrene-*co*-*n*-butyl acrylate)/clay films with 8.9, 7.0, 4.7, 0.0 weight % in clay content and 220 μm in thickness. On bottom: First derivative versus RH% of the top graph.

V.3.2.2. Influence of film thickness on the barrier properties of clay-polymer films

In real applications, a fine balance of the amount of clay used has to be considered in order to obtain the mechanical, barrier and flexibility properties desired. As well as polymer composition, polymer thickness is also fundamental in order to achieve the desired properties. For example, Chatham[42] showed that the oxygen permeability strongly decreases with the increase of polymer coating thickness of silicon rubber and polyethylene terephthalate (PET). Flandin and coworkers[43] demonstrated that increasing the Aluminum thickness on PET films surfaces, have a strong effect in the reduction of water vapor permeability of the polymer films. Alves[44] showed in his work a decrease of water/gas (oxygen and carbon dioxide) permeability with the increase of "mica" silica flakes content in polysaccharide films.

Herein, the polymer thickness influence on the barrier properties of polymer films made from poly(styrene-*co*-*n*-butyl acrylate) latex particles armored with Laponite clay is investigated. In **Figure V.16** and **Figure V.17**, it is shown, either in desorption and sorption curves, that thicker films have greater barrier properties compared to thinner polymer films (see also **Figure A. V-2** in appendix, that clear shows that the time of the first derivative maximum is larger for thicker films). The same shape curves are applied to all films thicknesses. An interesting aspect is the difference observed between the samples with 259 µm and 530 µm in thickness. Between these samples, it can be observed a big improvement in the water vapor barrier properties. With thicker films, it is more likely to have "dead ends" or discontinuity of the clay honeycomb structure, and

the molecules are more likely to stay trapped inside of the polymer films. Between these two thicknesses, we most presumably are in the presence of a critical thickness phase, where the effect of "dead ends" becomes more pronounced.

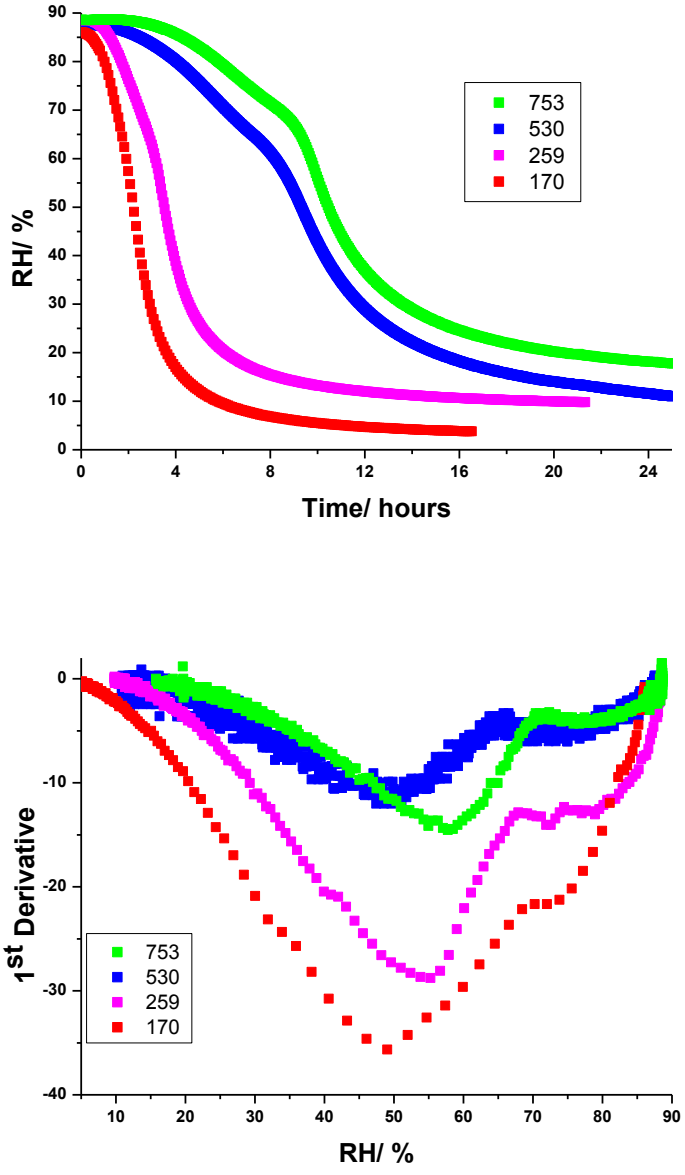

Figure V.16. On top: Desorption isotherm of relative humidity (RH %) versus time of poly(styrene-*co*-*n*-butyl acrylate)/clay films with 7.0 wt% in clay content and 753, 530, 259 and 170 μm in thickness. On Bottom: First derivative versus RH% of the top graph.

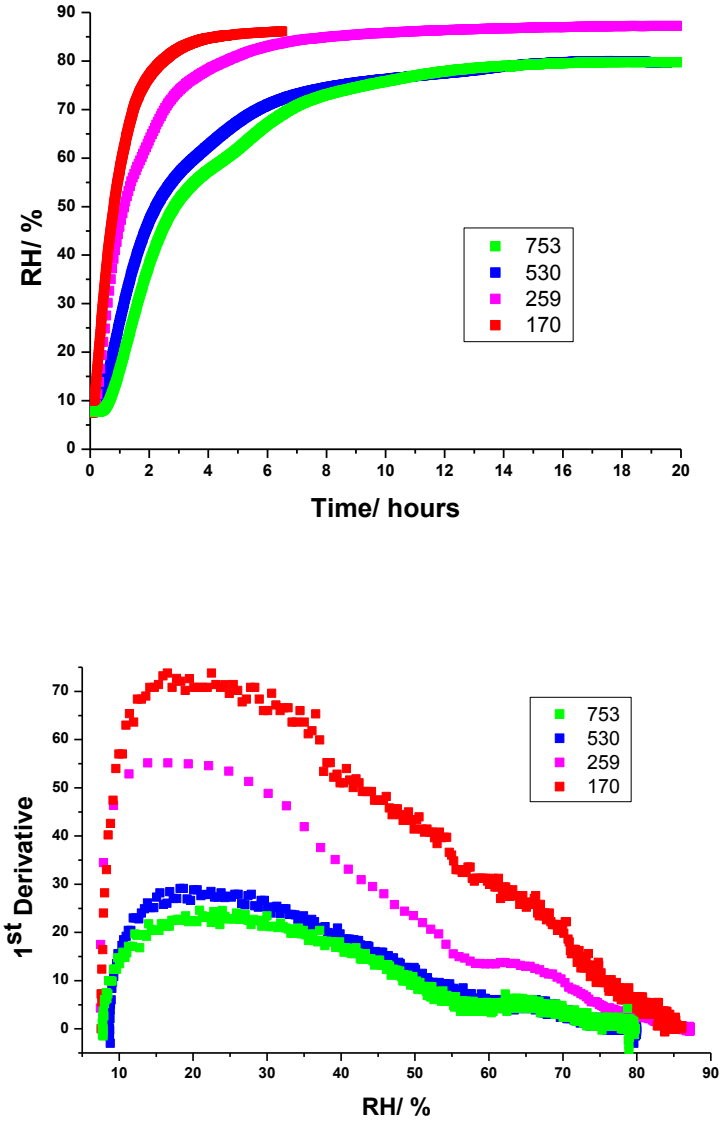

Figure V.17. On top: Sorption isotherm of relative humidity (RH %) versus time of poly(styrene-*co*-*n*-butyl acrylate)/clay films with 7.0 wt% in clay content and 753, 530, 259 and 170 μm in thickness. On Bottom: First derivative versus RH% of the top graph.

V.4. Conclusions

It was shown that the presence of Laponite clay XLS in polymer films prepared from "soft" polymer latexes particles armored with clay discs increases the water mass uptake capacity. It was demonstrated that polymer films with higher quantities of clay, have greater difficulty in the release of water due to capillary pressure forces provided by the honeycomb clay structure and due to strong chemical affinity between the hydrophilic Laponite clay and water molecules. It was shown that with increase in clay content, more interstitial spaces are present in the polymer films, increasing the capacity of the film to adsorb not only hydrophilic water molecules, but also hydrophobic octane molecules. It was verified that polymer films adsorbed water/octane close to linearity with the increase of humidity pressure until values of *ca* 40 RH% that are in agreement with the BET theory. However, for higher humidity pressures, the solvent sorption sharply increases due to capillary condensation of the solvent molecules into the porous clay channels. A blend polymer film made from the mixture of hybrid polymer latex particles armored with clay nanodiscs and non armored polymer particles was analyzed, showing similar water adsorption in comparison with a polymer film without any clay. This is clear evidence that the honeycomb structure plays an active role in the adsorption/desorption properties of polymer films. Freeze drying and HDMS treatments were successfully performed in order to alter the properties of polymer films from a relatively hydrophilic material to a relatively hydrophobic material. Finally, an innovative method to analyze water barrier properties was presented. We demonstrated that polymer films with higher loads of Laponite

clay improved the water barrier properties. In addition, we showed that in increasing the polymer films thicknesses; we also improved the water vapor barrier properties of nanocomposite polymer films.

V.5. References

(1) Negrete-Herrara, N.; Putaux, J.-L.; David, L.; De Haas, F.; E., Bourgeat-Lami, E., *Macromol. Rapid. Commun.* **2007**, *28*, 1567-1573.

(2) Faucheu, J.; Gauthier, C.; Chazeau, L.; Cavaille, J.-Y.; Mellon, V.; Bourgeat-Lami, E., *Polymer.* **2010**, *51*, 6-17.

(3) Diaconu, G.; Paulis, M.; Leiza, J. R., *Polymer.* **2008**, *49*, 2444-2454.

(4) Diaconu, G.; Paulis, M.; Leiza, J. R., *Macromol. React. Eng.* **2008**, *2*, 80-89.

(5) Agag, T.; Koga T.; Takeichi, T., *Polymer.* **2001**, *42*, 3399-3408.

(6) Gilman, J. W., *Appl. Clay Sci.* **1999**, *15*, 31-49.

(7) Inan, G.; Patra, P. K.; Kim, Y. K.; Warner, S. B., *Mater. Res. Soc. Symp. Proc.* **2003**, *708*, 289-295.

(8) Gilman, J. W.; Jackson, C. L.; Morgan, A. B.; Harris, R.; Manias, E.; Giannelis, E. P.; Wuthenow, M.; Hilton, D.; Phillips, S. H., *Chem. Mater.* **2000**, *12*, 1866-1873.

(9) Joanicot, M.; Wong, K.; Cabane, B. *Macromolecules.* **1996**, *29*, 4976-4984.

(10) Chevalier, Y.; Pichot, C.; Graillat, C.; Joanicot, M.; Wong, K.; Maquet, J.; Lindner, P.; Cabane, B., *Colloid Polym. Sci.* **1992**, *270*, 806-821.

(11) Eckersley, S. T.; Rudin, A., *J. Appl. Polym. Sci.* **1993**, *48*, 1369-1381.

(12) Feng, J.; Winnik, M. A., *Macromolecules.* **1997**, *30*, 4324-4331.

(13) Pichon, A., *Nat Chem* **2010** doi:10.1038/nchina.2010.128.

(14) Uğur, Ş.; Yargı, Ö.; Pekcan, Ö., *Polym. Comp.* **2010**, *31*, 77-82.

(15) Langmuir, I., *J. Am. Chem. Soc.* **1916**, *38*, 2221-2295.

(16) Lowry, H. H.; Kohman, G. T., *J. Phys. Chem.* **1927**, *31*, 23.

(17) Taylor, R. L.; Herrman, D. B.; Kemp, A. R., *INde. Ng. Chem.* **1936**, *28*, 1255.

(18) Brunauer, S.; Emmett, P. H.; Teller, E., *J. Am. Chem. Soc.* **1938**, *60*, 309-319.

(19) Fick, A., *Annal. Physik.* **1855**, *170*, 59-86.

(20) Atkins P. W., Physical Chemistry, *Oxford University Press, 6th ed.* **1998**.

(21) Eijkel, J. C. T.; Dan, B.; Reemeijer, H. W.; Hermes, D. C.; Bomer, J. G.; van den Berg, A., *Phys. Rev. Lett.* **2005**, *95*, 256107.

(22) Schramm, L. L., The Language of Colloid & Interface Science, *ACS: Washington, DC.* **1993**.

(23) Hunter, R.J., *Oxford University Press, 6th ed.* **2001**.

(24) Burgess, C. G. V.; Everett, D. H.; Nuttall, S., *Pur. Appl. Chem.* **1989**, *61*, 1845-1852.

(25) Tompsett, G. A.; Krogh, L.; Griffin, D. W.; Conner, W. C., *Langmuir* **2005**, *21*, 8214-8225.

(26) Meneghetti, P.; Qutubuddin, S., *Thermochim. Act.* **2006**, *442*, 74-77.

(27) Negrete-Herrera, N.; Putaux, J. L.; David, L.; De Haas, F.; Bourgeat-Lami, E., *Macromol. Rapid Comm.* **2007**, *28*, 1567-1573.

(28) Musto, P.; Mascia, L.; Mensitieri, G.; Ragosta, G., *Polymer.* **2005**, *46*, 4492-4503.

(29) Larobina, D.; Lavorgna, M.; Mensitieri, G.; Musto, P.; Vautrin, A., *Macromol. Symp.* **2007**, *247*, 11-20.

(30) Döppers, L.-M.; Breen, C.; Sammon, C., *Vibr. Spec.* **2004**, *35*, 27-32.

(31) Akovali, G.; Rzaev, Z. M. O.; Mamedov, D. H., *J. Appl. Polym. Sci.* **1995**, *58*, 645-651.

(32) Zhao, X. S.; Lu, G. Q., *J. Phys. Chem. B* **1998**, *102*, 1556-1561.

(33) More, Y. S.; Chang, T. C.; Liu, P. T.; Tsai, T. M.; Chen, C. W.; Yan, S. T.; Chu, C. J.; Pan, W. F.; Pan, F.M.; Lur, W.; Sze, S. M., *J. Vac. Sci. Technol. B* **2002**, *20*, 1334.

(34) Colard, C. A. L.; Cave, R. A.; Grossiord, N.; Covington, J. A.; Bon, S. A. F., *Adv. Mater.* **2009**, *21*, 2894-2898.

(35) Talalay, J. A., *US Patent 2* **1947**, *432*, 353.

(36) Talalay, L; Talalay, A., *US Patent 3* **1996**, *238*, 172.

(37) Zhong, Y.; Janes, D.; Zheng, Y.; Hetzer, M.; De Kee, D., *Polym. Eng. Sc.* **2007**, *47*, 1101-1107.

(38) Gain, O.; Espuche, E.; Pollet, E.; Alexandre, M.; Dubois, P., *J. Polym. Sc. B: Polym. Phys.* **2005**, *43*, 205-214.

(39) Priolo, M. A.; Gamboa, D.; Holder, K. M.; Grunlan, J. C., *Nano Lett.* **2010**, *10*, 4970-4974.

(40) Alexandre, B.; Langevin, D.; Médéric, P.; Aubry, T.; Couderc, H.; Nguyen, Q. T.; Saiter, A.; Marais, S., *J. Memb. Sci.* **2009**, *328*, 186-204.

(41) Rhim, J.-W.; Hong, S.-I.; Ha, C.-S., *LWT - Food Sci. Techn.* **2009**, *42*, 612-617.

(42) Chatham, H., *Surf. Coat. Techn.* **1996**, *78*, 1-9.

(43) Garnier, G.; Yrieix, B.; Brechet, Y.; Flandin, L., *J. Appl. Polym. Sci.* **2010**, *115*, 3110-3119.

(44) Alves, V. D.; Costa, N.; Coelhoso, I. M., *Carbohyd.. Polym.* **2010**, *79*, 269-276.

Chapter VI.

Synthesis of core-shell particles armored with Laponite clay discs using Pickering Emulsion Polymerization

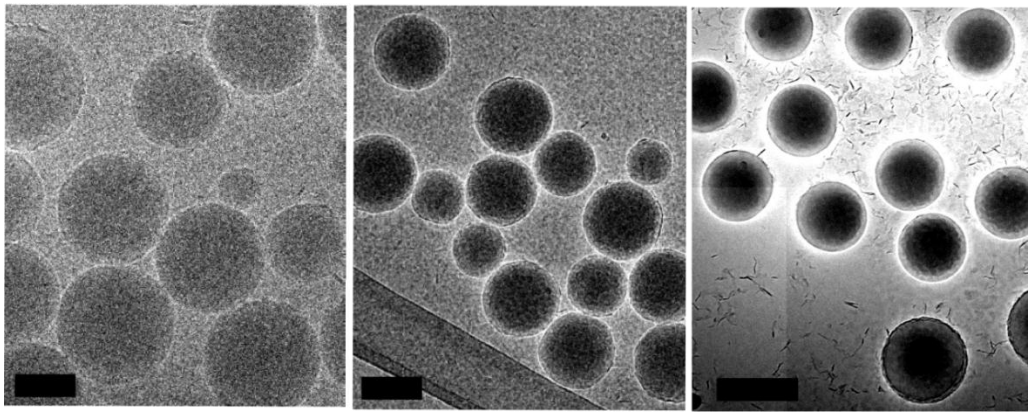

A versatile two step Pickering emulsion polymerization process is used to fabricate core-shell particles armored with Laponite clay XLS discs. In the first step, a seed of poly(styrene) latex particles is produced using soap-free emulsion polymerization in the presence of sodium styrene sulfonate as auxiliary monomer. In the second step, a soft shell of poly(styrene-co-n-butyl acrylate) (0.67 wt/wt) is grown around the seed latex particles in the presence of Laponite clay platelets that are adhered onto the surface of the core-shell particles.

VI.1. Introduction

The fabrication of multi-layered nanoparticles are of great interest, due their potential applications in diverse areas, from medicine and biotechnology to catalysis, encapsulation of cosmetics and paints.[1-5] Various methods to prepare hybrid multi-layered colloidal nanocomposites of different morphologies have been developed, such as layer-by layer,[6] miniemulsion polymerization,[7,8] emulsion polymerization[9] and dispersion polymerization.[10] The incorporation of fillers, such as silica and clay, into these polymer latex based materials can enhance material properties and performance and therefore have attracted considerable academic and industrial interest over the last decade.[11,12] Wu and coworkers[13] showed that polymer films of poly[styrene-*co*-(*n*-butyl acrylate)-*co*-(acrylic acid)] [P(St-BA-AA)]/silica have a remarkable hardness and solvent resistance improvements with increasing silica content. Keddie and collaborators[14] demonstrated that poly(lauryl acrylate) particles armored with Laponite clay RD considerably improved the tack adhesion energy of polymer film in comparison with a polymer of poly(lauryl acrylate) without any clay content. They showed that hybrid particles of poly(lauryl acrylate)/clay have much better tack adhesion properties than a polymer film formed from a simple blend mixture of clay discs and poly(lauryl acrylate).

In most cases, the studies of core-shell particles focus on the "hard-soft" combination or in colloidal particles with fillers.[15] Cabane *et al*.,[16] showed that polymer films made from core-shell particles with a glassy core and a rubbery shell are notably softer than the corresponding blend mixture of "soft" and

"hard" particles. Leibler and Dos Santos[17] demonstrated that core-shell particles with a "soft" core of poly(*n*-butyl acrylate) and a "hard" shell of poly(methyl methacrylate) had greater mechanical strength than the correspondent blend mixture.

Core-shell particles made of "soft" cores and "hard" fillers on the shell are of great importance in order to obtain homogeneity of the dispersed fillers and therefore better improvements on the mechanical properties. Asua and Keddie[18] showed that nanocomposites of poly(vinyl alcohol)/single walled carbon nanotubes P(VA/SWNT) strongly increased the stiffness of the material and energy dissipation in comparison with a blend mixture as a consequence of the better fillers distribution. Armes and coworkers[19] demonstrated that (co)polymer/silica nanocomposites can increase scratch and chemical resistance with increasing silica content.

Other type of core-shell particles are core-shell particles made from a "soft" core and a crosslinked shell. These particles are very interesting due to synergy between mechanical and viscoelastic properties. Lovell and collaborators[20] produced core-shell nanoparticles from the mixture of 1,3-butadiene and methacrylic acid nanoparticles after film formation based on the ionic crosslinking strength between both particles. The resultant films showed strong improvements in the mechanical properties as a result of the ionic crosslinking within a continuous structure that percolates the film. Creton *et al.*,[15] showed an interesting "soft-soft nanocomposite" of different crosslinked acrylic (co)polymers. These polymer films demonstrated a very good viscoelastic

behavior either at small and larger strains. They showed that the adhesion energy of a crosslinked "soft-soft nanocomposite" on polyethylene was up to 4 times bigger than a standard commercial product without crosslinking between the particles.

Colloidal crystals can be made from core-shell particles and have great interest, particularly in the fabrication of polymer films for electronic applications. Differences on the refractive indexes between core and shell and a periodic distribution of the core-shell particles in a polymer film will provide different light scattering and as a consequence color polymer films can be obtained. Lyon and coworkers[21] showed that colloidal crystals with good optical properties can be fabricated from crosslinked poly(N-isopropylacrylamide) p(NIPAm) core microgels and copolymer shell of p(NIPAm). Mangeney *et al*.,[22] showed that core-shell particles of poly(styrene-*co*-α-*tert*-butoxy-ω-vinylbenzylpolyglycidol) have great thermoresponsivity properties. They showed that these core-shell particles could be a good alternative to the common p(NIPAm) colloidal crystal. Zhu and collaborators[23] showed that a "soft" shell of poly(acrylic acid) around poly(styrene) "hard" particles is essential in the formation of microspheres colloidal crystals.

In this Chapter, core-shell particles armored with Laponite clay XLS are fabricated via two step emulsion polymerization process. In the first step, "hard" core poly(styrene) nanoparticles with sulfonate groups on the surface are synthesized. Then, in a second step, a "soft" layer of poly(styrene-*co*-*n*-butyl acrylate) (0.67 wt/wt)) armored with clay platelets is produced. The difference

in the refractive indexes between the core and the shell can potentially be of interest as a colloidal crystal material where the mechanical properties are strengthened by the Laponite clay dics.

VI.2. Experimental part

Materials: Styrene (Sty), *n*-butyl acrylate (BA), were purchased from Aldrich at 99 % or greater purity and used as received. Laponite clay XLS was obtained from Rockwood additives. Initiators azobisisobutyronitrile (AIBN), 99+% p.a.) and amonium persulfate (APS, 99+% p.a) were obtained from Fluka. Deionized water was used in all experiments. Sodium styrene sulfonate (NaSS) and sodium hydrogen carbonate ($NaHCO_3$) were purchased from Aldrich at 99 % purity.

Equipment: Emulsion polymerizations were carried out in double-walled cylindrical glass reactors (250 mL, Asynt) equipped with an external circulating heating bath (Julabo F-25 unit), a condenser, and a four-bladed teflon overhead turbine stirrer fitted at approximately 2 cm from the bottom of the reactor vessel (Cowie Ltd.) typically running at 300 rpm.

Average particle sizes and dispersities of the armored latexes were measured by dynamic light scattering using a Malvern Zetasizer Nano (data was analyzed using the CONTIN algorithm). SEM analyses were performed using a Zeiss Supra55VP FEGSEM with an EBSD camera and the samples were prepared on silicon wafers (kindly donated by Wacker Chemie AG) to be analyzed uncoated. TEM analyses were performed on a 1200EXII TEM with a 1K Gatan camera using Formvar-Film grids (200 Mesh Cu, Agar Sc. S138) and

cryo-TEM analyses were performed on a Jeol 2011 TEM (200KV LaB6) with 2K Gatan Ultrascan camera or on a Jeol 2010F TEM (200KV FEG) with 4K Gatan Ultrascan camera using Lacey-Carbon-Film grids (300 Mesh Cu, Agar Sc. S166-3H). An Analytical Balance (Precisa XT 220A) was used for accurate measurements. EELS (Electron Energy Loss Spectroscopy) analysis were performed in a JeoL 2100 STEM with a scanning mode and a Gatan Quantun SE energy filter.

Typical emulsion polymerization (synthesis of poly(styrene-co-(sodium styrene sulfonate)), first step): Typically, 0.11g of sodium styrene sulfonate (NaSS) and 0.11g of sodium hydrogen carbonate ($NaHCO_3$) were dissolved in 185g of deionized water and the mixture was placed under a nitrogen atmosphere by purging. Degassed monomer (styrene), 20.0 g was added. The reaction mixture was heated to 80ºC, whilst stirring at 300 rpm. The emulsion polymerization was started upon addition of 0.1180 g KPS dissolved in 2.0 g of water. Conversion of the emulsion polymerization was measured by gravimetry. Particle size and morphology were analyzed by dynamic light scattering and scanning electron microscopy (SEM).

Typical solids-stabilized seeded emulsion polymerization (synthesis of core-shell polymer particles): 9.39 g of latex solution of poly(styrene) seed particles was dispersed in 102 g of deionized water and placed under a nitrogen atmosphere by purging. The reaction mixture was heated to 80ºC, whilst stirring at 250 rpm. A mixture of 4.15 g of styrene (Sty) and 6.20 g of *n*-butyl acrylate (BA) was added to the previous mixture. The emulsion polymerization was

started upon addition of 0.0575 g of ammonium persulfate (APS) dissolved in 2.0 g of water. Particle size and morphology were analyzed by dynamic light scattering and scanning electron microscopy (SEM).

Typical solids-stabilized seeded emulsion polymerization (synthesis of armored core-shell polymer particles using APS, second step):): 9.39 g of latex solution of poly(styrene) seed particles was dispersed in 102 g of deionized water and placed under a nitrogen atmosphere by purging. The reaction mixture was heated to 80ºC, whilst stirring at 250 rpm. A mixture of (4.15 g of styrene (Sty) and 6.20 g of *n*-butyl acrylate (BA)) was added to the previous mixture. The emulsion polymerization was started upon addition of 0.0565 g of ammonium persulfate (APS) dissolved in 2.0 g of water. After 3 hours, 0.49 g of Laponite clay XLS dissolved in 2.0 g of water was added to the reaction. Particle size and morphology were analyzed by dynamic light scattering and scanning electron microscopy (SEM).

Typical solids-stabilized seeded emulsion polymerization (synthesis of armored core-shell polymer particle using AIBN, second step)): 9.39 g of latex solution of poly(styrene) seed particles was dispersed in 102 g of deionized water and placed under a nitrogen atmosphere by purging. The reaction mixture was heated to 80ºC, whilst stirring at 250 rpm. The emulsion polymerization was started upon addition of 0.0511 g of azobisisobutyronitrile (AIBN) dissolved in 0.5 g of *n*-butyl acrylate. A mixture of (4.15 g of styrene (Sty) and 6.20 g of *n*-butyl acrylate (BA)) was then fed at 0.054 g/min to the reaction. After 3 hours of the initiator addition, 0.49 g of Laponite clay XLS dissolved in

2.0 g of water was added to the reaction by shot addition. Particle size and morphology were analyzed by dynamic light scattering and scanning electron microscopy (SEM).

Table VI-1. Pickering emulsion polymerizations of styrene stabilized by sodium styrene sulfonate. Ammonium persulfate was used as initiator.

Sample	Sty/ water wt%	NaSS/ Sty wt%	HCO3/ Sty wt%	Initiator/ Sty wt%	Total solids wt%
Seed 1	11.22	0.53	0.53	0.53	10.2
Seed 2	11.12	0.24	0.53	0.53	10.1
RT-3-25	10.99	1.02	0.53	0.54	10.0
RT-3-26	11.01	0.0	0.53	0.53	9.9

Table VI-2. Pickering emulsion polymerization using a poly(styrene) latex as seed and Sty:BA (0.67 wt/wt). Ammonium persulfate was used as initiator.

Sample	Seed Latex	Monomer/ water wt%	Solid seed/ Monomer wt%	Initiator/ Monomer wt%	Total solids wt%
RT-3-42	Seed 1	10.62	7.9	0.57	9.7
RT-3-47	Seed 2	10.94	9.8	0.61	9.9

Table VI-3 Pickering emulsion polymerization using a poly(styrene) latex as seed and Sty:BA (0.67 wt/wt) in the presence of Laponite clay XLS. Ammonium persulfate was used as initiator.

Sample	Seed Latex	Monomer/ water wt%	Clay/ Monomer wt%	Solid seed/ Monomer wt%	Initiator/ Monomer wt%	Total solids wt%
RT-3-49	Seed 1	9.58	9.33	8.74	0.52	9.6
RT-3-45	Seed 2	9.77	9.82	10.26	0.50	9.7

Table VI-4. Pickering emulsion polymerization using a poly(styrene) latex as seed and Sty:BA (0.67 wt/wt) with shoot addition of Laponite clay XLS at X_M of 0.5. Ammonium persulfate was used as initiator.

Sample	Seed Latex	Monomer/ water wt%	Clay/ Monomer wt%	Solid seed/ Monomer wt%	Initiator/ Monomer wt%	Total solids wt%
RT-3-34	Seed 1	9.72	9.82	10.56	0.59	9.7
RT-3-48	Seed 2	10.76	9.32	8.83	0.60	10.5

Table VI-5. Pickering emulsion polymerization using a poly(styrene) latex as seed and Sty:BA (0.67 wt/wt) with shoot addition of Laponite clay XLS at X_M of 0.5. Azobisisobutyronitrile was used as initiator.

Sample	Seed Latex	Monomer/ water wt%	Clay/ Monomer wt%	Solid seed/ Monomer wt%	Initiator/ Monomer wt%	Total solids wt%
RT-3-61	Seed 1	10.10	9.86	9.07	0.58	10.0
RT-3-62	Seed 2	10.05	9.91	9.25	0.57	9.9
RT-3-89	Seed 1	10.02	9.95	19.99	0.57	11.0

VI.3. Results and Discussion

The preparation of core-shell particles armored with Laponite clay XLS was performed using a soap free emulsion polymerization process. Two experimental steps were undertaken. Firstly, the synthesis of "hard" core poly(styrene) latex particles with sulfonate groups on the surface was performed. Second, the synthesis of a core-shell particle with a "hard" core and a "soft" shell armored with Laponite clay was prepared.

VI.3.1. Synthesis of a poly(styrene) seed latex (core)

The preparation of poly(styrene) latexes without the use of emulsifiers has been studied extensively and the particles are often used as model colloids as a result of their narrow particle size distributions.[24] Stabilization of particles can be provided by strong acid groups of certain initiators like ammonium persulfate.[25,26] However, spontaneous hydrolysis and oxidation of the persulfate groups may occur over time resulting in the loss of colloidal stability.[27] Therefore, often monomers such as sodium styrene sulfonate having a strong and stable acid group, are employed to warrant colloidally stable latexes.[24]

Herein, sodium styrene sulfonate (NaSS-to-monomer ratio of 0.24, 0.53 and 1.02 wt %) was used to stabilize and control the particle size of polymer particles with sulfonate groups on the surface. The pH of the solutions were kept constant using sodium hydrogen carbonate as buffer solution at $NaHCO_3$-to-monomer ratio of 0.53 wt% and ammonium persulfate was used as initiator (initiator-to monomer ratio of 0.53-0.54 wt%) (recipes in **Table VI-1**). Scanning electron microscopy and dynamic light scattering analyses demonstrated the fabrication of relatively monodisperse poly(styrene) particles stabilized with sulfonate groups on the surface. The sulfonate groups on the surface of polymer particles create a surface charge that is fundamental to stabilize the particles by electrostatic repulsion. Higher loads of NaSS originated smaller particles, 0.53 wt% of NaSS based on monomer content, lead to *ca* 130 nm latex particles and 0.24 wt% of NaSS-to-monomer content lead to the formation of poly(styrene) particles with *ca* 216 nm. In addition, narrow particle size distribution were

obtained for higher content of NaSS used (D_I=0.002 and D_I=0.040 for 0.53 and 0.24 wt% in NaSS content). These results are in agreement with the work performed by Krieger,[28] in which 0.5 wt% of NaSS based on monomer content reduced the poly(styrene) particles to *ca*. 0.5-1 µm. Increasing the amount of sulfonate groups increases the stability of the polymer latex particles by electrostatic repulsion. The total charge increases, but the charge density per unit area does not increase leading to smaller particles and increasing the total surface area of the polymer particles. However, above 1.02 wt% of NaSS based on monomer content, secondary nucleation was observed. When very high amounts of NaSS are applied, p(NaSS) homopolymer will be formed in the water phase, which can act like a flocculant. On the other hand, emulsion polymerization without any amount of sodium styrene sulfonate led to complete coagulation due to low electrostatic stability.

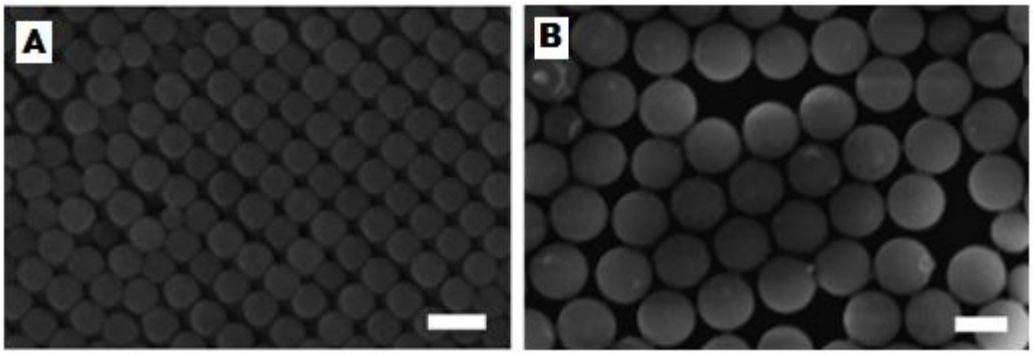

Figure VI.1. SEM pictures of poly(styrene) polymer particles with sulfonate groups on the surface prepared by emulsion polymerization. **A**: sample with 0.53 wt% of NaSS-to-monomer content (Seed 1). **B**: sample with 0.24 wt% of NaSS-to-monomer content (Seed 2). Both scale bars are of 200 nm.

The resulting poly(styrene) latexes (Seed 1 and 2) were dialyzed to remove impurities. The dialyzed latexes were then used as seed latex in a conventional second emulsion polymerization step.

VI.3.2. Preparation of core-shell particles by second step emulsion polymerization

A second step emulsion polymerization using poly(styrene) seed latex and styrene:*n*-butyl acrylate (0.67 wt/wt) comonomers using APS as initator was performed. The aim is to create a core-shell particle with a "hard" core and a "soft" shell armored with Laponite clay which can film form. Our first step towards the preparation of core-shell particles armored with clay discs was to prepare core-shell particles without the presence of Laponite clay via an emulsion polymerization process.

This synthesis of core-shell particles via emulsion polymerization was already undertaken by others, for example by Bourgeat-Lami[29] who demonstrated the preparation of poly(styrene) core particles armored with a shell of methacryloxypropyltrimethoxsilane via two step emulsion polymerization. The core-shell particles obtained using two different poly(styrene) seed particle sizes are presented in **Figure VI.2**.

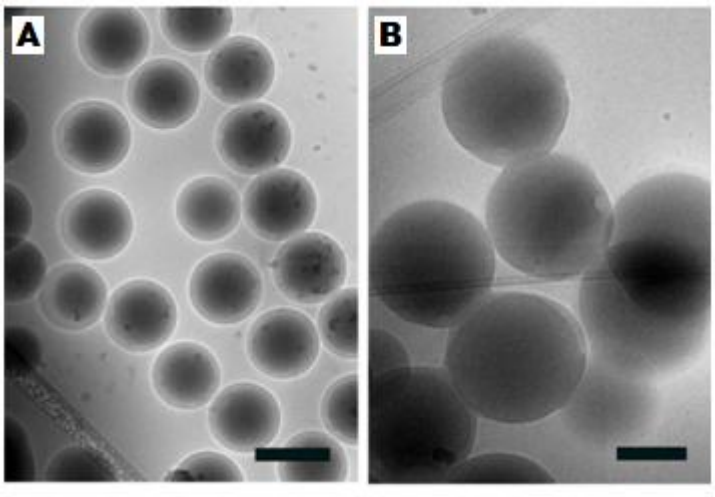

Figure VI.2. Cryo-TEM pictures of core-shell particles with a "hard" core poly(styrene) with sulfonate groups on the surface and a "soft" shell of poly(styrene-*co*-*n*-butyl acrylate) prepared through two step emulsion polymerization process. **A**: core-shell particles with smaller seed particles (seed 1). **B**: core-shell particles with larger seed particles (seed 2). Scale bars are of 200nm.

Figure VI.2 shows core-shell particles obtained through the emulsion polymerization process. This is particularly evidenced on the picture using seed latex 1 (smaller particles). Smaller seed poly(styrene) particles increase the total surface area of the latex particles, increasing the probability of the oligomeric radicals of poly(styrene-*co*-*n*-butyl acrylate) to collide with and/or swell the seed particles. Note that batch emulsion polymerizations were undertaken. Under these conditions the comonomers Sty:BA could have swollen the poly(styrene) seed particles and the reason for the core-shell structure could be due to phase separation of the polymers. On the other hand, localized polymerization in the shell region may have occurred. Particles are not very

small, so entry and propagation could potentially favor the shell region, especially if the core is not fully swollen.

VI.3.3. Preparation of core-shell particles armored with Laponite clay XLS

After the synthesis of core-shell particles, a new series of experiments (**Table VI-3**) were made using the same two different "hard" core seed poly(styrene) particles (Seed 1 and 2) with the comonomers styrene:*n*-butyl acrylate (0.67 wt/wt) in the presence of Laponite clay XLS (clay-monomer ratio 9.32-9.82 wt%) in order to obtain core-shell particles armored with Laponite clay (APS was used as initiator at initiator-to monomer ratio of 0.52-0.60 wt%). Batch emulsion polymerizations of both types of hard core seed particles led to secondary nucleation, confirmed by DLS (D_I above 0.5 in both cases). With the presence of clay discs into the recipe, competition between the clay and the seed latex particles for growing oligomeric radicals in the water phase to undergo "entry" will occur. This phase transfer event is governed by surface area. Due to the high total surface area of clay, the probability of secondary nucleation is high. The resulting latexes, will mainly consists of a new crop of poly(styrene-*co*-*n*-butyl acrylate) particles armored with Laponite clay XLS and the seed poly(styrene) particles. Just a few poly(styrene) "hard" particles end up as core-shell particles. The overall particle size did not change significantly (*ca.* 150nm) due to the formation of new polymer particles instead of core-shell particles.

To try to resolve these problems, emulsion polymerizations with later addition (X_M of 0.5) of Laponite clay XLS were performed (**Table VI-4**). The

latter addition of Laponite radically reduced the secondary nucleation (D_I of 0.137 for small seed particles and D_I of 0.198 for bigger seed particles); however poor adhesion of clay nanodiscs was observed on the "soft" shell of the polymer particles as evidenced in **Figure VI.3**.

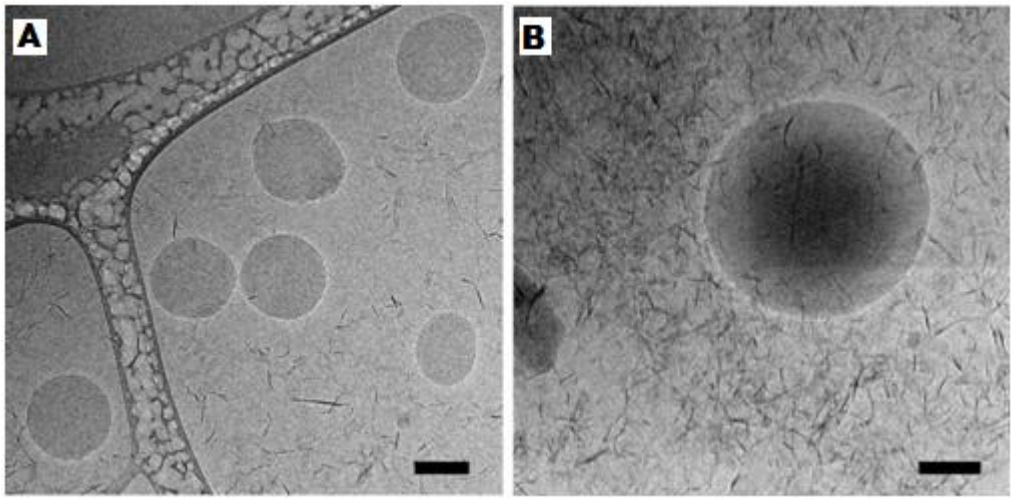

Figure VI.3. Cryo-TEM pictures of core-shell particles armored with Laponite clay XLS prepared through Pickering emulsion polymerization using APS as initiator and shot addition of clay at X_M of 0.5. **A**: core-shell particles using Seed 1. **B**: core-shell particles using Seed 2. Both Scale bars are of 100 nm.

A plausible explanation for the poor clay adhesion on the polymer particles surface is the presence of too many negative charges on the polymer surfaces provided by the negatively charge initiator (ammonium persulfate). Comparing these core-shell particles with our armored particles fabricated in chapter III (same recipe, but without the seed latex particles), we verify that the core-shell particles are bigger in size. This increase in the particle size reduced the total surface area of the polymer particles and therefore more negative sulfate groups (from the negative initiator) per unit area are present. In **Figure VI.3**.A, it is also

difficult to see the core-shell structure of the particles, making us believe that the poly(styrene) seed particles may have swollen and no polymerization of Sty:BA comonomers occurred on the shell surface. Alternatively, the lack of contrast between the core and shell in **Figure VI.3**.A could be as a result of the relatively small differences in the refractive indexes between poly(styrene) and poly(styrene-co-*n*-butyl acrylate) making it hard to observe by cryo-TEM.

To eliminate these problems, a new series of experiments was performed (**Table VI-5**), replacing the negatively charged ammonium persulfate by an initiator of neutral charge, azobisisobutyronitrile (AIBN). Starved-feed addition of comonomers styrene:*n*-butyl acrylate (0.67 wt/wt) was undertaken in order to avoid monomer swelling and to make sure that the polymerization occurs on the surface of the seed latex particles. The addition of Laponite clay was done by shot addition at X_M of 0.5.

The resulting core-shell particles showed a more visible core-shell structure and much better adhesion of clay platelets on the surface of the core-shell particles, as shown in **Figure VI.4**. The armored core-shell particles produced from the smaller seed latex particles showed better adhesion of clay nanodiscs (**Figure VI.4**. B and C) and had a lower dispersity (D_I of 0.125 for small seed particles and D_I of 0.191 of larger seed particles) as a result of the bigger total surface area. The monodispersity of the armored core-shell particles was improved in a new reaction, using twice the amount of seed 1 latex solution (D_I of 0.040) (**Figure VI.4** C).

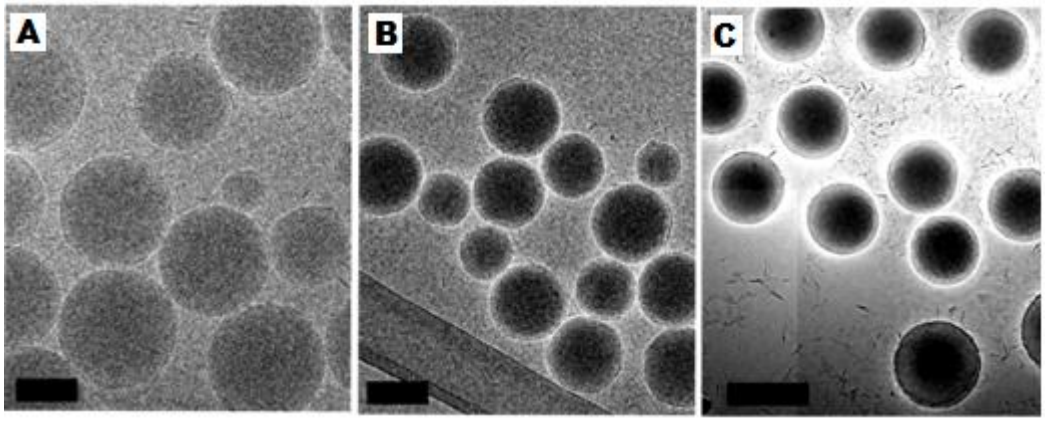

Figure VI.4. Cryo-TEM pictures of core-shell particles armored with Laponite clay XLS prepared through two step emulsion polymerization process using AIBN as initiator. **A**: core-shell particles using larger seed latex particles (seed 2). **B**: core-shell particles using smaller seed latex particles (seed 1). **C**: core-shell particles using twice the amount of the smaller seed latex particles (seed 1). Scale bars are of 200 nm.

Despite the improvements made, the adhesion of clay onto the shell of the core-shell polymer particles was not as strong as the armored poly(styrene-*co*-*n*-butyl acrylate) particles obtained in chapter III. The later addition of Laponite clay could be one plausible reason. Note, that in chapter III, Laponite clay is added in the beginning of the polymerization, working as a buffer solution and keeping the pH under basic conditions. Is discussed in chapter III that the clay adhesion into P(Sty-*co*-BA) surface can be due to the hydrolysis of *n*-butyl acrylate under basic conditions. Here, with the latter addition of Laponite clay, the pH of the reaction is kept under acidic or neutral conditions and no hydrolysis of *n*-butyl acrylate is expected. Note that, in chapter III, the presence of a small amount of methacrylic acid allowed much better adhesion of clay discs onto the poly(styrene-*co*-2-ethyl hexylacrylate) particles.

Due to a non clear proof of the adhesion of clay discs onto the core-shell particles surface, EELS (Electron Energy Loss Spectroscopy) analysis (for the sample using more amount of seed latex 1 (sample showed in **Figure VI.4**.C)), was performed. The results show a clear adhesion of clay nanodiscs onto the polymer particles surface, as evidenced in the next figure.

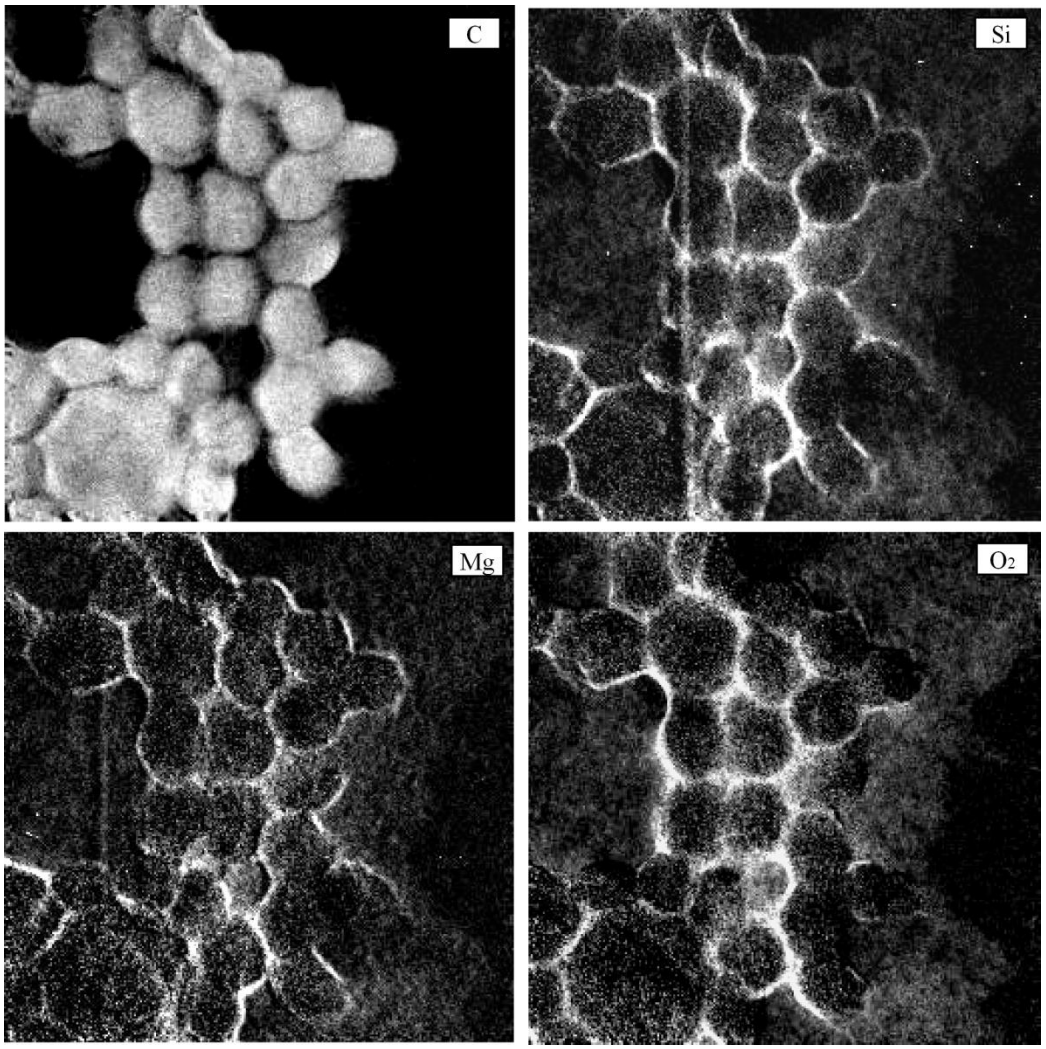

Figure VI.5. EELS (Electron Energy Loss Spectroscopy) analysis of four different elements present in the sample of core-shell particles using twice the amount of smaller seed latex particles (seed 1). Element content increases with the bright color.

Figure VI.5 confirms the presence of Laponite clay on the core-shell particle surface. The EELS analysis shows brighter colors when a certain element is present, being brighter with increasing elemental content. Taking into account that the polymers are largely carbon based, and the Laponite clay contains silicon, magnesium and oxygen, we can clearly see brighter colors around the polymer particles for the silicon, magnesium and oxygen elements. On the other hand, the carbon analysis shows, as expected, brighter colors in the polymer particles.

VI.4. Conclusions

The fabrication of core-shell particles armored with clay platelets via two steps Pickering emulsion polymerization was investigated. Firstly, hard core poly(styrene) polymer particles with sulfonate groups on the surface were prepared. The sulfonate groups on the surface were obtained by adding of sodium styrene sulfonate to the polymerization recipe. We found that the use of NaSS creates an active surface charge that is fundamental to stabilize the particles by electrostatic repulsion. The particle size and dispersity were also influenced by the use of sodium styrene sulfonate. For higher amounts of NaSS used, smaller and more monodisperse particles were obtained. In a second step emulsion polymerization, initially without clay discs, core-shell particles were obtained using hard core poly(styrene) particles with sulfonate groups on the surface as seed latex with comonomers styrene:*n*-butyl acrylate (0.67 wt/wt) using ammonium persulfate as initiator.

When it was introduced clay into the second emulsion polymerization step, competition between the clay and the hard core particles to absorb the oligomeric radicals of styrene:*n*-butyl acrylate (0.67 wt/wt) occurred leading to secondary nucleation, with a latex composition essentially of poly(styrene-*co*-*n*-butyl acrylate) particles armored with Laponite clay XLS and seed poly(styrene) particles. To overcome this problem, latter addition of clay particles was done (X_M of 0.5). The dynamic light scattering analysis on this latex showed much better monodispersity. However poor adhesion of Laponite clay platelets was verified. A plausible reason for the poor adhesion of clay is the presence of negative charge provided by the initiator ammonium persulfate. A new series of experiments were performed, replacing the ammonium persulfate by the neutral initiator azobisisobutyronitrile in the second emulsion polymerization step. In addition, starved-feed monomer addition was performed, in order to avoid monomer swelling. These changes allowed much better adhesion of clay nanodiscs onto the core-shell particles surfaces as confirm by cryo-TEM and EELS analysis.

VI.5. References

(1) Yin, Y.; Rioux, R. M.; Erdonmez, C. K.; Hughes, S.; Somorjai, G. A.; Alivisatos, A. P., *Science* **2004**, *304*, 711-714.

(2) Caruso, F.; Caruso, R. A.; Moehwald, H., *Science* **1998**, *282*, 1111-1114.

(3) Ohnuma, A.; Cho, E. C.; Camargo, P. H. C.; Au, L.; Ohtani, B.; Xia, Y., *J. Am. Chem. Soc.* **2009**, *131*, 1352-1353.

(4) Im, S. H.; Jeong, U. Y.; Xia, Y. N., *Nat. Mater.* **2005**, *4*, 671-675.

(5) Li, G.; Zeng, D. L.; Wang, L.; Baoyu; Zong; Neoh, K. G.; Kang, E. T., *Macromolecules.* **2009**, *42*, 8561-8565.

(6) Caruso, F.; Lichtenfeld, H.; Giersig, M.; Mohwald, H., *J. Am. Chem. Soc.* **1998**, *120*, 8523-8524.

(7) Tiarks, F.; Landfester, K.; Antonietti, M., *Langmuir* **2001**, *17*, 5775-5780.

(8) Landfester, K., *Adv. Mater.* **2001**, *13*, 765-768.

(9) Colver, P. J.; Colard, C. A. L.; Bon, S. A. F., *J. Am. Chem. Soc.* **2008**, *130*, 16850-16851.

(10) Agarwal, G. K.; Titman, J. J.; Percy, M. J.; Armes, S. P., *J. Phys. Chem. B* **2003**, *107*, 12497-12502.

(11) Alexandre, M.; Dubois, P., *Mater. Sc. Eng. R: Rep.* **2000**, *28*, 1-63.

(12) Sinha Ray, S.; Okamoto, M., *Prog. Polym. Sci.* **2003**, *28*, 1539-1641.

(13) You, B.; Wen, N.; Cao, Y.; Zhou, S.; Wu, L., *Polym. Inter.* **2009**, *58*, 519-529.

(14) Wang, T.; Colver, P. J.; Bon, S. A. F.; Keddie, J. L., *Soft Matter* **2009**, *5*, 3842-3849.

(15) Deplace, F.; Rabjohns, M. A.; Yamaguchi, T.; Foster, A. B.; Carelli, C.; Lei, C.-H.; Ouzineb, K.; Keddie, J. L.; Lovell, P. A.; Creton, C., *Soft Matter* **2009**, *5*, 1440-1447.

(16) Chevalier, Y.; Hidalgo, M.; Cavaillé, J. Y.; Cabane, B., *Macromolecules.* **1999**, *32*, 7887-7896.

(17) Dos Santos, F. D.; Leibler, L., *J. Polym. Sc. Part B: Polym. Phys.* **2003**, *41*, 224-234.

(18) Wang, T.; Lei, C. H.; Dalton, A. B.; Creton, C.; Lin, Y.; Fernando, K. A. S.; Sun, Y. P.; Manea, M.; Asua, J. M.; Keddie, J. L., *Adv. Mater.* **2006**, *18*, 2730-2734.

(19) Schmid, A.; Tonnar, J.; Armes, S. P., *Adv. Mater.* **2008**, *20*, 3331-3336.

(20) Pinprayoon, O.; Groves, R.; Lovell, P. A.; Tungchaiwattana, S.; Saunders, B. R., *Soft Matter* **2011**, *7*, 247-257.

(21) Suzuki, D.; McGrath, J. G.; Kawaguchi, H.; Lyon, L. A., *J. Phys. Chem. C* **2007**, *111*, 5667-5672.

(22) Griffete, N.; Dybkowska, M.; Glebocki, B.; Basinska, T.; Connan, C.; Maître, A. S.; Chehimi, M. M.; Slomkowski, S.; Mangeney, C., *Langmuir* **2010**, *26*, 11550-11557.

(23) Meng, Q.; Li, Z.; Li, G.; Zhu, X. X., *Macromol. Rapid Comm.* **2007**, *28*, 1613-1618.

(24) Tamai, H.; Niino, K.; Suzawa, T., *J. Colloid Interf. Sci.* **1989**, *131*, 1-7.

(25) Furusawa, K.; Norde, W.; Lyklema., J., *Kolloid Z. Z. Polymer.* **1972**, *250*, 908.

(26) Ono, H.; Saeki, H., *Brit. Polym. J.* **1975**, *7*, 21-31.

(27) Goodwin, J. W.; Hearn, J.; Ho, C. C.; Ottewill, R. H., *Brit. Polym. J.* **1973**, *5*, 347-362.

(28) Juang, M. S.-D.; Krieger, I. M., *J. Polym. Sc.: Polym. Chem. Ed.* **1976**, *14*, 2089-2107.

(29) Ni, K. F.; Shan, G. R.; Weng, Z. X.; Sheibat-Othman, N.; Fevotte, G.; Lefebvre, F.; Bourgeat-Lami, E., *Macromolecules.* **2005**, *38*, 7321-7329.

Chapter VII.

Final Remarks and Future Work

In this chapter, the main goals and achievements of each chapter are summarized. The industrial interest of the work performed is discussed. Finally, a brief outlook towards future developments is addressed.

Polymer dispersions can conveniently be synthesized through emulsion polymerization. The fabrication of polymer latexes using this waterborne process is of industrial relevance with applications in coatings, adhesives, printing inks, asphalt, dipped goods, etc..[1] The incorporation of fillers into these polymer latex based materials can enhance material properties and performance. However, a non-even distribution of inorganic fillers and pigments upon film formation leads to cracks and brittle films. Therefore, there is a clear need to design more complex nanocomposite polymer particles. This work focused on the development of armored polymeric particles with a layer of inorganic nanoparticles through Pickering emulsion polymerization process. This solids-stabilized emulsion polymerization process relies on the adhesion of solid particles to soft interfaces, a phenomenon known as Pickering stabilization.

Silica nanoparticles of *ca* 25 nm in diameter (Ludox TM-40) when used in Pickering emulsion polymerization they allow the formation of raspberry shaped hybrid polymer particles. It was demonstrated that silica nanopartices adhere to a variety of soft interfaces i.e. poly(*n*-butyl acrylate) P(BA), poly(methyl methacrylate-*co*-*n*-butyl acrylate) P(MMA-*co*-BA) and poly(vinyl acetate) P(VAc). Monitoring the adhesion of silica nanoparticles onto the polymer latex particles throughout the emulsion polymerization process is key not only for reaction process optimization but also to tailor the composition of the final composite dispersion. This has direct consequences on the film properties. It was shown that disc centrifugation can be used as a powerful quantitative tool to analyze and determine the concentration of nanoparticles in the water phase throughout solids-stabilized emulsion polymerizations.[2]

Laponite clay XLS are disc shaped silicates of low heavy metal content with 25 nm in diameter and a 0.92 nm height. We showed that clay nanoparticles can adhere to soft polymer latex interfaces hereby allowing the fabrication of armored structures. We have shown the fabrication of "soft" clay armored nanocomposite polymer latexes of poly(methyl methacrylate-*co*-*n*-butyl acrylate) P(MMA-*co*-BA), poly(styrene-*co*-*n*-butyl acrylate) P(Sty-*co*-BA) and poly(styrene-*co*-2-ethyl hexyl acrylate) P(Sty-*co*-2-EHA) using Pickering emulsion polymerization.[3] Cryo-TEM analysis confirmed the adhesion of clay nanodiscs onto the latex particles. It was demonstrated that the use of high water solubility monomers, which easily hydrolyze under basic conditions, should be restricted. Different amounts of clay were used to see its influence on the polymerization rates, and average polymer particle size and its distribution. The overall rate of polymerization was increased when larger amounts of clay were used. The average particle size measured as a function of monomer conversion showed a substantial effect of the clay, with particles being considerably smaller when clay was used. This is clear evidence that clay plays an important role in the particle formation stage of the Pickering emulsion polymerization process. Particle formation now involves heterocoagulation of a clay disc with a precipitating oligomer of critical chain-length from the waterphase or with a colloidally unstable primary latex particle. From the dispersity of the particle size, again plotted as function of monomer conversion, it can be seen that prolonged periods of nucleation occur at higher amounts of clay leading to broader particle size distribution.

Polymer films made from poly(styrene-*co*-*n*-butyl acrylate)/clay armored particles prepared through Pickering emulsion polymerization were investigated. It was shown that the presence of clay improves the mechanical and thermal properties of P(Sty-*co*-BA) films. Improvements on the storage modulus upon increasing amounts of clay were shown. Very interestingly, polymer films made from these hybrid nanocomposite particles showed a very good recovery after deformation, showing elastic behavior. It was verify that the presence of a honeycomb clay network lead to better mechanical improvements in comparison with a blend mixture of the same composition. It was demonstrated that the presence of clay improves the thermal decomposition of polymer films. It was also shown that the presence of Laponite clay leads to much smoother polymer films.[4]

In chapter V, it was shown that the presence of a honeycomb structure provided by the clay platelets in the polymer films enhanced the capacity to absorb not only more water but also more hydrophobic octane molecules. It was shown that for low humidity pressures values (till *ca* 40 RH %) the solvent adsorption is relative linear with the humidity pressure; however for high humidity pressures the solvent adsorption strongly increases due to capillary condensation of solvent molecules in the clay channels network. To prove the importance of a honeycomb, a polymer film made from a blend mixture of hybrid polymer latex particles armored with clay and non armored polymer particles was analyzed. It was verified that the blend mixture adsorbed much less solvent molecules than a polymer film made just with hybrid nanoparticles. The importance of the continuous honeycomb structure was shown to be crucial

since the blend polymer film adsorbed roughly the same amount of water than a simple polymer film without any amount of clay. An innovative method to measure barrier properties was addressed. It was shown that the presence of clay improves the water vapor barrier properties of hybrid polymer films.[4]

In chapter VI, the fabrication of complex nancomposite latexes particles made via two steps Pickering emulsion polymerization process was addressed.[5] Core-shell particles armored with a layer of clay nanodiscs on the outer shell were produced. These versatile nancomposites have a "hard" core made of poly(styrene) and a "soft" shell made of poly(styrene-*co*-*n*-butyl acrylate) armored with Laponite clay. The difference in the refractive indexes between the "hard" core and the "soft" shell makes these particles attractive for potential use as colloidal crystals.

Future work

Further investigation of core-shell particles armored with fillers produced by Pickering emulsion polymerization as well as characterization of the corresponding polymer films are the next logical steps of this work. The synergetic effects between the "hard" core, "soft" shell and fillers make these particles very attractive for a wide range of applications. The influence of the solid-stabilizer geometry in the final polymer films properties is also an interesting aspect to be investigated. Barrier properties and mass uptake capacity of waterborne polymer films should be extended to others solvents of interest to the packing, coating and painting industries.

List of papers related to this PhD thesis

(1) Teixeira, R. F. A.; Bon, S. A. F. *Adv. Polym Sci*. **2010**, 233, 19-52.

(2) Colard, C. A. L.; Teixeira, R. F. A.; Bon, S. A. F. *Langmuir* **2010**, 26, 7915-7921.

(3) Teixeira, R. F. A.; Mckenzie, H. S.; Boyd, A. A.; Bon, S. A. F. *Macromol.* **2011**, 44, 7415-7422..

(4) Teixeira, R. F. A.; Bon, S. A. F., Influence of clay discs on the barrier properties of cellular nanocomposite "soft" polymer films, in preparation

(5) Teixeira, R. F. A.; Bon, S. A. F., Fabrication of armored core-shell nanoparticles via two step Pickering emulsion polymerization process, in preparation

VII.1. Quotes:

Research is what I am doing when I do not know what I am doing.

By: Wernher Von Braun

The most exciting phrase to hear in science, the one that heralds the most discoveries, is not "Eureka!" (I found it!) but "That's funny..."

By: Isaac Asimov

Science is simply common sense at its best.

By: Thomas Huxley

The greatest discoveries of science have always been those that forced us to rethink our beliefs about the universe and our place in it.

By: Roberto L. Park, New York Times (1999)

I am among those who think that science has great beauty. A scientist in his laboratory is not only a technician: he is also a child placed before natural phenomena which impress him like a fairy tale.

By: Marie Curie

Appendix

Appendix of Chapter II - Pickering Emulsion polymerizations stabilized with silica nanospheres

The calibration data for the signal intensity of the detector versus the concentration of the silica nanoparticles dispersed in water could be fitted with a linear expression for the range of concentrations investigated (linear fit: $R^2 > 0.95$)., that is up to ca. 0.40 wt% of silica nanoparticles in water. To correlate the detector signal to concentration we used three different methods of data analysis; that is the full area of the peak, lower half-area of the peak and the base-line corrected peak height. The peak shape of the Ludox TM-40 was constant throughout the series of calibration standards. The method measuring the height of the peak was most straightforward and accurate; the base-line corrected height measurements were not as sensitive to noise observed at small diameters on the left hand side of the peak. All further data was analyzed using this method.

In the disc centrifugation analysis of waterborne dispersions often a sucrose gradient of the aqueous spinning fluid is used in to minimize peak broadening. We found that in order to get reliable and reproducible quantitative data great accuracy had to be taken in preparation of this sucrose gradient. The underlying reason is that variation in the sucrose concentration influences the differential

refractive index, the turbidity and hence the signal intensity. The maximum sucrose molality used was 0.70 mol kg^{-1} of water with a corresponding density of ~ 1.064 g ml^{-1} and viscosity of ~ 1.3 cP.[1] This is less than the density of the nanocomposite polymer latexes and the ludox silica, and therefore allows sedimentation upon imposing the centrifugal force by rotation of the disc.[2]

Disc centrifuge measurements

The CPS was used to correlate intensity of the detection signal to the concentration of nanoparticles. Our gradient was built from two solutions; sucrose of 8.0 wt% (0.23 mol kg^{-1}) and 24.0 wt% (0.70 mol kg^{-1}).

We initially injected a series of calibration standards of Ludox TM-40 silica nanoparticles dispersed in water. Representative data is shown in **Figure A. II-1** for various concentrations of silica nanoparticles, 0.11 wt%, 0.22 wt%, 0.28 wt%, 0.33 wt% and 0.39 wt%.

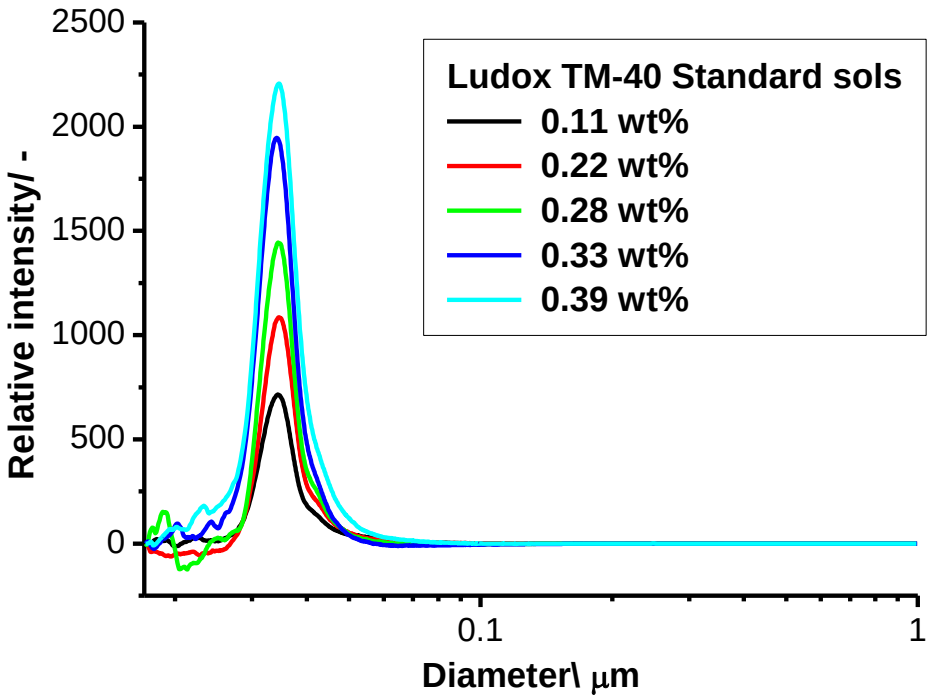

Figure A. II-1. Traces obtained by CPS analyses of approximately 0.1 g for each Ludox TM-40 standard sol of known concentration in colloidal silica nanoparticles prepared from a 40 wt% Ludox TM-40 sol.

Note that the position of the silica particles according to the disc centrifuge lies at 35 nm which differs from our TEM mean value. We believe that this difference is due to separation on hydrodynamic volume rather than dry, the silica particles are not of perfect spherical shape, and the density is an estimated value. However the mean position of the peak is not important as we are interested in the intensity of the detector signal, and the shape of the signal, which does not change throughout emulsion polymerization.

In order to measure intensity of the detector signal, we compared three different methods to analyse the traces (**Figure A. II-2**). We used the CPS software to measure (1) the full area under the peak, (2) the area of half of the peak, and finally, (3) the height corrected by the baseline (subtracting the

intensity at a diameter of 0.26 nm to the highest intensity of the peak). This diameter was chosen arbitrarily to attempt to minimise the errors induced by the noise observed at the end of the runs (settings parameters are specified in the experimental part).

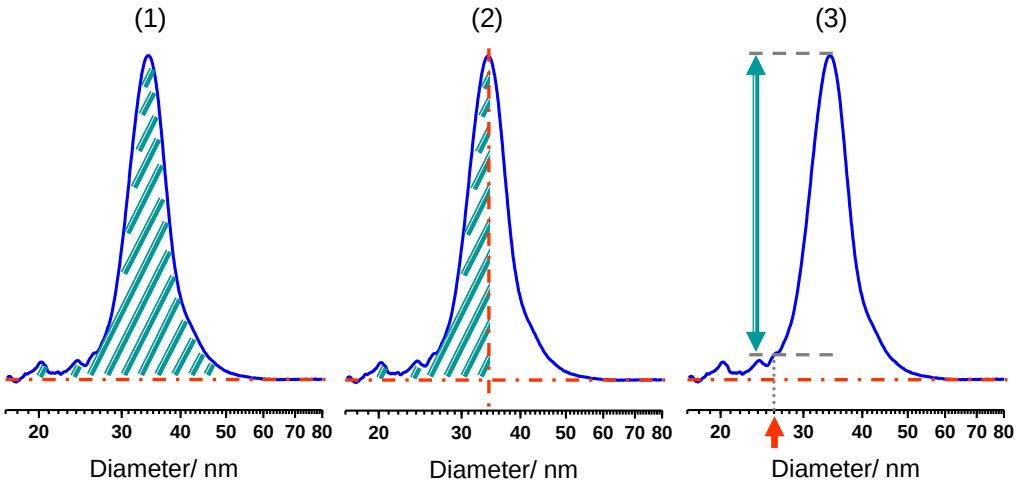

Figure A. II-2. Cartoon of the three types of analysis performed for each trace (1) by full-area, (2) by half-area and (3) by height after 'baseline correction'. The y-axis is the relative light intensity measured by the detector. The horizontal red dashed-line represents the 'zero' made by the software at a diameter of 17 nm.

Each colloidal silica standard was injected 3 times and all traces obtained were analysed by methods (1), (2) and (3), and corrected by the mass of sample injected. The average of the three measurements is plotted with the standard deviation against the concentration in colloidal silica in **Figure A. II-3**.

(1) Full-area

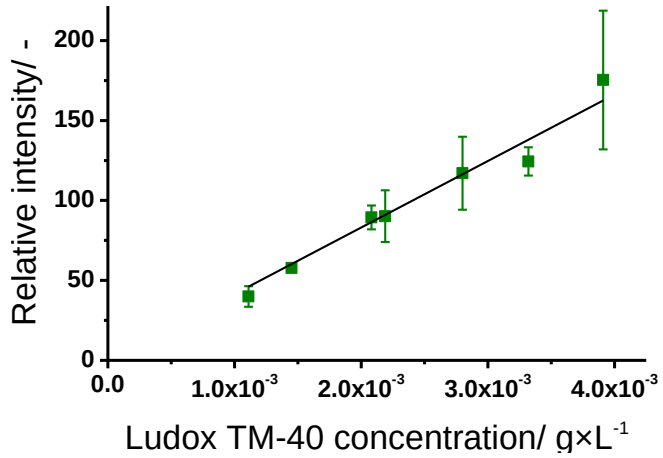

(2) Half-area

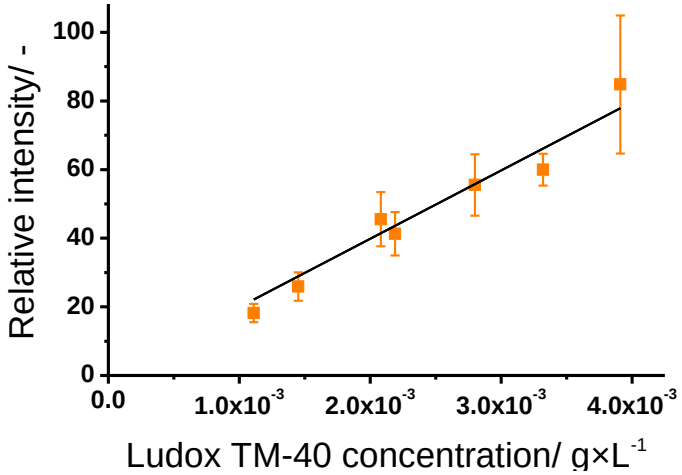

(3) Height

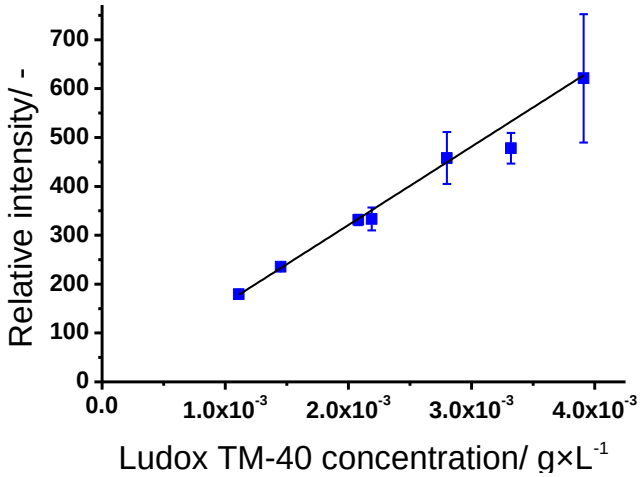

Figure A. II-3. Graphs of dependence between the concentration in silica nanoparticles and the relative intensity of the peak obtained by CPS

measurements for the three different analysis methods described. (1) Full-area (linear fit: y = 41555 x, R^2 = 0.967), (2) Half-area (linear fit: y = 19919 x, R^2 = 0.955) and (3) Height (linear fit: y = 155598 x, R^2 = 0.983).

By plotting relative signal intensities versus concentration in colloidal silica, a linear trend is observed for the three types of analysis with excellent linear regression (R^2 over 0.95). The peak is uniform in shape and size which gives a good indication for reproducibility and comparison between samples.

In order to determine the most accurate methods of the three methods to analyze, relative standard deviations, σ_{rel}, were compared and plotted in **Figure A. II-4**. They were calculated over three measurements made for each concentration in nanoparticles and normalized by dividing by the relative intensity of the signal measured. The irregularities observed on the graph are simply attributed to the fact that each sample was injected only 3 times.

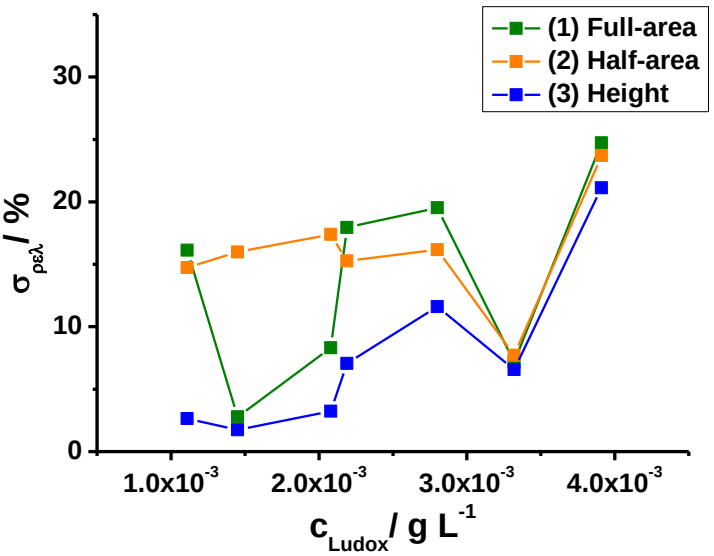

Figure A. II-4. Graph of the relative standard deviations, σ_{rel}, from the analysis with the three different methods of the Ludox standard sol CPS measurements.

From these analyses we found a very clear linear trend between the concentration in colloidal silica nanoparticles and the signal intensity given by the CPS. All cases, reported a high R^2, from 0.955 with method (2), 0.967 with method (1) and 0.982 with method (3). However the differences between standard deviations are less negligible as can be seen in **Figure A. II-4**. The third method (**Figure A. II-3**)), using the height of the peak exhibits a smaller standard deviation and hence more accurate for single measurements, especially for smaller concentration in silica nanoparticles. We therefore further pursue the analyses of emulsion polymerisation samples using this method.

Reproducibility and variation between gradient fluids

This technique has demonstrated exemplary reproducibility due to the injection of PVC calibration standard prior to each injection of samples. However in our case, as we are not analyzing the particle size distribution but intensity of the detected signal, more parameters have to be taken into account.

The intensity of the scattered light depending on the refractive index of the dispersed medium, we expect the sucrose concentration to be determinant for the detection of the nanoparticles. Since a sucrose gradient fluid cannot be used for longer than 5 or 6 hours, several gradients had to be prepared in order to analyze Ludox standards and series of samples with each injection taking

approximately half an hour. Herein we checked the influence of which on the measurements. The detector is located at the edge of the rotating disc where the sucrose concentration of the gradient is highest.. In **Figure A. II-5**, the graph displays the results obtained using 8.0 – 20.0 wt% gradient in comparison with 8.0 – 24.0 wt% gradient to investigate the influence on detection of the nanoparticles. A noticeable shift in the detector response was found.

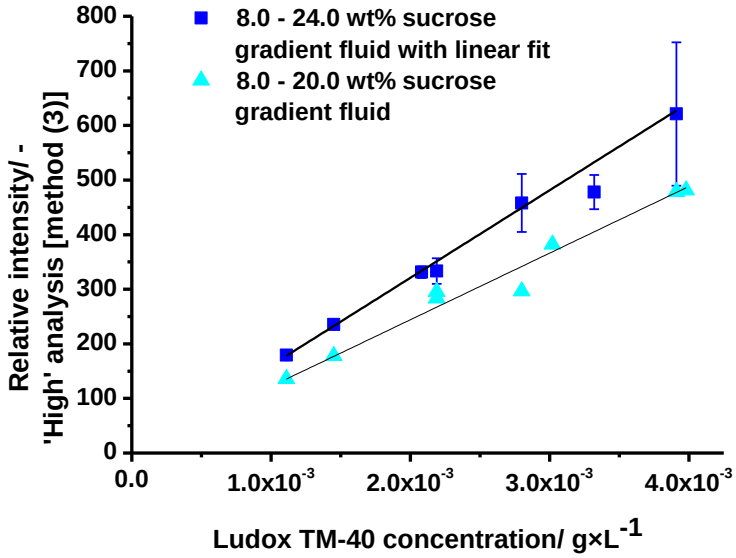

Figure A. II-5. Relative intensity from the colloidal silica analysed by CPS versus concentration using two different gradient fluids of sucrose: 8.0 to 24.0 wt% (■) and 8.0 to 20.0 wt% (▲).

Stability of the gradient fluid

We also tested the repeatability of the measurement as a function of time using the same sucrose gradient fluid. Two different samples were alternatively injected four times each over a period of four hours. After analyzing the data as described above, the variation between the different traces was found to be random. Any change in the refractive index of medium, induced by a warm-up

during the centrifugation process for instance, was minimal and could not be observed.

References

(1) Analytik Ltd analytical solutions, C. I. E., *CPS Disc Centrifuge DC24000, System Documentation* **2009**.

(2) Hu, Y.-F.; Zhang, Z.-X.; Zhang, Y.-H.; Fan, S.-S.; Liang, D.-Q., *J. Chem. Eng. Data* **2006,** *51*, 438-442.

Appendix of Chapter III - Pickering Emulsion Polymerization using Laponite Clay as Stabilizer to prepare Armored "Soft" Polymer Latexes

In the next tables is presented the raw data of all reactions from **Table III-3** and **Table III-4**:

HM-1				**HM-2**			
Time	X_M	D_z/ *nm*	*D*/ -	**Time**	X_M	D_z/ *nm*	*D*/ -
0	0	66.82	0.174	0	0.01	80.87	0.198
15	0.01	90.01	0.046	15	0.02	56.05	0.129
30	0.01	106.7	0.017	30	0.03	59.29	0.079
45	0.02	122.0	0.013	45	0.05	69.73	0.072
60	0.04	150.2	0.020	60	0.07	83.13	0.059
90	0.06	176.5	0.018	90	0.11	97.19	0.071
120	0.06	214.1	0.015	120	0.16	116.3	0.109
180	0.09	255.9	0.008	180	0.23	123.4	0.095
240	0.14	290.1	0.035	240	0.29	131.6	0.105
300	0.15	303.8	0.174	300	0.34	137.2	0.073
330	0.18	305.0	0.029	330	0.38	141.4	0.059
360	0.2	355.0	0.114	360	0.43	141.6	0.06
390	0.26	342.5	0.013	390	0.47	146.5	0.104
420	0.29	360.7	0.035	420	0.53	153.2	0.07
450	0.32	361.5	0.012	450	0.58	156.2	0.076
480	0.8	609.4	0.027	480	0.87	184.3	0.032

HM-3				HM-4			
Time	X_M	D_z/ *nm*	*D*/ -	**Time**	X_M	D_z/ *nm*	*D*/ -
0	0.02	74.53	0.147	0	0.06	74.55	0.184
15	0.03	82.24	0.113	15	0.12	96.98	0.042
30	0.04	90.12	0.102	30	0.17	109.5	0.630
45	0.08	111.7	0.101	45	0.22	127.8	0.030
60	0.11	144.4	0.102	60	0.29	159.8	0.036
90	0.13	172.3	0.136	90	0.38	187.1	0.051
120	0.16	195.2	0.206	120	0.48	304.2	0.149
180	0.21	180.1	0.225	180	0.6		
240	0.30	190	0.284	240	0.7		
300	0.33	190	0.24	300	0.72		
330	0.37	189.4	0.218	330	0.88		
360	0.42	185.3	0.114	360	0.82		
390	0.46	194.6	0.09				
420	0.49	198.5	0.055				
450	0.49	206.2	0.004				
480	0.90	216.5	0.021				

HM-5				HM-6			
Time	X_M	D_z/ *nm*	*D*/ -	**Time**	X_M	D_z/ *nm*	*D*/ -
15	0.01	81.75	0.461	15	0.04	77.26	0.226
30	0.06	60.91	0.14	30	0.09	74.25	0.124
45	0.12	72.83	0.064	45	0.16	88.83	0.151
60	0.19	86.67	0.027	60	0.2	100.2	0.095
90	0.32	114	0.027	90	0.35	120.2	0.046
120	0.43	127.4	0.031	120	0.4	128.8	0.054
180	0.57	144.1	0.006	180	0.53	144.9	0.034
240	0.69	154.5	0.021	240	0.6	158.2	0.039
300	0.81	168.8	0.043	300	0.71	168.7	0.029
330	0.88	172.8	0.031	330	0.76	171.0	0.103
360	0.91	174.8	0.02	360	0.8	176.2	0.104
390	0.94	175.1	0.002	390	0.84	179.6	0.061
420	0.96	177.0	0.006	420	0.89	182.1	0.103
450	0.97	179.7	0.027	450	0.93	186.4	0.026
480	0.98	177.0	0.02	480	0.93	184.5	0.113

HM-7				*RT-2-50*			
Time	X_M	D_z/ *nm*	*D*/ -	**Time**	X_M	D_z/ *nm*	*D*/ -
15	0.02	63.26	0.139	26	0.07	90.49	0.287
30	0.21	79.87	0.089	40	0.09	73.53	0.326
45	0.31	91.24	0.064	68	0.14	72.11	0.246
60	0.39	100.2	0.069	90.5	0.19	73.5	0.215
90	0.52	112.4	0.049	124	0.26	77.15	0.203
120	0.62	121.5	0.057	167	0.37	76.87	0.17
180	0.79	137.8	0.036	222	0.51	85.23	0.156
240	0.97	152.5	0.061	268	0.67	92.28	0.162
300	1	149.3	0.069	324	0.80	94.9	0.132
330	0.99	151.1	0.086	365	0.76	97.07	0.13
360	1	150.3	0.058	800	1	121.5	0.203
390	1	151.2	0.029				
420	0.98	149.2	0.022				
450	0.97	148.8	0.055				
480	1	150.6	0.037				

RT-2-52				RT-2-51			
Time	X_M	D_z/ *nm*	*D*/ -	**Time**	X_M	D_z/ *nm*	*D*/ -
15	0.04	58.42	0.24	22.3	0.04	50.26	0.115
33	0.07	58.89	0.21	50.5	0.1	55.00	0.148
61	0.13	59.75	0.183	83	0.16	56.54	0.081
105	0.21	62.16	0.133	120	0.27	61.82	0.062
140	0.31	64.35	0.107	152	0.37	68.45	0.051
177	0.38	67.17	0.126	167	0.42	68.98	0.082
220	0.53	73.04	0.116	200	0.51	73.04	0.073
267	0.66	80.16	0.074	240	0.63	82.00	0.041
315	0.73	87.79	0.117	280	0.74	86.72	0.070
355	0.86	91.77	0.092	315	0.85	91.85	0.065
420	0.87	95.7	0.108	340	0.90	93.25	0.048
800	1	115.4	0.174	370	0.94	95.58	0.033
				800	0.97	102.5	0.085

RT-2-54				**RT-2-56**			
Time	X_M	D_z/ *nm*	*D*/ -	**Time**	X_M	D_z/ *nm*	*D*/ -
5	0.01	60.23	0.200	5	0.02	56.37	0.095
10	0.02	56.02	0.158	14	0.04	61.14	0.077
16	0.03	56.28	0.132	30	0.08	66.51	0.064
25	0.04	56.77	0.105	48	0.1	72.02	0.051
44	0.08	64.64	0.12	61	0.13	74.91	0.024
67	0.12	69.33	0.08	87	0.18	81.98	0.024
97	0.19	72.51	0.038	139	0.27	94.7	0.03
125	0.27	83.89	0.07	191	0.4	104.4	0.013
167	0.39	93.7	0.056	238	0.51	112.1	0.026
251	0.59	108.3	0.041	308	0.66	125.6	0.02
295	0.71	115	0.048	358	0.74	128.3	0.011
340	0.75	119.2	0.07	800	0.86	131.1	0.012
377	0.81	123.7	0.079				
800	0.95	126.3	0.048				

RT-2-55				**RT-2-57**			
Time	X_M	D_z/ *nm*	*D*/ -	**Time**	X_M	D_z/ *nm*	*D*/ -
6	0.01	71.85	0.09	4	0.01	64.81	0.142
10	0.04	75.84	0.102	10	0.02	72.77	0.069
13	0.02	78.91	0.056	16	0.03	77.73	0.074
18	0.04	83.46	0.033	25	0.05	83.65	0.074
24	0.06	87.43	0.040	40	0.07	92.87	0.042
32	0.07	91.4	0.028	74	0.13	109.5	0.022
45.5	0.10	98.59	0.056	107	0.19	123.5	0.011
64.5	0.14	109.7	0.03	145	0.27	137.4	0.04
86	0.20	117.7	0.017	187	0.34	148.1	0.016
103	0.23	125.3	0.024	224	0.38	155.1	0.004
135	0.32	139.5	0.012	273	0.53	167.0	0.023
159	0.37	144.4	0.021	326	0.66	175.0	0.038
200	0.48	156.6	0.018	800	0.95	201.4	0.002
250	0.61	166.7	0.017				
312	0.64	174.0	0.048				
800	1.00	193.4	0.039				

RT-2-53			
Time	X_M	D_z/ *nm*	*D*/ -
17.5	0.02	95.96	0.018
30	0.04	116.5	0.003
49	0.05	136.9	0.014
64	0.07	154.2	0.012
113	0.14	208.1	0.034
165	0.23	228.7	0.074
201	0.33	243.2	0.045
248	0.37	253.7	0.019
300	0.48	263.2	0.042
333	0.59	262.3	0.041
370	0.63	270.2	0.032
800	0.82	278.8	0.051

Appendix of Chapter V - Influence of Laponite clay on the adsorption/desorption and barrier properties of cellular nanocomposite "soft" polymer films

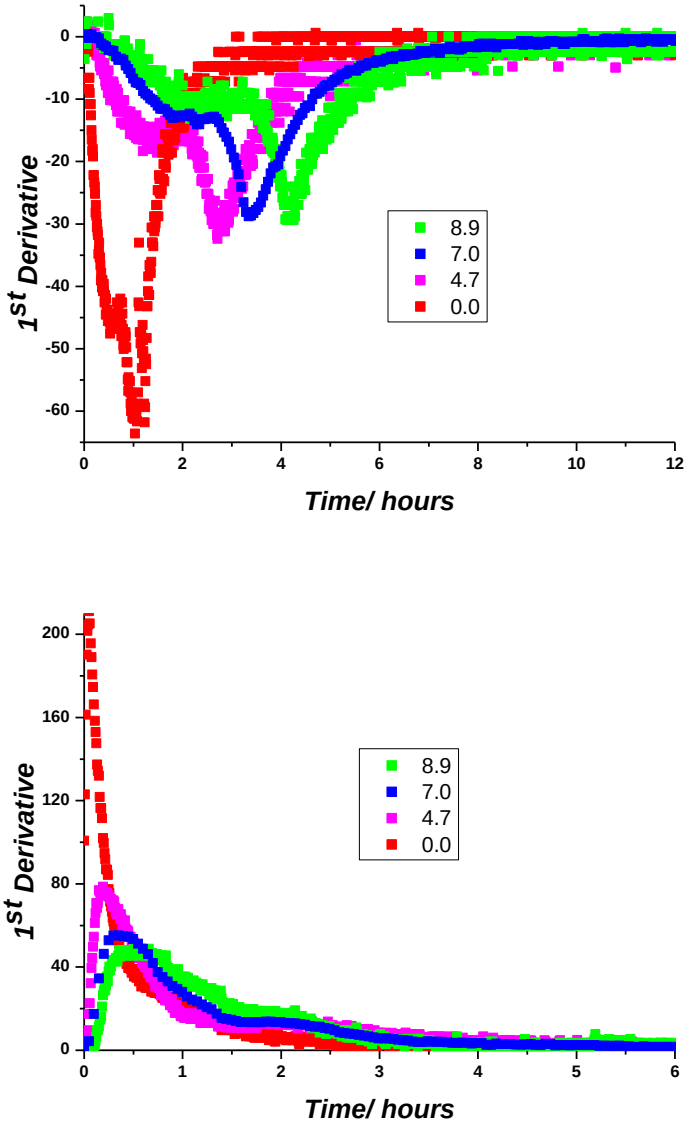

Figure A. V-1. On top: First derivative versus time of sorption isotherm of poly(styrene-*co*-*n*-butyl acrylate)/clay films with 8.9, 7.0, 4.7, 0.0 weight % in clay content. On bottom: First derivative versus time of desorption isotherm of

poly(styrene-*co*-*n*-butyl acrylate)/clay films with 8.9, 7.0, 4.7, 0.0 weight % in clay content.

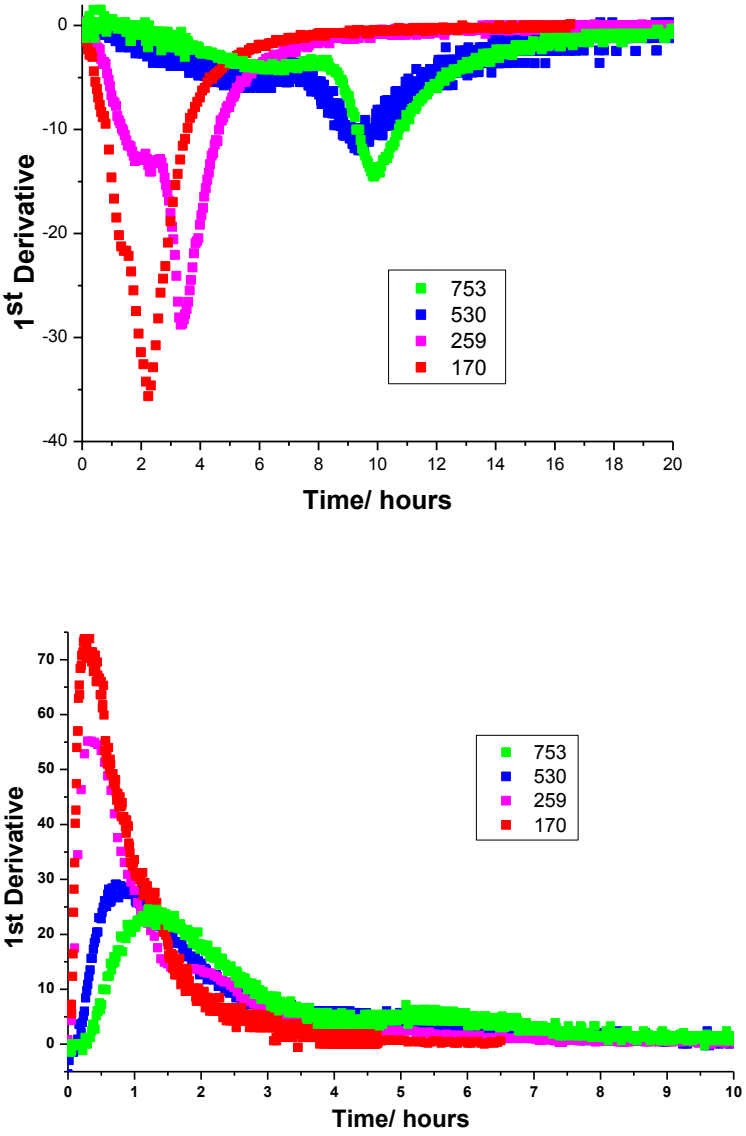

Figure A. V-2. On top: First derivative versus time of sorption isotherm of poly(styrene-*co*-*n*-butyl acrylate)/clay films with 7.0 wt% in clay content and 753, 530, 259 and 170 µm in thickness. On Bottom: First derivative versus time of desorption isotherm of poly(styrene-*co*-*n*-butyl acrylate)/clay films with 7.0 wt% in clay content and 753, 530, 259 and 170 µm in thickness.